Design and Implementation of an RF Front End for the NeXtRAD Radar System

Adrian Dale Stevens

A dissertation submitted to the
Department of Electrical Engineering,
University of Cape Town,
in partial fulfilment of the requirements for the degree of
Master of Science in Engineering
specialising in
Radar and Electronic Defence.

July 2017

Declaration

I know the meaning of plagiarism and declare that all the work in the document, save for that which is properly acknowledged, is my own. This thesis/dissertation has been submitted to the Turnitin module (or equivalent similarity and originality checking software) and I confirm that my supervisor has seen my report and any concerns revealed by such have been resolved with my supervisor.

Signed by candidate

Cape Town
03 July 2017

Abstract

This dissertation presents the design of the RF front end for use on the *NeXtRAD* radar system. The system is intended for research purposes to investigate potential target detection benefits to be derived from a multistatic, dual-band (X- and L-band), polarimetric radar architecture, particularly within dense clutter environments such as the maritime environment.

By examining the high-level system requirements and objectives, requirement specifications for the RF front end were derived and a suitable architecture, making use of commercial off-the-shelf components, proposed. This architecture was modified in order to meet cost constraints — subsequently offering reduced levels of functionality but suitable for an initial build.

Using this modified RF front end architecture, design verification and system analysis was conducted, both analytically and with the aid of *SystemVue*, in order to predict both the front end and overall radar detection performance. Once the front end design was found to be satisfactory, it was built and tested in a laboratory environment. Test results revealed a general improvement in performance when compared with the design predictions, yielding peak transmitter power levels in excess of 61 dBm at L-band, and 54 dBm at X-band. Some non-conformances were also identified, but these were as a result of component problems and not system design. Since the front end could not yet be integrated into the radar, performance modelling was repeated using the final lab test results. This indicated a negligible improvement in receiver single-pulse signal-to-noise ratio, but confirmed that the system performed as predicted.

Based on the lab test results, it was concluded that the 'as-built' front end design closely matched the design goals and would be suitable for eventual integration into the first revision of the NeXtRAD system. It was, however, recommended that a concerted effort be made to secure funding to implement the original front end architecture in order to achieve the full system functionality originally desired.

Acknowledgements

I would like to express my gratitude to the following persons/entities who provided various forms of support during the course of this project:

My supervisor, Professor Riana Geschke, for her guidance, support and patience during the rather protracted process of completing this dissertation.

Professor Michael Inggs for offering this project to me and securing funding for it during my time of unemployment. Also for the important advice and guidance provided.

Professor Barry Downing, who functioned as my co-supervisor for a brief period of time and provided valuable insight and guidance over the course of this project.

Dr. Rodolfo Lima from the Brazilian Navy Research Institute (IPqM), for his continual assistance and advice, particularly during the design and testing phases of the project.

My wife, Siddeeqa, for the support and encouragement, and the many sacrifices that were made whilst I undertook this degree.

Reutech Radar Systems for stimulating my interest in radar, sending me to do the the Radar Masters programme, and providing funding towards the degree. Also for the support and mentorship provided during my time of employment there.

Armscor and the Institute for Maritime Technology for partially funding this degree through the Ledger fund, and for supporting its completion whilst under their employ.

Contents

List of Figures

List of Tables

List of Abbreviations

ADC	Analogue-to-Digital Converter
ATP	Acceptance Test Procedure
BIM	Built-In Monitoring
BPF	Band Pass Filter
BW	Antenna Beamwidth
CoC	Certificate of Conformance
COTS	Commercial Off-The-Shelf
CW	Continuous Wave
DAC	Digital to Analogue Converter
DC	Duty Cycle or Direct Current
FET	Field Effect Transistor
FPGA	Field-Programmable Gate Array
GaN	Gallium Nitride
GPSDO	Global Positioning System (GPS) Disciplined Oscillator
H-Pol	Horizontally Polarised
HPA	High Power Amplifier

HPBW	Half Power Beamwidth
IEEE	Institute for Electrical and Electronic Engineers
IF	Intermediate Frequency
IL	Insertion Loss
IRC	IF Receive Chain
ITU	International Telecommunication Union
L-Band	Frequency band spanning 1 – 2 GHz
LFM	Linear Frequency Modulated
LNA	Low Noise Amplifier
LO	Local Oscillator
MTBF	Mean Time Between Failure
NF	Noise Figure
PIN	P-type, Intrinsic, N-type
Pre-Amp	Pre-Amplifier
PRF	Pulse Repetition Frequency
PRI	Pulse Repetition Interval
PW	Pulse Width
RCS	Radar Cross Section
REC-L	RF Exciter Chain, L-band
REC-X	RF Exciter Chain, X-band
REX	Receiver/Exciter unit
RF	Radio Frequency
RRC	RF Receive Chain, located in the REX

RRS Reutech Radar Systems, Pty. Ltd

Rx Receive

S-Band Frequency band spanning 2 – 4 GHz

s/n Serial Number

SFDR Spurious Free Dynamic Range

SLL Side Lobe Level

SNR Signal-to-Noise Ratio

SPDT Single Pole Double Throw

STC Sensitivity Time Control

T/R Transmit/Receive

TRx Transceiver

TTL Transistor-Transistor Logic

Tx Transmit

UCL University College London, United Kingdom

UCT The University of Cape Town, South Africa

V-Pol Vertically Polarised

VGA Variable Gain Amplifier

VNA Vector Network Analyser

VSWR Voltage Standing Wave Ratio

X-Band Frequency band spanning 8 – 12 GHz

List of Symbols

A	Area
B	Bandwidth
C	Capacitance, measured in Farad, or coupling factor
E	Pulse energy
F	Noise figure
G	Gain
L	Loss
N_i	Input noise power
N_o	Output noise power
P_{1dB}	1 dB power compression point
P	Power
R	Target range
T_a	Antenna noise temperature
T_e	Equivalent noise temperature
T	Temperature
η	Antenna aperture efficiency
κ	Thermal conductivity
λ	Wavelength

ρ	Thermal resistivity
σ	Target RCS
τ	Pulse width
θ	Thermal resistance
c	Speed of light ($\approx 3 \times 10^8\ m.s^{-1}$)
f	Frequency
k	Boltzmann's constant

Chapter 1

Introduction

1.1 Project Background

The NetRAD project was a collaborative effort between the University of Cape Town (UCT) and University College London (UCL), which culminated in a number of trials which took place along coastal regions of the United Kingdom and South Africa from 2009 until 2011 [1]. These trials, or measurement campaigns, were primarily used to acquire sea clutter data for off-line processing and analysis, to further research into target detection in dense clutter environments in the littoral region.

The system itself consisted of an S-band pulse-Doppler radar in a bistatic configuration (also known as a 'netted' radar, from where the name 'NetRAD' was derived), and was produced using mostly commercial off-the-shelf (COTS) components. The transmitter and receiver were capable of functioning in both vertical and horizontal polarisation modes, subject to manual reconfiguration, and had a peak output power of 400 W which allowed for a bistatic range of 5–10 km. The system also allowed for the simultaneous capture of bistatic and monostatic measurements, allowing for direct comparison of detection performance for each configuration.

Deployment of the NetRAD system involved the use of mobile transmitter and receiver nodes, powered using generators, and with the electronic equipment placed inside the back of a vehicle to provide some protection against the elements. Antennas were mounted onto tripods, which provided a reasonably stable support

Figure 1.1: A typical deployment of a mobile node of the original *NetRAD* system is shown. The tripod-mounted antenna system can be seen, as well as the electronics and operator laptop located in the back of a vehicle.

platform, but required manual adjustment of the antenna orientation in order to acquire targets or change polarisation. A typical NetRAD deployment is shown in Figure 1.1.

Operation of the NetRAD system was found to be cumbersome, due to the manual antenna alignment process involved. Polarisation changes had to be done by physically rotating the antenna, which left room for human error and possible inconsistency between datasets. Pointing the antennas at targets was also time consuming because care had to be taken to ensure that both antennas were accurately aimed at the target, and that the desired polarisation had been configured.

Nonetheless, the system was considered successful and as a result of the NetRAD trials, a successor system called '*NeXtRAD*' was proposed. The aim of this new system was to expand the capabilities of the older NetRAD system, whilst simultaneously overcoming any shortcomings identified. It was thus decided that the new system would function as a dual-band radar operating in L- and X-band (from where the 'X' in '*NeXtRAD*' originates), and offering enhanced polarimetric capabilities. It was also proposed that the system be scalable to allow for multistatic configuration — a requirement which adds layers of complexity, particularly to the timing and synchronisation of the remote nodes of the netted system.

NeXtRAD was subsequently commissioned, with teams located at UCT and UCL working simultaneously on research and development of the system.

1.2 Project Description

The purpose of this project was to design and implement the radio frequency (RF) front end for the *NeXtRAD* system based on the system requirements derived prior to, and over the course of, the project. The RF front end incorporates all the components between the receiver/exciter (REX) subsystem and the antennas; for the purposes of this project, all ancillary components required to provide functionality (such as power supplies, timing, control and monitoring) were also required. These components were either to be procured or, where necessary, requirement specifications derived in order for them to be developed as separate projects.

When compared with the original NetRAD system, the *NeXtRAD* system is unique in that it incorporates a dual-band RF subsystem with dual-polarised transmission and polarimetric reception at higher power levels. These improvements give it the advantage of longer detection range, along with enhanced detection capabilities due to the dual-band, polarimetric datasets which will be captured. The desire to change polarisation on a pulse-to-pulse basis significantly increases the hardware costs and complexity, and solutions were thus investigated for keeping costs within the relatively modest budget allocated to a research project of this nature, whilst aiming to achieve the desired system functionality.

In order to place this project in context, Figure 1.2 shows a typical deployment of the *NeXtRAD* system along a coastline. A primary active node functions as a monostatic radar, transmitting and receiving returns from the illuminated target

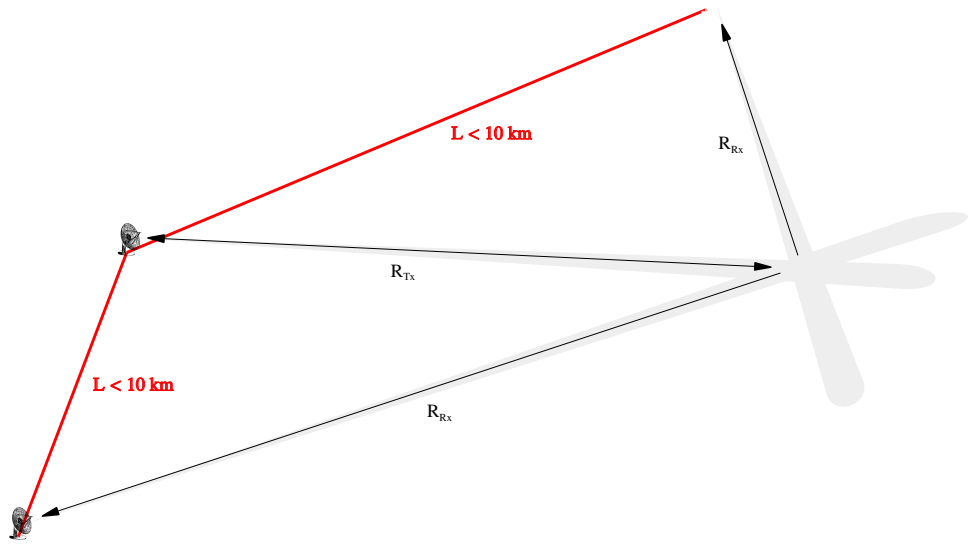

Figure 1.2: Diagram of a typical deployment of the *NeXtRAD* multistatic system. A primary active node transmits, whilst two passive nodes as well as the active node receive returns from the same target. Careful antenna alignment is necessary to ensure all nodes are viewing the same scene of interest.

or scene of interest. Two secondary passive nodes, pointed at the same target or scene of interest, receive target returns resulting from the emissions originating at the primary node. Baseline distances, L, between the primary and secondary nodes can be varied independently up to approximately 10 km (constrained by point-to-point Wi-Fi command and control links), while bistatic target ranges are intended to be up to 15 km.

The design of the antennas did not form part of this project, but their configuration is important to the overall system, and therefore taken into consideration in the design process of the RF front end. From a practical perspective, the difficulties associated with aiming a complex antenna system can be seen when considering a scenario such as that depicted in Figure 1.2, whereby multiple antennas from multiple nodes are all required to be accurately pointed at the same target area.

Design and implementation of the RF front end thus takes into account numerous other subsystems and their requirements, in order to achieve the necessary system capabilities for the *NeXtRAD* system.

1.3 Terms of Reference

The terms of reference for this project were to:

- Review the high-level system requirements as specified in Section 2.3 and perform a basic requirements analysis.
- Identify requirement specifications for the RF front end, including requirements for any other subsystems influencing or influenced by the RF front end.
- Develop a functional solution based on the requirements specifications.
- Model the functional solution using suitable system modelling software and verify that it meets the identified RF front end requirements.
- Identify suitable hardware for implementation of the functional solution, update the system model with the hardware specifications, and verify that the updated model still meets the system requirements.
- Acquire the identified hardware components and test and integrate them to create the RF front end.
- Perform final verification testing of the RF front end and provide recommendations on changes required to improve the system performance.

Beyond the scope of this dissertation, the requirement also existed to integrate the functional RF front end with the full *NeXtRAD* system, to be used for trials in a coastal environment. Whilst this integration does not feature within the dissertation, it implies that the system design and assembly be done to reliability, safety and performance standards exceeding those of conventional laboratory based systems.

Due to the high cost of certain components, it was accepted that the assembled system my not contain all of the components identified in the functional solution. For these components an alternative solution was to be implemented in order to achieve a level of functionality as close to the system requirements as possible.

1.4 Plan of Development

This dissertation presents the *NeXtRAD* RF front end subsystem design in a manner that remains mindful of the higher level system requirements for the *NeXtRAD* system. It is structured as follows:

Chapter 2 discusses the background to the project and the requirements for the RF front end, which sets the framework for this dissertation. It includes details on the proposed *NeXtRAD* architecture, as this influences the RF front end requirements and design process. The content of this chapter originates from various papers and meetings with stakeholders, where the project was road-mapped and detailed requirements were developed, based on earlier proposals.

Chapter 3 discusses the system design process for the RF front end. It starts by laying out various design constraints which had been identified. This is followed by details on the front end design and how it was derived in order to achieve the required functionality. The chapter is then concluded with modifications to the original design architecture, as a result of the high costs identified during the initial design process.

Chapter 4 evaluates the expected system performance based on the design developed in the preceding chapter. This is first done at a hardware level to confirm that the design meets the system requirements, particular when considering signal levels through the front ends. This is followed by an analysis of the signal integrity through the front end, in order to determine the expected signal-to-noise ratio (SNR) at the final intermediate frequency (IF) output of the receiver. This includes modelling and simulation of the front end using *Keysight SystemVue*.

Chapter 5 focuses on testing of the individual components used for the RF front end, as well as the final results from the integration process. This is important since the design calculations were based on the manufacturer specifications for the full operational bandwidth of the individual components, whilst testing determined the performance for the narrower operational bandwidth of the *NeXtRAD* system. Comparisons were subsequently drawn between the design predictions, system simulation and integration test results. These are discussed in Chapter 6.

The final chapter draws conclusions and makes recommendations for future work, based on deviations from the original requirement specifications, as well as potential improvements which could be accomplished.

Chapter 2

NeXtRAD Concept

2.1 System Overview

The *NeXtRAD* system is the successor to the original NetRAD system, which was jointly developed by UCT and UCL. The NetRAD system was a netted or multistatic radar system operating in the IEEE S-band. It consisted of a primary transceiver (TRx) node for transmit (Tx) and receive (Rx), and a secondary receive-only node located remotely from the primary node. Together they formed a bistatic radar configuration which was used to perform sea clutter measurements in both bistatic and multistatic mode. Additionally, polarisation could be switched between vertical and horizontal planes after manual reconfiguration of the antenna systems, allowing some degree of diversity in the measurements.

After a number of successful measurement campaigns, an upgraded system was proposed. One of the reasons for proposing a new system was to move away from the S-band frequency range, where the rapid growth of commercial Wi-Fi posed an increasing risk of undesired interference. Another reason was the desire to perform measurements in more than one frequency band simultaneously. This was to allow the capture of separate measurement datasets of a target, taken at different frequencies but at the same time. This would allow for investigations into the improvement in target identification at different frequency bands, and particularly, the effects of clutter on probability of detection of a given target in different frequency bands. Based on these and other objectives, an initial set of potential system requirements were drawn up and are detailed below:

- The system shall operate in two frequency bands, with S-band specifically excluded.
- The system shall be able to function as a multistatic system, having a single primary TRx and multiple secondary Rx only nodes. When used with only the primary node, the system functions as a traditional monostatic radar.
- All nodes shall have the same performance characteristics to ensure comparable target detection and measurement congruency.
- The remote nodes shall be linked via wireless network.
- A highly accurate timing system shall be used to synchronise all nodes and to timestamp their captured data.
- The system shall offer some level of polarimetric operation, allowing for changes in polarisation to take place without the need for mechanical reconfiguration.

A high-level graphical depiction of the system is shown in Figure 2.1.

2.2 System Measurement Goals

The *NeXtRAD* system is the next generation of the NetRAD system, thus it's primary purpose is to further the results achieved by NetRAD. Due to the change in operating frequency, the system is required to duplicate the functionality offered by NetRAD, after which further capabilities are incorporated into the system in order to perform more advanced research. Since the NetRAD system performed many sea clutter measurements, the requirement clearly existed to repeat sea clutter measurements in L- and X-bands. In the most elementary case this allows for a performance comparison between L-, S- and X-bands by making use of the *NeXtRAD* and historic NetRAD datasets.

A number of more significant achievements are, however, desired. These include, inter alia [1],[2]:

- Measurements of sea clutter in varying sea states and system geometries. This includes forward scatter measurements, which refers to measurements

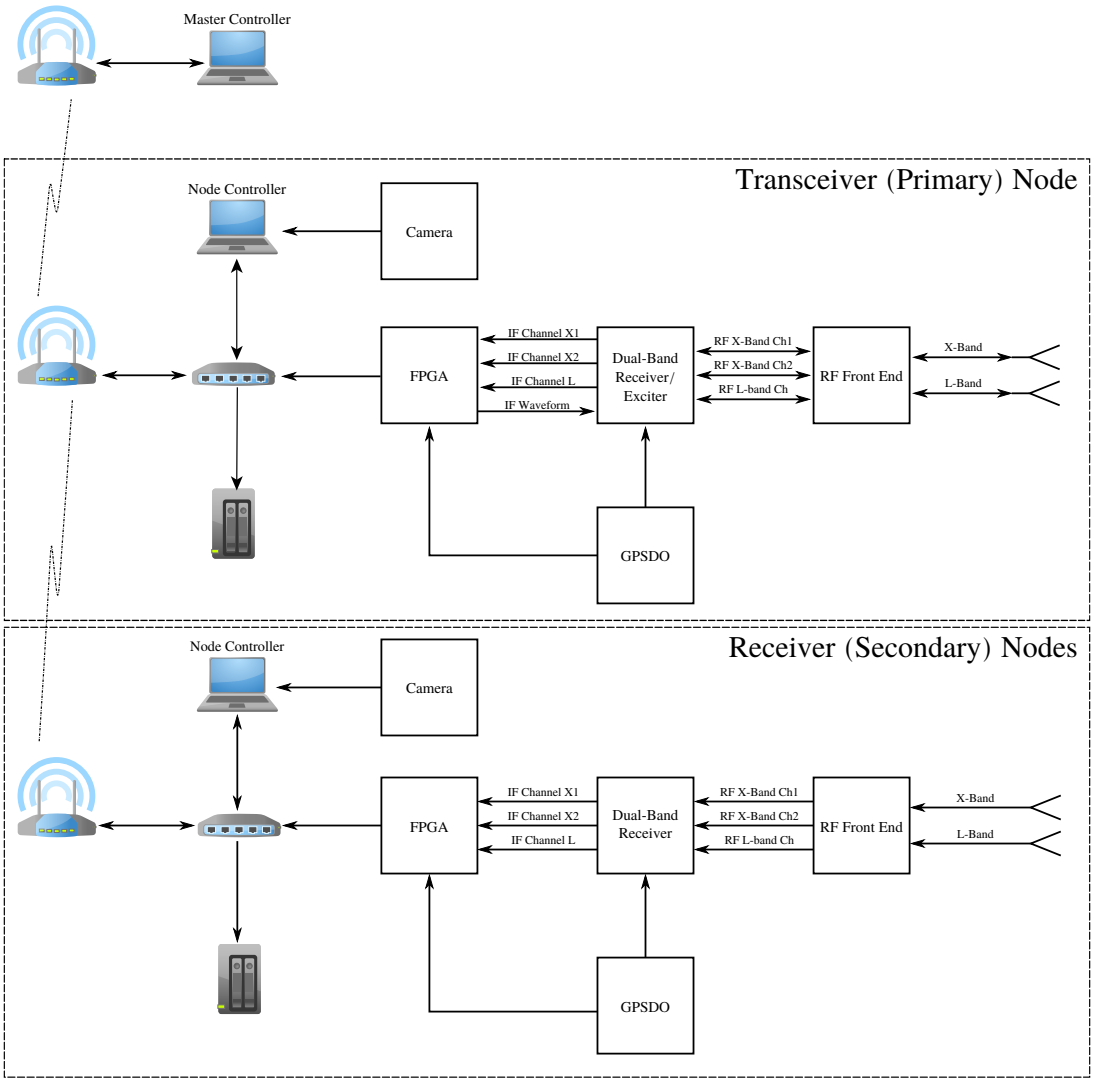

Figure 2.1: High-level system diagram showing the proposed *NeXtRAD* multistatic system configuration.

taken with a system geometry having the transmitting and receiving nodes directly opposite and pointing towards each other.

- Measurements of maritime targets such as small boats, swimmers, etc.
- Measurements of terrestrial clutter using the multistatic configuration.
- Investigations into benefits derived from the multistatic configuration at wind turbine sites. (It is well known that wind turbines pose a major problem for radar systems, particularly those used for coastal security, due to the huge radar cross section (RCS) presented by these turbines [3].)
- Trialling of adaptive waveforms for matched illumination of targets.
- Real-time tracking in the multistatic geometry.

As is evident from the above mentioned objectives, many of these will generate significant amounts of research material once measurement campaigns have been completed. Coupled with the fact that all measurements will be dual-band, multistatic (including monostatic) and polarimetric, research using the gathered data is expected to extend for many years, generating many publications and practical applications. The outcomes from these goals will thus hold both academic and practical value for future radar research and development.

Achieving these goals will require measurement campaigns conducted at various locations and under differing conditions. Careful site selection will be required and this will likely include sites used for the NetRAD trials, as well as new sites in the United Kingdom and South Africa. Factors which would have to be included during the site selection process would include:

- Site elevation (i.e. grazing angle).
- Line of sight between nodes (for Wi-Fi data links).
- Baseline between nodes.
- Presence of undesired interference (e.g. naval or navigation radar systems).

The achievement of these measurement goals will thus provide significant advancements in the results attained with the NetRAD system and allow better assessment of the potential advantages of multistatic, dual-polarised radar, through further study of the target and clutter properties to be gathered by the system.

2.3 System Requirements

A detailed list of system requirements was generated by the members of the design teams at both UCT and UCL, and these were based on the original desired system requirements, as detailed in Section 2.1, as well as additional requirements which were decided on in various meetings and work sessions. The final list of requirements was a refined version of the original list, as progress on the project often highlighted the need for changes due to requirements being unrealistic, unnecessary or too costly. The final list of requirements relating to the RF subsystems, as developed by the design teams and detailed below, sets the ground work for this dissertation.

1. The system shall operate in two frequency bands, namely IEEE L-band and X-band.

2. The L-band frequency range shall be 1.235 – 1.365 GHz, with the nominal operating frequency centred at 1.300 GHz.

3. The initial X-band operating frequency range shall be 8.475 – 8.525 GHz, but the system shall be designed to function from 8.475 – 10.500 GHz, or as close to this range as possible. The nominal operating frequency shall be centred at 8.500 GHz.

4. An instantaneous bandwidth of 50 MHz shall apply to both frequency bands, to accommodate the use of pulse compression waveforms.

5. An existing X-band high power amplifier (HPA) shall be used (*Microwave Amps* AM89-8.5S-56-56P). This HPA is designed for use in the frequency range 8.400 – 8.500 GHz.

6. A pre-selected L-band HPA (*RFHIC* RRP131K0-10) shall be acquired and used.

7. The system shall be capable of transmitting and receiving in both vertical and horizontal polarisation modes.

8. The REX shall be a *Reutech Radar Systems* (RRS) supplied subsystem. The RF front end shall be designed around the specifications and limitations of this REX.

9. The antenna system shall be designed as part of a PhD at UCL and shall be incorporated into the system at a later stage. An interim antenna system shall be designed (as a separate project) and used with the first revision of the *NeXtRAD* system.

10. All necessary ancillary components required to support the RF front end (e.g. power supplies) shall be procured, preferably as COTS components, or if necessary, designed and built.

11. A system timing plan shall ensure that hardware events occur timeously.

12. A built-in monitoring (BIM) system shall monitor critical hardware components and report on failures or non-compliance.

13. A dedicated house-keeping processor shall handle system timing and BIM.

2.4 Scope of Work

Based on the context of the project, it was necessary to develop a list of objectives and deliverables for this dissertation in order to clearly define its scope. While the focus is on the RF front end, certain subsystems and components not falling into this category had to be considered and investigated due to the interaction between them.

The scope of this project is thus:

1. Design an RF transmitter front end operating at L-band, with the ability to switch between vertically and horizontally polarised antennas on a pulse-to-pulse basis.

2. Design an RF transmitter front end operating at X-band, with the ability to switch between vertically and horizontally polarised antennas on a pulse-to-pulse basis.

3. Design an RF receiver front end operating at L-band with the ability to accept two antenna feeds (vertically and horizontally polarised) and selectively feed them into a single receive chain on a pulse-to-pulse basis. The output of the front end shall at all times comply with signal level requirements and limits as specified by the REX.

4. Design an RF receiver front end operating at X-band which accepts two antenna feeds (corrsponding to vertically and horizontally polarised returns), and feeds them to two RF receive chains. The output of the front end shall at all times comply with signal level requirements and limits as specified by the REX.

5. Propose modifications to the aforementioned front end receiver designs, if necessary, for use at the passive multistatic nodes.

6. Simulate all designed RF front ends to verify their performance.

7. Determine the timing requirements for switching, control and monitoring of all components, and document this in a timing schedule or timing diagram for implementation in a separate project.

8. Determine the power supply requirements and design and/or acquire the necessary components to power the front end.

9. Acquire all necessary hardware and build and test the RF front ends. Verify its performance with that of the model.

10. Comment on any improvements and suggest future upgrades for achieving the initial *NeXtRAD* objectives.

Chapter 3

Design Synthesis

This chapter discusses the design and selection process for the components forming the RF front end and its supporting subsystems. It examines the design constraints in order to derive a functional solution which addresses the system requirements.

This chapter focuses on the process for deriving and designing the functional system, whilst Chapter 4 discusses some of the detailed design calculations and performs an analysis of the expected system performance. Whilst they are written as two separate chapters, the contents of the chapters were generally derived concurrently and iteratively in order to develop the final solution.

3.1 Constraints

As with any project, various design constraints usually limit aspects of the design process. In the case of the *NeXtRAD* project a number of pre-existing or pre-selected components imposed constraints on the design process. Furthermore, the high cost of RF and microwave components required the design process to be mindful of the cost implications of proposed solutions and, where necessary, consider alternative designs in order to reduce cost — whilst sticking as closely as possible to the original system requirements. The various design constraints are detailed below.

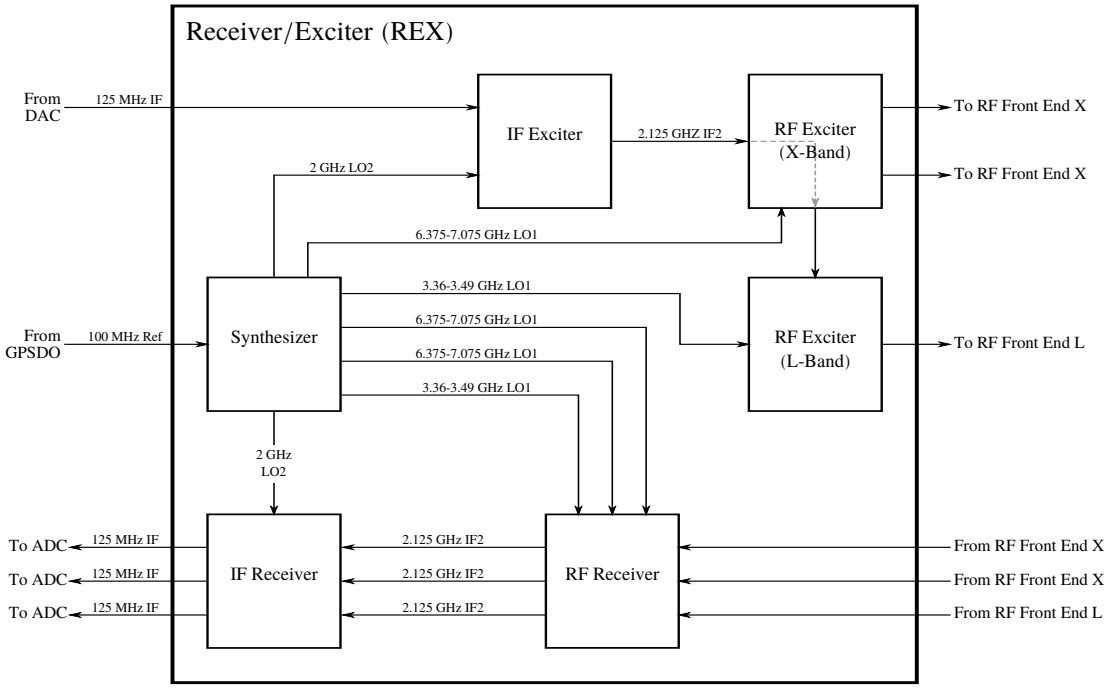

Figure 3.1: A simplified block diagram of the REX functionality and RF interfaces.

3.1.1 Receiver/Exciter Subsystem

The REX is a major subsystem of the *NeXtRAD* system, and was designed and built by RRS. Its purpose, as the name suggests, is to perform two primary functions: (1) taking a waveform (e.g. linear frequency modulated (LFM) chirp) at an IF of 125 MHz and upconverting it to the required RF, and (2) receiving the RF and downconverting it back to IF. A simplified block diagram depicting the REX functionality is shown in Figure 3.1.

The design was based on an existing RRS system, with only minor specification changes requested as per the *NeXtRAD* requirements. These changes focused on specifications such as phase noise, system bandwidth, control and programming interfaces, etc. while input and output signal levels remained as per the original RRS product specifications. It was therefore required that all input and output signals interfacing with the REX be designed to meet these specifications.

From the REX specifications [4], the following requirements and constraints were imposed on the RF front end:

1. L-band Tx front end input power level: 16 dBm ±2 dB.

2. X-band Tx front end input power level: 0 dBm ±2 dB.
3. L- and X-band Rx front end nominal output power level: 0 dBm.
4. L-band Rx front end absolute maximum output power level: $\leq$ 10 dBm.
5. X-band Rx front end absolute maximum output power level: $\leq$ 20 dBm.
6. L-band operational bandwidth: 1.235 - 1.365 GHz.
7. X-band operational bandwidth: 8.500 - 10.500 GHz.
8. IF and RF instantaneous bandwidth: 50 MHz.
9. L- and X-band Tx front end input VSWR: $\leq 1.9 : 1$.
10. L- and X-band Rx front end output VSWR: $\leq 1.9 : 1$.

3.1.2 Digital Back End

The digital back end consists of a Virtex-6 field-programmable gate array (FPGA), mated with a Pentek Cobalt 71620 analogue front end consisting of three 200 MHz analogue-to-digital converters (ADCs), and two 800 MHz digital-to-analogue converters (DACs). One of these DACs drive the IF input on the REX, while the ADCs accept the IF outputs for digitisation. The full scale input level of the ADC dictates the optimal and maximum acceptable power levels of the REX IF output. Similarly, the DAC output power level should comply with the requirements of the REX IF input. From the Pentek user manual [5] it was found that the full scale input power level of the ADC was +8 dBm, and the full scale output of the DAC +4 dBm. Both of these ports were transformer coupled with a transformer insertion loss of 0.58 dBm. As a result of this, the Pentek analogue signal levels were determined to be:

- Maximum acceptable full scale analogue input level (maximum permissible REX output): 8.58 dBm
- Maximum achievable full scale analogue output level (maximum possible REX input): 3.42 dBm

These figures assume negligible cable losses between the REX and Pentek analogue ports.

Examining the REX IF output specifications [4], it was found to have a 1dB output compression point of +7 dBm, whilst the maximum output power level in limiting mode was $\leq +13.5$ dBm. This meant that the required full scale output of 8.58 dBm would not be achievable within the linear region of the REX, and that precautions needed to be taken to prevent overloading the ADC when the REX output enters compression. Furthermore, the REX IF input specifications required a signal level of +5 dBm ±2 dB, which meant that the full scale analogue output from the Pentek was below this level. Use of reduced IF drive levels could be compensated for in the RF front end design, but this was likely to have negative effects on the REX specifications, such as reducing spurious free dynamic range (SFDR), increasing harmonic levels, etc.

Addressing the Pentek output power levels required thorough testing of it in order to determine the necessary steps to be taken, but this was outside of the scope of this project and was to be addressed by a Masters research project undertaken by another student. It was therefore assumed that DAC drive levels fell within the specified requirement of +5 dBm ±2 dB for the rest of this dissertation.

3.1.3 L-Band High Power Pulse Amplifier

The selection of the L-band pulse HPA was done prior to commencement of the RF front end design process. Its selection was based on its compact size, high peak output power level and excellent power-to-cost ratio. Being a Gallium Nitride (GaN) based amplifier, it also had the added benefit of high efficiency and high power density, when compared to other HPA architectures [6].

Since the L-band HPA was a pre-selected item and did not form part of the front end design and selection process, its specifications were considered constraints since the design and selection of the remaining L-band transmitter front end components was influenced by the HPA specifications.

The datasheet [7] for the *RFHIC* manufactured L-band HPA (model number RRP131K0-10) contained all the relevant specifications but did not include detailed application notes. Previous experience with this specific amplifier model revealed a number of potential usage pitfalls. The design requirements and constraints for the transmitter front end were thus derived from the specifications in [7], as well as the lessons learned from previous experience and verified during lab tests (see Section 5.1.3.1).

For the L-band HPA RF interfaces we have the following requirements:

1. Nominal input pulse power level: 7 dBm
2. Maximum input pulse power level: 10 dBm
3. Typical peak output power level: 60.79 dBm (1 200 W)
4. Maximum pulse width: 500 μs
5. Maximum duty cycle: 20 %
6. Maximum input VSWR: 1.5:1
7. Maximum output VSWR: 1.5:1

It is critical to note that the datasheet specifies a typical output power level of 1 200 W, with no maximum power level specified. A figure of 1 500 W (61.76 dBm) was chosen to provide a safety margin due to prior experience indicating a peak output power level exceeding the specified typical value. For the calculations done in this report, the lower value of 1 200 W is used for general performance analysis, whilst the value of 1 500 W is used where a higher than expected power level could have adverse effects on the system, such as damaging other component.

In addition to the RF interface requirements, the power, control and monitoring systems had their own requirements and specifications which needed to be considered during the design phase. These are detailed below.

Power requirements:

1. Primary supply voltage: 50 ± 2.5 VDC
2. Secondary supply voltage: 12 ± 0.6 VDC
3. Primary supply current (peak): 80 A
4. Primary supply current (average): 16 A
5. Secondary supply current (average): 0.2 A

Control and monitoring:

1. Shutdown control input signal: TTL 0 V On, TTL 5 V Off
2. Standby control input signal: TTL 0 V On, TTL 5 V Off
3. Peak power monitor output range: 0–5 V
4. Junction temperature monitor output range: 0–5 V
5. Power-up sequence: Secondary supply (12 VDC) followed by primary supply (50 VDC)
6. Power-down sequence: Primary supply (50 VDC) followed by secondary supply (12 VDC)

The power sequencing information was not detailed in the datasheet, but previous experience revealed that the HPA locked up in an undesired state if the primary supply was applied prior to the secondary supply during the power-up sequence. Since the 50 V supply is used to bias the field-effect transistors (FET), it was theorised that the 12 V supply is used to power the internal electronics. This would suggest that the power-down sequence should be the reverse of the power-up sequence, in order to ensure that the high voltage is removed from the HPA prior to disabling the control circuitry. This would prevent any potential damage to sensitive low voltage semiconductors. Whilst there was no confirmation that this theory was correct, it was decided to settle on this conclusion and specify this power-down sequence as a requirement. This theory was supported by the power sequencing provided in the X-band HPA datasheet.

The final constraints which needed to be considered were those for thermal management — constraints which are critical for ensuring reliability and longevity of the HPA.

Thermal limits:

1. Maximum junction temperature: 225 °C
2. Maximum flange temperature: 75 °C

3.1.4 X-Band High Power Amplifier

The *Microwave Amps* class A X-band HPA (model number AM89-8.5S-56-56P) was an existing unit belonging to UCL. Whilst the bandwidth of this HPA did not match perfectly with that of the REX, it was decided to still make use of this unit due to the high cost of alternative X-band solid state HPAs (circa USD100k upwards). While the International Telecommunication Union (ITU) X-band radar frequency band covers 8.50 – 10.68 GHz [8], the HPA operational bandwidth was 8.40 – 8.50 GHz and the REX operational bandwidth 8.50 – 10.50 GHz. Thus the X-band operating frequency was limited to 8.5 GHz as it was the only common frequency between the REX and HPA, and coincided with the start of the ITU radar band. The instantaneous radar bandwidth of 50 MHz meant that actual spectrum usage would be 8.475 – 8.525 GHz, which is 25 MHz below the ITU band and 25 MHz above the HPA bandwidth, but this was unfortunately unavoidable.

The requirements for the X-band HPA interfaces were as follows [9]:

1. Nominal input pulse power level: 3 dBm
2. Maximum input pulse power level: 15 dBm
3. Typical peak output power: 56.5 dBm (447 W)
4. Maximum pulse width: unspecified
5. Maximum duty cycle: 10 %
6. Maximum input VSWR: 1.5:1
7. Maximum output VSWR: 1.5:1

The datasheet did not specify the nominal input power level, so the value of +3 dBm was assumed based on the minimum small signal power gain $G = 53$ dB, and the minimum 1dB gain compression point $P_{1dB} = 55$ dBm. The 1dB compression point is considered the maximum safe and practical operating point for an RF amplifier [10], thus at P_{1dB} the ideal linear output would be 56 dBm, and with a gain of 53 dB the input power level required would be $P_{in} = 3$ dBm. This was subject to verification through lab testing.

Power requirements:

1. Primary supply voltage: $+12 \pm 0.1$ VDC
2. Secondary supply voltage: -10 ± 2 VDC
3. Primary supply current (peak): 140 A
4. Secondary supply current (peak): 0.2 A

Control and monitoring:

1. Standby control input signal: TTL 5 V On, TTL 0 V Off
2. Peak power monitor output: 5 V(nom.)
3. Over temperature alarm output: +12 V
4. Power-up sequence: Secondary supply (−8 VDC) at least 1 μs prior to primary supply (+12 VDC)
5. Power-down sequence: Primary supply (+12 VDC) followed by secondary supply (−8 VDC)

3.1.5 Antennas

The antennas used for the system do not impose true constraints on the front end design, but they are included here due to the fact that they have some influence on its implementation and the final performance of the radar. The initial system architecture proposed a complex antenna system which would be developed as part of a PhD. Since no progress on these antennas had occurred, a set of interim antennas were proposed and developed as two separate MSc projects. Some of the important requirements for the antenna design were:

- dual polarisation capability
- high power handling (1500 W at L-band and 450 W at X-band)
- the ability to be tripod mounted
- capable of withstanding windy conditions

A half power beamwidth (HPBW) of 10° was settled on for both antennas, even though a narrow beam, high gain X-band antenna would have been desirable to compensate for the lower peak power of the X-band HPA.

The L-band antenna design was based on a prime focus parabolic reflector antenna. A 2.45 GHz Wi-Fi reflector antenna was modified, with the aid of extensive calculations and *FEKO* simulations, in order to achieve an antenna system which would operate at 1.3 GHz. A circular waveguide was used for the feed, as this was found to be the optimal feed type for the dual-polarisation requirement. Two probes were positioned orthogonally in the feed, in order to produce vertically and horizontally polarised emissions. Wind loading on the reflector was reduced through the use of wire mesh instead of a solid reflector surface. Details on this antenna can be found in [11].

For the X-band antenna, an conical horn was selected. A circular waveguide feed was also used, with probes positioned orthogonally in order to achieve dual polarisation. Manufacturing limitations meant that the final product deviated slightly from the design, due to the fact that the aluminium horn had to be formed by bending the sheet metal, rather than smoothly rolling it. The end result was still found to be satisfactory, when compared with the simulation results. Further details on this antenna design can be found in [12].

A summary of the antenna specifications, as tested by the designers [11],[12], is shown in Table 3.1. The full bandwidth of the antennas is not clear, but in both cases exceeds the 50 MHz *NeXtRAD* instantaneous bandwidth. Figure 3.1 shows both antennas installed onto a single tripod, as they are intended to be used in the system.

In the event of a narrow beamwidth X-band antenna eventually being implemented, Figure 3.3 shows the effect of the narrow beam X-band main lobe overlaid on the wide beam L-band main lobe. Misalignment of these two antennas could result in a target being illuminated at one frequency band but not at the other, defeating the purpose of the system. For the initial antenna designs presented here, misalignment has less of an effect on the system due to the 'wide' beamwidth at both bands, but careful alignment of the two antennas was still done to ensure accurate dual-band target illumination. This alignment included ensuring that optical equipment (video camera and rifle scope), fitted to the pedestal to aid in target acquisition, was aligned with the electrical boresight of the antennas.

Figure 3.2: The L-band reflector antenna and X-band conical horn antenna are shown installed on a single pedestal and aligned to point in the same direction.

Table 3.1: Critical specifications of the dual-polarised antennas designed for the NeXtRAD system.

	L-band	X-band	Units
Aperture Type	Parabolic Reflector	Conical Horn	–
Centre Frequency	1.3	8.5	GHz
Gain	19.65	23.37	dBi
HPBW (Azimuth)	12.4 (V-Pol) 13.9 (H-Pol)	10.4 (V-Pol) 9.1 (H-Pol)	°
HPBW (Elevation)	20.0 (V-Pol) 19.6 (H-Pol)	9.2 (V-Pol) 9.9 (H-Pol)	°
SLL (Azimuth)	-16.4 (V-Pol) -17.4 (H-Pol)	-36.0 (V-Pol) -24.0 (H-Pol)	dBi
SLL (Elevation)	-15.8 (V-Pol) -15.7 (H-Pol)	-23.6 (V-Pol) -31.9 (H-Pol)	dBi
Bandwidth	<100	>50	MHz

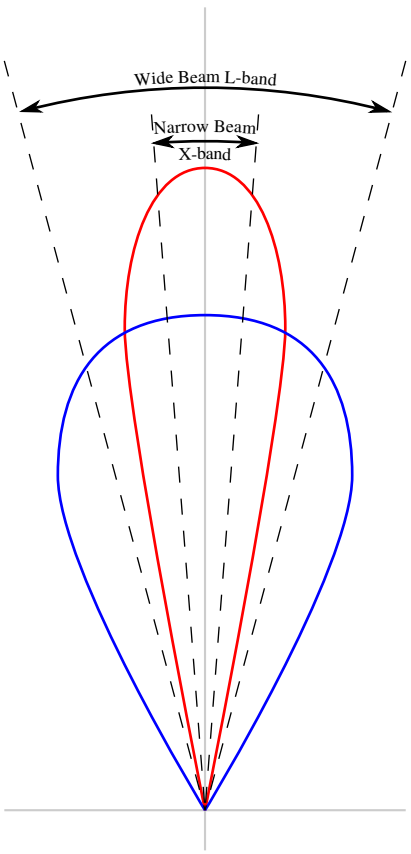

Figure 3.3: Wide beamwidth L-band and narrow beamwidth X-band antenna main lobes overlaid to illustrate the importance of correctly aligning the antennas with each other.

Table 3.2: Pulse width (in microseconds) as a function of PRF and duty cycle.

Duty	**Pulse Repetition Frequency (kHz)**									
(%)	1.0	2.0	3.0	4.0	5.0	6.0	7.0	8.0	9.0	10.0
1.0	10.0	5.0	3.3	2.5	2.0	1.7	1.4	1.3	1.1	1.0
2.0	20.0	10.0	6.7	5.0	4.0	3.3	2.9	2.5	2.2	2.0
3.0	30.0	15.0	10.0	7.5	6.0	5.0	4.3	3.8	3.3	3.0
4.0	40.0	20.0	13.3	10.0	8.0	6.7	5.7	5.0	4.4	4.0
5.0	50.0	25.0	16.7	12.5	10.0	8.3	7.1	6.3	5.6	5.0
6.0	60.0	30.0	20.0	15.0	12.0	10.0	8.6	7.5	6.7	6.0
7.0	70.0	35.0	23.3	17.5	14.0	11.7	10.0	8.8	7.8	7.0
8.0	80.0	40.0	26.7	20.0	16.0	13.3	11.4	10.0	8.9	8.0
9.0	90.0	45.0	30.0	22.5	18.0	15.0	12.9	11.3	10.0	9.0
10.0	100.0	50.0	33.3	25.0	20.0	16.7	14.3	12.5	11.1	10.0

3.1.6 Pulse Parameters

This section lists the radar pulse parameters derived from the *NeXtRAD* requirements and the various aforementioned constraints. Whilst these parameters do create some design constraints, they are provided here mostly for reference and completeness. The use of pulse compression means that the bandwidth is fixed at 50 MHz, and therefore is not affected by the pulse widths used in the system.

The first set of parameters are obtained from the pulse repetition frequency (PRF) and duty cycle (DC). Using the PRF, we take the inverse to obtain the pulse repetition interval (PRI), and then use the duty cycle to determine the pulse width, τ. Mathematically:

$$\tau = \frac{1}{PRF} \times DC$$

For a PRF in the range 1 000 Hz to 10 000 Hz and a duty cycle between 1 % and 10 %, we get a corresponding range of pulse widths spanning from 1 μs to 100 μs. Table 3.2 shows the full list of pulse widths for each combination of PRF and duty cycle. In general, the pulse width is likely to be around $\tau_{typ} = 10\,\mu$s, but all possible combinations need to be considered as they will influence the design requirements.

We also consider the first blind zone as a function of pulse width, as this plays a role in the timing requirements for the monitoring and control. The blind range is the period during which the radar is transmitting and is unable to see target

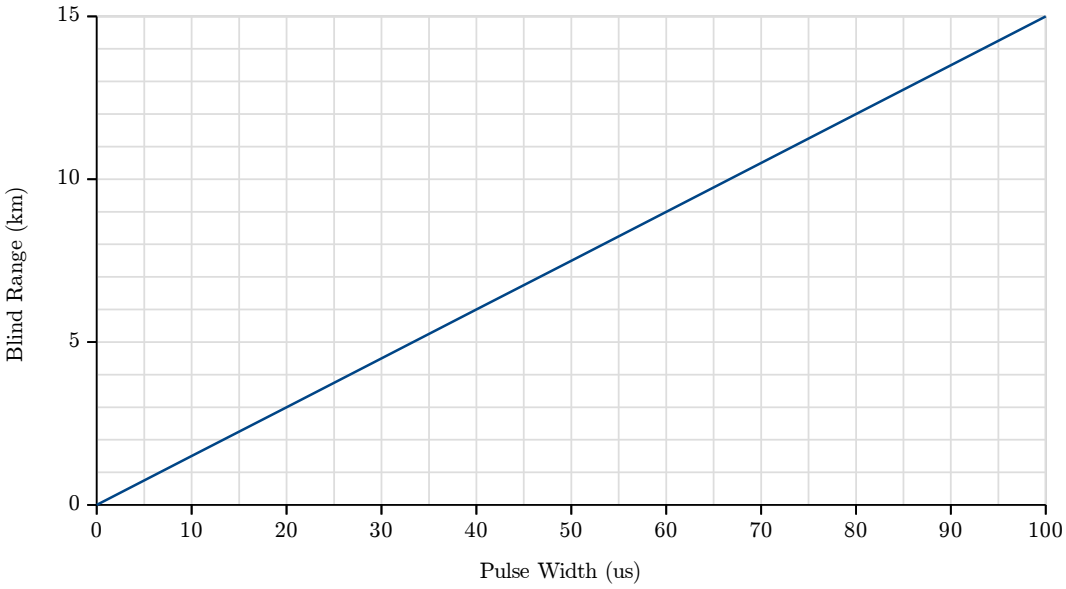

Figure 3.4: Minimum blind range vs pulse width.

returns [13]. This range is a function of the pulse width, τ, and is calculated as:

$$R_{blind} = \frac{c\tau}{2}$$

Note that this applies only for the monostatic case, so in the *NeXtRAD* system this implies a blind range for the primary node only. In the case of the secondary nodes, blind ranges do not exist since these passive nodes are constantly 'listening' for target returns and do not radiate their own pulses. The blind range as a function of pulse width is depicted in Figure 3.4. For our typical expected pulse width of $\tau_{typ.} = 10\,\mu$s, we have a blind range of $R_{blind} = 1\,500\,$m.

3.2 Design Process

In this section we discuss the RF front end design which meets the system requirements and provides the required functionality to the system. Trivial design details are omitted, but some justification or explanation is given for design choices where this is considered important.

The design process needs to take into account the entire analogue signal path, shown in Figure 3.5. This starts at the DAC, then passes through the exciter, transmitter, the natural environment and target, the receiver, and finally termi-

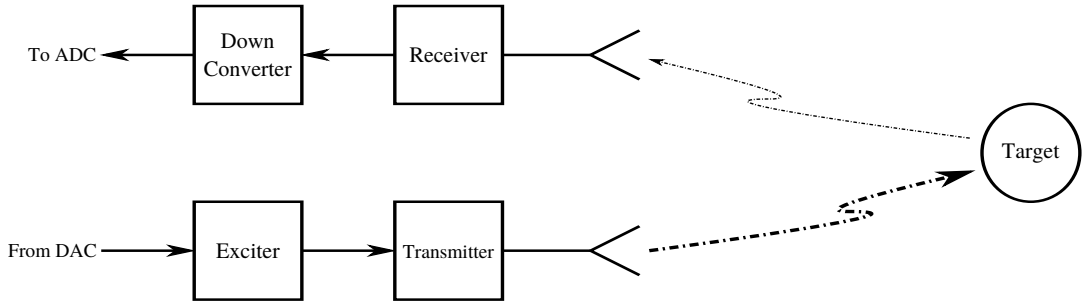

Figure 3.5: Block diagram showing analogue signal path for a generic radar system.

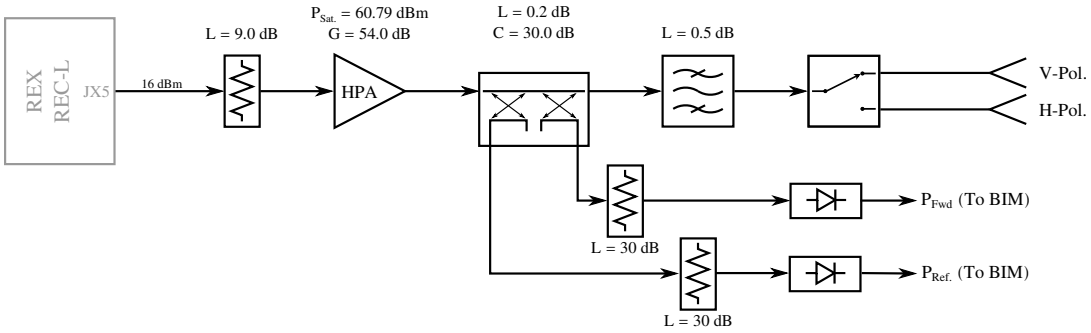

Figure 3.6: L-band Transmitter Front End

nates at the ADC. Thus, while the transmitter and receiver front ends are in some ways separate subsystems, they cannot be designed in isolation as they all form part of the signal path. The same applies to the supporting subsystems of the RF front end, such as power supplies, timing and control, monitoring, etc.

3.2.1 L-Band Transmitter Front End

In developing the L-band transmitter front end, depicted in Figure 3.6, the relevant design constraints discussed in Section 3.1 were used as the starting point. Specifically, these were the output specifications of the REX, and the input and output specifications of the L-band HPA.

A 9 dB attenuator was placed between the REX and HPA in order to reduce the REX output power level from +16 dBm to +7 dBm, as required by the HPA. This has the added advantage of improving the VSWR at the output of the REX, as any reflections at the HPA input are attenuated twice before arriving back at the REX output. This results in a VSWR $\leq$ 1.3:1, which is well below the specified

limit of 1.9:1 for the REX.

The dual-polarisation requirement could be achieved in a number of different ways. The first requirement for achieving this is to ensure a suitable antenna system is used. This can consist either of two separate antenna apertures, one with a vertically orientated feed and the other with a horizontally orientated feed, or a single antenna aperture with both vertical and horizontal feeds located at the focal point. Both of these configurations have pros and cons associated with them, e.g. the separate apertures provide better isolation from each other, but at the cost of a larger physical system configuration and component count, making set-up and operation more complex, and subjecting the antenna mounts to additional wind loading. Whilst the antennas are being developed as a separate project, the requirements for feeding the antenna terminals remain the same regardless of the configuration settled on.

To address the dual-polarised transmitter requirement, a separate antenna feed is required for each polarisation plane, regardless of the final antenna configuration settled on. Since the system is only required to transmit in one polarisation plane at a time, this is achieved with the placement of a single pole double throw (SPDT) RF switch within the transmitter front end path, allowing the feed to be switched to the required antenna when necessary. This switch was placed on the high power side of the RF front end, directly before the antenna. Subsequently, it was necessary that this switch be capable of handling peak power levels of at least 62 dBm, in accordance with the HPA power rating.

For pulse-to-pulse polarisation switching to occur, the maximum allowable switching time is determined by the PRF and duty cycle. The switching speed therefore needs to be less than the inter-pulse period at the maximum expected PRF. For the *NeXtRAD* system, $PRF_{max} = 10\,\text{kHz}$ and the maximum possible duty cycle is 10 %, as constrained by the X-band HPA. This gives a $PRI = 1/PRF = 100\,\mu\text{s}$ and at 10 % duty cycle that translates to an inter-pulse interval of $90\,\mu\text{s}$. Hence the switching speed was required to be less than $90\,\mu\text{s}$.

This switching speed exceeds the limits of typical mechanical RF switches or relays [14] and would quickly exceed the actuator lifespan [15] in this application. A solid state RF switch (e.g. PIN diode switch) was therefore necessary, as it offers significantly higher switching speeds and eliminates the possibility of mechanical failure [16]. This fulfils the requirement for polarisation switching.

Whilst the above mentioned components allowed for the basic functional requirements of the transmitter front end to be achieved, the design was suboptimal since it failed to mitigate the effects of a number of undesirable scenarios. Specifically, it was necessary to account for possible: (1) failure within the transmitter chain and, (2) unwanted spurious and out of band emissions.

For the former scenario it was necessary to consider the path between the HPA and the antenna, and the effects of a mismatch resulting from a cable failure or similar undesirable event along this path. In a worst-case scenario, this could result in a full-power reflection back into the output port of the HPA (0 dB return loss or an infinite VSWR), resulting in damage to sensitive components. Examination of the HPA datasheet, however, indicated the presence of internal isolators able to handle full-power reflections at the output port. This eliminated the need for an external isolator at the HPA output. This was also important since antenna impedance bandwidth is typically specified as the frequency range over which the VSWR $\leq$ 2:1 [17], which implies the need for the HPA output port to handle a VSWR of up to 2:1 under normal operating conditions, depending on the final antenna performance figures.

A dual directional coupler was added between the HPA output and the antenna to provide BIM for the transmitter. The HPA has an internal BIM system for reporting back on power levels and temperatures, but is primarily geared towards providing feedback on the output performance of the HPA. The addition of the dual directional coupler and power detectors allowed for monitoring of the actual transmitted and reflected power levels of the transmitter, allowing for more comprehensive performance analysis, including the identification of failure conditions external to the HPA itself — such as the case of a damaged antenna feed cable.

Finally, spurious signals within the transmitter chain needed to be accounted for. This was especially important with the high power levels which are to be transmitted, since the risk of interfering with systems operating in other frequency bands increases. Furthermore, spectrum regulatory authorities would require that emissions are compliant with the rules for systems operating in the ITU radar bands. To mitigate this problem, a filter was added to reject out of band signals and harmonics. The requirements for this filter, to be designed by an undergraduate student, were specified as:

- Passband: 1.235 – 1.365 GHz

- Passband Insertion Loss: $< 0.5\,\text{dB}$
- Passband Ripple: $< 0.1\,\text{dB}$
- Passband Return Loss: $> 20\,\text{dB}$
- Cut Off Frequency ($-3\,\text{dB}$): $1.2\,\text{GHz}$ and $1.4\,\text{GHz}$
- Power Handling Capability: $\geq 62\,\text{dBm}$ peak, $\geq 52\,\text{dBm}$ average.
- Filter Order: n ≥ 5

This filter was placed between the coupler and polarisation switch in order to filter the output of the HPA.

3.2.2 L-Band Receiver Front End

When designing the receiver front end for a radar system we need to design for high dynamic range due to the unpredictable target returns, and the significant effect that varying target range has on the received power due to the $1/R^4$ factor in the radar equation [13]. For the case of a very weak signal close to the noise floor, we need to make use of a low noise, high gain amplifier, as is typical for the front end of any RF receiver system [18]. This allows us to maximise the SNR in the analogue receive chain, after which further improvements can be achieved using pulse integration techniques once the signal has been digitised [13].

The combined L-band Tx and Rx front end is shown in Figure 3.7. Focussing on the Rx front end, selection of the correct low noise amplifier (LNA) is critical as it is usually the first component in the receive chain, and sets the noise figure, F, for the entire receiver. This is evident when analysing the equation for the noise figure of a cascaded system, given by [18]:

$$F = F_1 + \frac{F_2 - 1}{G_1} + \frac{F_3 - 1}{G_1 G_2} + \cdots \tag{3.1}$$

where F is the cascaded noise figure, F_i is the noise figure of the ith component and G_i is the gain of the ith component (all values in linear units). From this it is evident that the gain and noise figure of the first stage dominates the cascaded noise figure. By selecting a suitable high gain low noise amplifier for the front end we can minimise the receiver noise figure, as required. Thus for the Rx front end

shown in Figure 3.7, a *Mini-Circuits* LNA (part number ZX60-P162LN+) was identified as a good candidate, having $G = 20.5\,\text{dB}$ and $F = 0.56\,\text{dB}$ at 1.3 GHz.

For the path between the LNA and the REX, the limiter and attenuator were added to ensure the input to the REX could not exceed the $P_{in} \leq 10\,\text{dBm}$ limit. For the selected LNA the datasheet specified $P_{1dB} \approx 20\,\text{dBm}$. Since there was no mention of the saturated output power level, it was assumed that the peak output voltage would approach, but not exceed, the DC supply voltage of the LNA. For the typical 4 V supply specified in the datasheet, we calculate the saturated output power as:

$$P_{sat} = \frac{V_{rms}^2}{Z_{in}} = \frac{(V_{pk}/\sqrt{2})^2}{Z_{in}} = \frac{(4/\sqrt{2})^2}{50} = 0.16\ W = 22.04\ dBm$$

which corresponds with the general rule of thumb of $P_{sat} \approx P_{1dB} + 2\,\text{dB}$ [10].

Using this value for P_{sat}, a total of 12 dB attenuation would be required to ensure that the REX would not get damaged if the LNA were saturated. This would mean that small signals would also be attenuated, resulting in the signal at the ADC falling well below the full-scale range of the ADC. Thus to avoid this problem a limiter with leakage rating of $P_{out} = 11.5\,\text{dBm}$ was placed directly after the LNA, followed by a 4 dB attenuator. The benefit of this configuration is that when the output of the LNA is small (say less than 0 dBm) the limiter is inactive and the signal is attenuated by the limiter insertion loss (0.2 dB) and the 4 dB attenuator. On the other hand, when the input signal is large the limiter maintains it at 11.5 dBm and the attenuator brings it down another 4 dB to prevent damage to the REX RF receive chain (RRC).

For a pulsed radar system we have the options of using a single antenna for both transmitting and receiving, since the system never performs both functions at the same time; or one antenna for transmitting and a separate antenna for receiving — which provides better isolation. Due to the preference for a minimalistic mechanical configuration for the *NeXtRAD* system, the single-antenna configuration was selected.

The use of a single antenna requires a duplexer to control the path of the Tx and Rx signals in the front end. This is typically achieved with a passive device such as a circulator, or alternatively an actively controlled transmit/receive (T/R) switch [19]. Whilst the T/R switch provides superior isolation when compared with the circulator [20], the switching speed and power requirements for the system

meant that a circulator had to be settled on instead, due to its low cost. This was also acceptable since the pulse train was to be formed by using a pulsed waveform and shutting down the HPA between pulses, and not by switching the T/R switch between Tx and Rx paths whilst outputting a continuous wave (CW) signal from the HPA — the latter being a technique which is often employed but would necessitate an isolation figure of about 80 – 100 dB in order to avoid masking target returns due to leakage from the transmitter into the receiver [21].

The use of the circulator and single antenna means that high power levels in the Rx chain can result from three possible mechanisms: (1) coupling of the high power transmission within the circulator, (2) reflections at the antenna port during transmission, and (3) high power emissions entering the antenna from the environment. Handling of these high power levels is done using a receiver protector — in this case a limiter — capable of handling the full transmitter output power level (60.79 dBm) for a duration equal to the maximum system pulse width (100 μs), in order to protect the receiver in the event of a broken or disconnected antenna feed cable (which would result in a full-power reflection entering the receiver). External sources of high power entering the receiver are harder to protect against as their power levels are unpredictable, and therefore only the transmitter power level is accounted for. Placement of the limiter before the LNA therefore provides the necessary protection to the sensitive LNA, but with the trade off of an increase in receiver noise figure.

One of the most important components in the L-band Rx front end is the polarisation switch. This is necessary because there is only one L-band RF receiver input on the REX, meaning that in order to capture a polarimetric dataset we need to switch between vertical and horizontal polarisation on a pulse-to-pulse basis in order to synthetically populate the polarisation matrix. In order to accomplish this we include the same solid state switch used in the Tx front end, placed between the circulators and the limiter. Finally, a filter identical to the one used in the Tx front end was placed between the switch and limiter in order to reject out-of-band emissions which would otherwise enter the receiver.

3.2.3 X-Band Transmitter Front End

For the X-band front ends we are faced with the problem of increased component cost, insertion and propagation losses, along with decreased power handling capa-

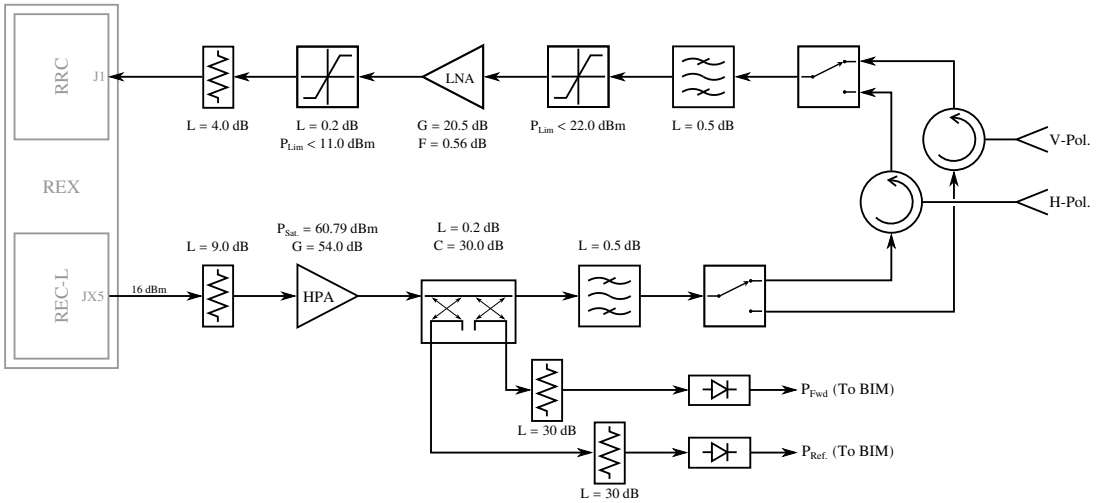

Figure 3.7: L-band Receiver Front End

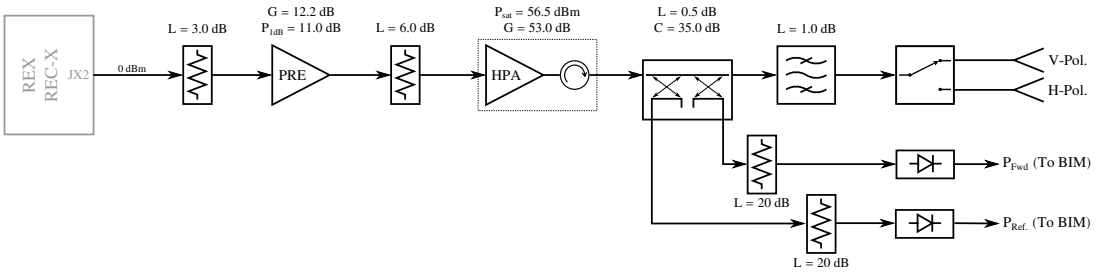

Figure 3.8: X-band Transmitter Front End

bilities. This creates a complication since received power $P_R \propto \lambda^2$, where $\lambda = c/f$ [13], which makes it desirable to increase the power level accordingly with frequency, and keep system losses to a minimum. With the X-band HPA having been preselected, the only parameter which could be controlled to some extent was the system losses. An increase in antenna gain resulting from the use of narrower beamwidth antennas would provide an improvement in detection range, but at the expense of differing angular resolution between the two operating bands, resulting in some inconsistency between the scene of interest in the two bands. However, for the initial system setup and for all work done in the remainder of this report, the 10° beamwidth antenna described in Section 3.1.5 will be used.

For the X-band transmitter front end shown in Figure 3.8, the placement of a pre-amp between the REX and the HPA was necessary to increase the 0 dBm output of the REX to the required +3 dBm input level for the HPA. Since the selected pre-amp had a gain of 12.2 dB, the input and output was padded in order to bring the signal level down to the required magnitude, whilst improving the

REX output VSWR.

As with the L-band HPA, the X-band unit included an isolator to handle full power reflections at the output port. This isolator is located external to the HPA and is therefore represented separately on the block diagram. It was assumed that the HPA output power rating included the insertion loss of the isolator, since they were supplied together.

Internal BIM is also included in the HPA, but an external coupler followed by attenuators and detector diodes on the coupled ports was used in order to obtain more comprehensive power monitoring of forward and reflected power. The combination of 35 dB coupling and 20 dB attenuator keeps the peak power level close to 0 dBm at the detector diodes, which is well below the 20 dBm limit of the *Aeroflex* ACSP-2504 diodes — surplus components in the lab which were identified as being suitable for the task.

For the polarisation switch we had the same 90 ns maximum switching time as required for the L-band system in order to switch on a pulse-to-pulse basis. This meant that a solid state switch was again selected, but with lower peak power requirement due to the lower X-band HPA output power rating.

For the filter we follow the same principles as with the L-band one. Due to the fact that it was decided by the *NeXtRAD* team that the filter design be allocated as an undergraduate student project, the requirements are somewhat relaxed since filtering is also present within the REX. Low-level design decisions were left to the undergraduate student and supervisor, but high-level specifications which were required to be met were:

- Passband from 8.45 – 8.55 GHz minimum. The preferred passband would be 8.45 – 10.5 GHz, but this is not expected to be achievable in the time allocated for completion of a final year undergraduate project.
- Insertion loss as low as possible ($\leq$ 1 dB recommended).
- Passband ripple $\leq$ 0.5 dB, but should aim to make this as low as possible.
- Out of band rejection: No specific requirement, but the use of a 5th order or higher filter is recommended.
- Power Handling Capability: $\geq$ 58 dBm peak, $\geq$ 48 dBm average.
- N-type coaxial connectors.

- Absorptive configuration highly desirable.

The intention was that once these filters were built and tested they would be evaluated to determine their suitability and, if necessary, redesigned to improve on any shortcomings. This does not form part of this dissertation.

3.2.4 X-Band Receiver Front End

For the X-band receiver front end, shown in Figure 3.9, the same basic design as the L-band front end was followed, with the primary difference being the fact that the REX has two independent receiver channels at X-band, making it necessary to duplicate the front end design for each channel. This eliminated the need for a switch to select the polarisation since both v-pol and h-pol are received by the REX simultaneously, allowing for true polarimetric measurement.

For the Rx filters, the same filter design as for the Tx front end was used. Since the filter is the first component in the receive chain (after the antenna) we can see the importance of obtaining the lowest possible insertion loss so as to keep the noise figure contribution to a minimum. This is compounded by the the insertion loss of the limiter which fits between the filter and LNA.

For the LNA a number of COTS options were considered but a bespoke unit was settled on which was designed and developed by *Amplitech Inc.* in accordance with our requirement specifications, namely:

- Operating frequency: 8.5 – 10.5 GHz.
- Noise figure: ≤ 1 dB
- Gain: ≥ 30 dB
- Gain flatness: ± 1.5 dB
- Output P_{1dB}: ≥ 15 dBm
- P_{in}: ≤ 19 dBm
- Input and output VSWR: ≤ 2.0:1

Since the LNA had a specified $P_{1dB} \geq 15$ dBm, and the maximum input power level for the REX on the X-band receiver channels was 20 dBm, it was reasonable

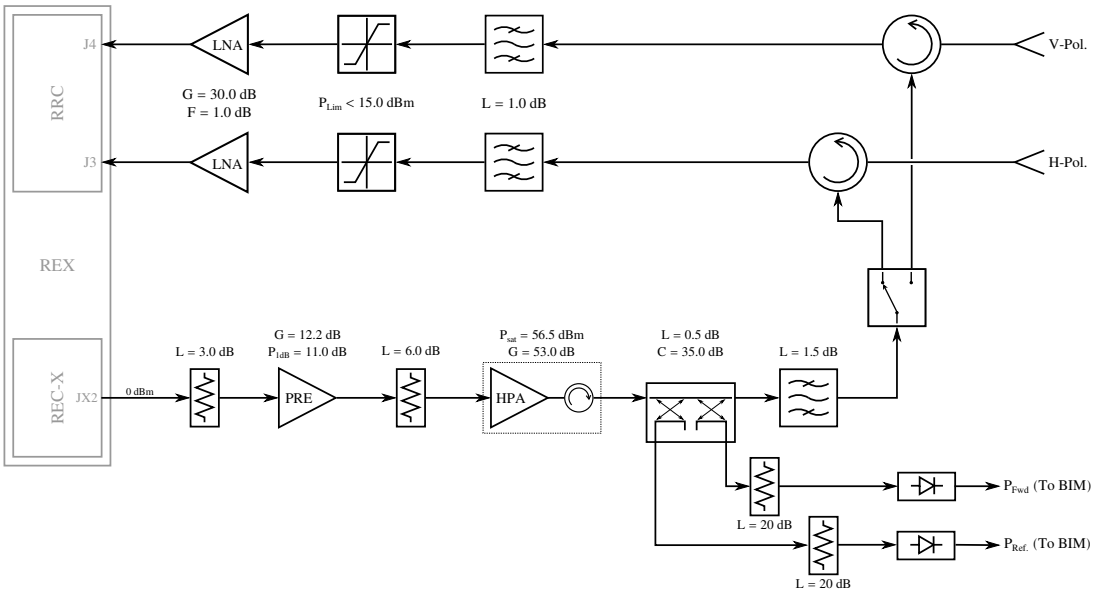

Figure 3.9: Combined X-band transmitter and receiver front end.

to assume that the saturated output power level of the LNA would not exceed this value, since it is generally related to the P_{1dB} point by our previously mentioned rule of thumb: $P_{sat} \approx P_{1dB} + 2\,\text{dB}$ [10], which in this case gave $P_{sat} \approx 15 + 2 = 17\,\text{dBm}$. This allowed us to connect the LNA output directly to the input of the REX without any further attenuation. Furthermore, with the maximum input rating of 19 dBm for the LNA, a COTS limiter (*Aeroflex* ACLM-4571FC31K) was selected, having a flat leakage rating of 13 dBm and a peak input power rating of 1 000 W or 60 dBm. Whilst the limiter does not specify the peak leakage value, it was once again reasonable to assume that it would not exceed the 19 dBm input limit of the LNA. Nonetheless, both the limiter and the LNA would require testing to confirm the assumptions made on the peak leakage and saturated output power levels, respectively.

3.2.5 L-Band HPA Thermal Analysis

While the X-band HPA was supplied with a pre-fitted heat sink and cooling fans, the L-band HPA was supplied as a bare amplifier without any thermal management in place. It was therefore necessary to determine the thermal load which needed to be dissipated and implement suitable cooling measures. Since the final integrated *NeXtRAD* system will have its own thermal requirements based on the final mechanical configuration, the aim of this analysis is to determine a suitable

heat sink size/design in order to ensure that the HPA is operated within its thermal limits, in an ambient temperature of up to 30 °C, using natural convection. This should then allow sufficient leeway to operate the system in an environment with higher ambient temperature, if necessary, by adding fans for forced convection. A more detailed analysis of the *NeXtRAD* thermal management study can be found in [22].

In order to determine the required thermal resistance of the heat sink we use the equation [23]:

$$T_J = T_A + (\theta_{JC} + \theta_{CS} + \theta_{SA})\, P \tag{3.2}$$

where T_J is the desired maximum junction temperature of the device, T_A is the maximum ambient operating temperature, θ_{JC} the thermal resistance (in degrees per Watt) from junction to case, θ_{CS} the thermal resistance from case to heat sink, θ_{SA} the thermal resistance from heat sink to ambient, and P the power to be dissipated.

Since the datasheet for the HPA does not provide a value for θ_{JC} but does provide a maximum case temperature (referred to as 'flange temperature' in the datasheet), we modify Equation 3.2 by substituting the maximum junction temperature T_J with the maximum case temperature T_C and removing the junction to case thermal resistance θ_{JC}. This yields:

$$T_C = T_A + (\theta_{CS} + \theta_{SA})\, P \tag{3.3}$$

where T_C is the maximum desired case temperature. Since the maximum case temperature specified in the datasheet is 75 °C, we need to select a maximum operating temperature below this to ensure reliable operation. By setting $T_C = 65\,°\text{C}$ we allow 10 °C headroom as a safety margin.

In order to determine the required thermal resistance of the heat sink we need to determine the power to be dissipated by it. From the HPA datasheet we see that its minimum efficiency is 40 %, and with an estimated peak output power of 1 500 W (as per Section 3.1.3) we obtain a worst-case instantaneous thermal load of $P_{pk} = 1\,500 \times (1 - 0.4) = 900\,\text{W}$. Due to the combination of the thermal mass of the heatsink and the PRI of the system, the temperature of the HPA is determined by average power and not peak power, thus giving $P_{max} = 900/10 = 90\,\text{W}$ at a maximum duty cycle of 10 %.

The remaining variable needed before we can identify a suitable heat sink is θ_{CS}.

In the hypothetical case of a perfectly flat mating surface on both the heat sink and the case, heat would flow seamlessly from the case to the heat sink. However, in real world applications the mating surfaces are not perfectly flat, resulting in an air interface forming between the two surfaces [24]. This impedes the heat flow, resulting in a high θ_{CS} value. Good metal-to-metal contact is typically achieved across 40 – 60 % of the surface area, thus to overcome this problem a thin layer of thermal compound is placed between the two mating surfaces to fill the air gaps and reduce θ_{CS} [25]. This layer of compound should be sufficiently thin so as not to prevent metal-to-metal contact, but simultaneously thick enough to fill in these air gaps.

An Electrolube HTSP compound was selected, having a thermal conductivity of $\kappa = 2\,\mathrm{W/m.K}$. By taking into account the surface finish of the HPA and its total surface area ($A \approx 0.0375\,m^2$), a maximum compound thickness of $t = 0.2\,\mathrm{mm}$ was assumed. The thermal resistance was then determined using the equation [26]:

$$\theta_{CS} = \frac{\rho \times t}{A} = \frac{(1/2) \times 0.0002}{0.0375} = 2.67 \times 10^{-3}[K/W]$$

where $\rho = 1/\kappa$ is the thermal resistivity of the compound. Equation 3.3 was then solved to determine the maximum acceptable θ_{SA}, giving:

$$\theta_{SA} = \frac{T_C - T_A}{P} - \theta_{CS} = \frac{65 - 30}{90} - 0.003 = 0.386\ K/W$$

A Fischer Elektronik SK520 heat sink was selected, having a thermal resistance of $\theta_{SA} \approx 0.35\,\mathrm{K/W}$. This was sufficient for use in a lab environment with natural convection cooling, whilst the use of forced convection cooling in the final system would further reduce the effective thermal resistance of the heat sink, ensuring a lower operating temperature [27].

3.2.6 Power Supplies

A number of different power supplies were required for the various active front end components. Most of these components required a +5 V DC supply, but the HPAs had special requirements which need to be addressed. For the +5 V components, COTS power supplies were selected and the components powered directly off them. This also applied to the X-band LNAs which required a +12 V supply.

Both HPAs draw large current pulses during and after transmission of RF pulses, in order to maintain constant RF power and recharge their internal capacitor banks prior to the next pulse. If the power supplies are not able to source sufficient current to recharge the HPA capacitor banks prior to the transmission of the next pulse, the HPA performance will be degraded and could result in them shutting down completely.

For the L-band HPA the power supply is required to provide +50 V ±5 % at an average current of up to 16 A. This current consumption value applies for a duty cycle of 20 % at a pulse width of 200 μs. For *NeXtRAD* the maximum duty cycle is 10 %, meaning that the average current requirement becomes 8 A, which translates to a peak current requirement of up to 80 A. The datasheet therefore recommends the use of a 10 000 μF capacitor on the supply rail.

A power supply was identified (*Mean Well* SPV-1500-48) offering an adjustable output of 48 V ±5 % and maximum current of 32 A, for a total power rating of 1 536 W. Operating the power supply at 50 V would require derating the current rating accordingly, therefore resulting in a maximum current rating of $I = P/V = 1\,536/50 = 30.72$ A. If the previously mentioned peak current draw of 80 A is assumed correct, external capacitors would be required to supply the 49.28 A deficit during pulse transmissions. The ±5 % HPA voltage tolerance means that the resulting voltage drop on these capacitors may not exceed $dV = 2.5$ V if the HPA is operated at a nominal voltage of 50 V. Subsequently, for a maximum pulse width of $\tau = 100\,\mu$s the minimum required capacitance can be calculated as [23]:

$$I = C\frac{dV}{dt}$$

$$\therefore C = I\frac{dt}{dV} = 49.28\frac{100 \times 10^{-6}}{2.5} = 1\,971.2\ \mu F$$

where $dt = \tau$ is the period over which the voltage decay takes place. This calculation confirms that the 10 000 μF capacitance specified in the datasheet is sufficient to maintain the supply voltage within specification with the selected power supply. For additional headroom a total of capacitance of 47 000 μF was selected, providing a theoretical maximum supply voltage droop of:

$$dV = \frac{I}{C}dt = \frac{49.28}{0.047}100 \times 10^{-6} = 0.105\ V$$

or 0.21 % of 50 V, which is well within the specified tolerance.

For the +12 V secondary supply the current requirement is only 200 mA which is easily supplied by a standard COTS power supply (a *Mean Well* RT-85B unit was selected). Over and above the voltage and current requirements, the +12 V secondary supply is required to be applied prior to the +50 V primary supply. Due to the inherent set up and rise time of the primary supply being 1 600 ms and the secondary supply being 520 ms, this biasing sequence is inadvertently taken care of by the supply design as long as the AC power is always applied to both supplies simultaneously.

The requirement for the X-band HPA primary power supply is +12 V ±0.1 V at a peak current of 140 A. Using another 1 500 W *Mean Well* power supply (SPV-1500-12) with maximum current rating of 125 A, the necessary capacitance required to sustain the 15 A shortfall within the 0.1 V tolerance is

$$C = I\frac{dt}{dV} = 15\frac{100 \times 10^{-6}}{0.1} = 15\,000\ \mu F$$

This was addressed with a 22 000 μF capacitor, resulting in a maximum expected voltage droop of $dV = \frac{I}{C}dt = (15/0.022)(100 \times 10^{-6}) = 68.2\,\text{mV}$.

For the −12 V X-band HPA secondary supply the same RT-85B unit selected for the L-band HPA was used, as it contained three channels (+5 V, +12 V, −12 V), with the −12 V able to provide sufficient current for the requirement. Furthermore, the biasing sequence was addressed by the inherent set up and rise time of the power supplies, as before.

The HPA power cables were kept as short as possible in order to minimise voltage overshoot resulting from the combination of large current and cable inductance.

The power distribution to the RF front end components can be seen in Appendix A.

3.2.7 Timing and Control

Timing of the control and monitoring functions are a critical part of a radar system as it ensures all events occur as and when they should. An event occurring at the wrong time could have a detrimental effect on the radar functionality, or even worse, inconsistent captured data which could go undetected. For example, if an HPA is not biased early enough prior to the transmission of RF, the transmitted pulse would be distorted as the bias time overlaps the rise time, resulting in a

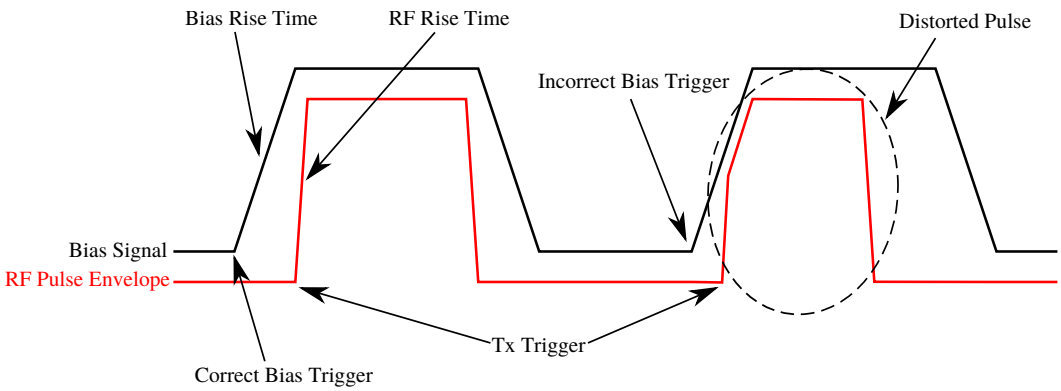

Figure 3.10: Example of distorted pulse resulting from incorrect control timing.

power ramp rather than a pulse, as shown in Figure 3.10. Or premature switching of a polarisation switch would result in an inconsistent dataset which could go undetected. These are two examples of the many possible effects of erroneous timing.

In order to develop an appropriate timing scheme, a thorough knowledge of the system operation is required in order to account for all necessary control and monitoring signals, and the relevant timing requirements of these. Once the system operation is fully understood, the appropriate component datasheets are required to develop a detailed timing diagram based on system requirements and inherent timing limitations and restrictions of individual components. In this section we will discuss the system operation which drives the timing requirements applicable to the RF front end, without going into the extensive low-level timing diagram derivation.

The system consists of both static and dynamic timing which needs to be accounted for. Generally speaking, static timing is fixed and determined by the various components of the system (e.g. the amplifier bias time specification will dictate how much time needs to elapse before the RF pulse can be transmitted), while dynamic timing varies based on the system configuration at any given time (e.g. the selected pulse width will dictate the duration between HPA bias and HPA shutdown).

At a high level, the system operates in one frequency band at a time, alternating after a batch of pulses has been transmitted and received. The two frequency bands have some subtleties between them, owing primarily to the single L-band

and dual X-band receive channels. The sequences of events describing system operation and used for developing the timing diagrams follows:

Power-Up events:

1. L-band HPA into shutdown mode
2. L-band HPA into standby mode
3. X-band HPA into standby mode
4. Apply HPA secondary supplies
5. Apply HPA primary supplies
6. Apply other front end power supplies
7. L-band HPA out of shutdown mode

Shutdown events:

1. L-band HPA into standby mode
2. L-band HPA into shutdown mode
3. X-band HPA into standby mode
4. Remove HPA primary supplies
5. Remove HPA secondary supplies
6. Remove other front end power supplies

L-band events:

1. Set Tx switch to v-pol
2. Set Rx switch to v-pol
3. HPA out of standby mode
4. Transmit RF
5. Measure peak power while transmitting
6. Measure reflected power while transmitting
7. HPA into standby mode after RF pulse
8. Measure HPA junction temperature
9. Wait for target returns
10. Set Rx switch to h-pol
11. Repeat steps 3–9
12. Set Tx switch to h-pol
13. Repeat steps 3–9

14. Set Rx switch to v-pol
15. Repeat steps 3–9

X-band events:

1. Set Tx switch to v-pol
2. HPA out of standby mode
3. Transmit RF
4. Measure peak power while transmitting
5. Measure reflected power while transmitting
6. HPA into standby mode after RF pulse
7. Check for HPA over-temperature alarm
8. Wait for target returns
9. Set Tx switch to h-pol
10. Repeat steps 2–8

The timing and control module is to be implemented as a separate project, but the guideline timing schedule derived in this project is included in Appendix B, for use as an input for the final implementation.

3.3 Architecture Modification for Cost Reduction

After developing the initial design, the next step was to identify and procure suitable components. With the limited budget and high cost of many of the components, this necessitated making changes to the design in order to have a system which fell within the available budget whilst offering as much of the required functionality as possible. From a cost perspective, the items identified as being prohibitively expensive were:

- The high power receiver protectors which were critical for protecting the LNAs and receiver.
- The high power solid state switches which were required to implement pulse-to-pulse switching for polarimetric operation.

Removal of the solid state switch removes critical functionality from the system, whilst removal of the receiver protectors places the entire system at risk of damage — an option which could not be considered. By making some changes to the architecture, however, it was possible to reduce the cost of the system and maintain an acceptable amount of functionality which could serve as a first revision setup, with scope for upgrading to achieve the preferred design and functionality as more funding becomes available.

The first step taken was to reduce the power levels within the Rx front end, so as to lower the power handling requirements of the receiver protectors and the L-band Rx switch. In the current configuration a portion of the transmitted pulse is reflected from the antenna port into the Rx front end. The magnitude of this reflection is determined by the return loss of the antenna — typically around 15 – 20 dB. This means that under normal operating conditions with a peak power level of 61.76 dBm the L-band Rx front end would need to handle power levels as high as 46.76 dBm — a number which is still considered moderately high.

The reduction in Rx power levels was achieved by using separate Tx and Rx antennas, and subsequently doing away with the circulators, in order to isolate the Tx and Rx front ends. Whilst the dual-antenna architecture was less desirable from a mechanical perspective, it was a necessary sacrifice in order to provide sufficient protection for the receiver within the available budget. This new configuration had the advantage of removing the need to handle a full power reflection in the event of a cable break between the HPA and Tx antenna, since such reflections would return to the output of the HPA, which is already designed to handle an infinite VSWR.

The implication of using separate Tx and Rx antennas is that the system would now require that the transmit antennas for both bands be located on one tripod (as seen in Figure 3.2), and an identical setup for the the receive antennas be co-located on another tripod. Careful alignment would then be necessary to ensure that the electrical boresight of the antennas for both bands are aligned, and that the transmit and receive pedestals (and subsequently the antennas) can be accurately pointed at the same target or scene of interest.

With the high power direct feed now removed from the receiver front end, a low power solid state switch (*Mini-Circuits* ZFSWA2-63DR+) was selected for the L-band Rx front end. A limiter (*Mini-Circuits* VLM-63-2W+) was used for the receiver protector and moved to before the polarisation switch in order to protect

the switch as well as the LNA. The power handling capability of this limiter should be determined by the greater of the Tx-Rx antenna isolation and the maximum expected echo which may occur. A large echo would typically occur during an undesirable condition, such as a person or object moving in front of the antennas at close range. Whilst it was desirable to choose a limiter meeting the requirements of the aforementioned scenarios, the need to obtain low cost COTS units meant that the most sensible solution was to identify a limiter with a reasonable power rating and use these ratings to calculate the necessary antenna isolation and minimum 'target' distance to ensure these limits are not exceeded. This would of course not account for jamming or saturation by other emitters, but the range to such emitters is expected to be sufficiently large such that the signals would not exceed damage levels.

For the Rx filter it was decided to use a unit donated by RRS while the UCT filter was being developed. This filter offered low insertion loss (0.2 dB) and in-band ripple, and covered the same operational bandwidth as the system.

Similarly for the X-band system, changing to a dual antenna configuration meant that the receiver no longer had to handle reflections from the antenna port (up to 41 dBm for an antenna return loss of 15 dB), with the biggest reflection occurring in the event of a close-in 'target'. The *Aeroflex* limiter initially selected was kept, with the benefit that the peak power into the receiver front end would now be well below the specified 60 dBm peak level specified for the limiter – a figure which is only valid for a pulse width of $\leq 1\,\mu$s at duty cycle not exceeding 0.001 % and PRF ≤ 1 kHz.

Returning to the transmitter front end, removal of the solid state switch meant that a mechanical switch needed to be used in order to be able to maintain the dual-polarised functionality. Such mechanical switches do not have the fast switching speed of the solid state variants, and typically have a mean time between failure (MTBF) of between 1–10 million switching cycles [14],[15]. This makes them only suitable for switching after a batch of pulses rather than on a pulse-to-pulse basis. This impacts the operational capability of the system, but is a viable temporary solution which can be substituted with a solid state variant at a later stage, without requiring any changes to the system architecture. Whilst a *Teledyne* and *Mini-Circuits* option was identified, a further decision by the *NeXtRAD* team meant that the procurement of the mechanical switch was decided against, thus requiring physically changing the coaxial cable between the two polarisation feeds on the

antenna between measurements. The switch, however, is maintained as part of the system architecture diagrams as it symbolises functionality, regardless of its method of implementation (physical switch or manual changing of cables).

The final change made to the design was to replace the *Aeroflex* ACSP-2504 X-band power detectors, due to their requirement of an external biasing circuit. A decision was made to make use of the same *Mini-Circuits* ZX47-40+ power detectors used for the L-band front end. Whilst these detectors are only specified to operate up until 8.0 GHz, their low cost and internal bias circuitry made them a viable option for consideration. This was coupled to the fact that their application in the front end was only for monitoring and reporting of transmitter performance, and that they could be characterized in the lab to determine their performance at X-band to ensure calibrated measurements of transmitter power levels.

The aforementioned changes to the initial design concluded the design process, leaving us with a final design as shown in Figure 3.11.

3.4 Summary

By taking into consideration the design requirements derived in the various system design discussions, and the specifications of the other subsystems, constraints for the RF front end design were derived. These constraints focussed primarily on the frequency bands and power levels required at the inputs and outputs of the front end.

The constraints were combined with the functional requirements of the system in order to develop a front end design which would realise all the necessary functionality of the system. A detailed design process was followed, which included the design and selection of the RF front end, power supplies, thermal management for the L-band HPA, and timing requirements for the front end components.

Due to budgetary constraints, the design was modified in order to achieve a reduced level of functionality which could be implemented as a first build, and subsequently upgraded. This modified architecture did away with the ability to perform pulse-to-pulse switching on transmit, and increased transmit-receive isolation by using separate antennas — at the cost of increased antenna count and mechanical complexity. This resulted in a system which met the budget limitations and offered acceptable levels of functionality for an initial build.

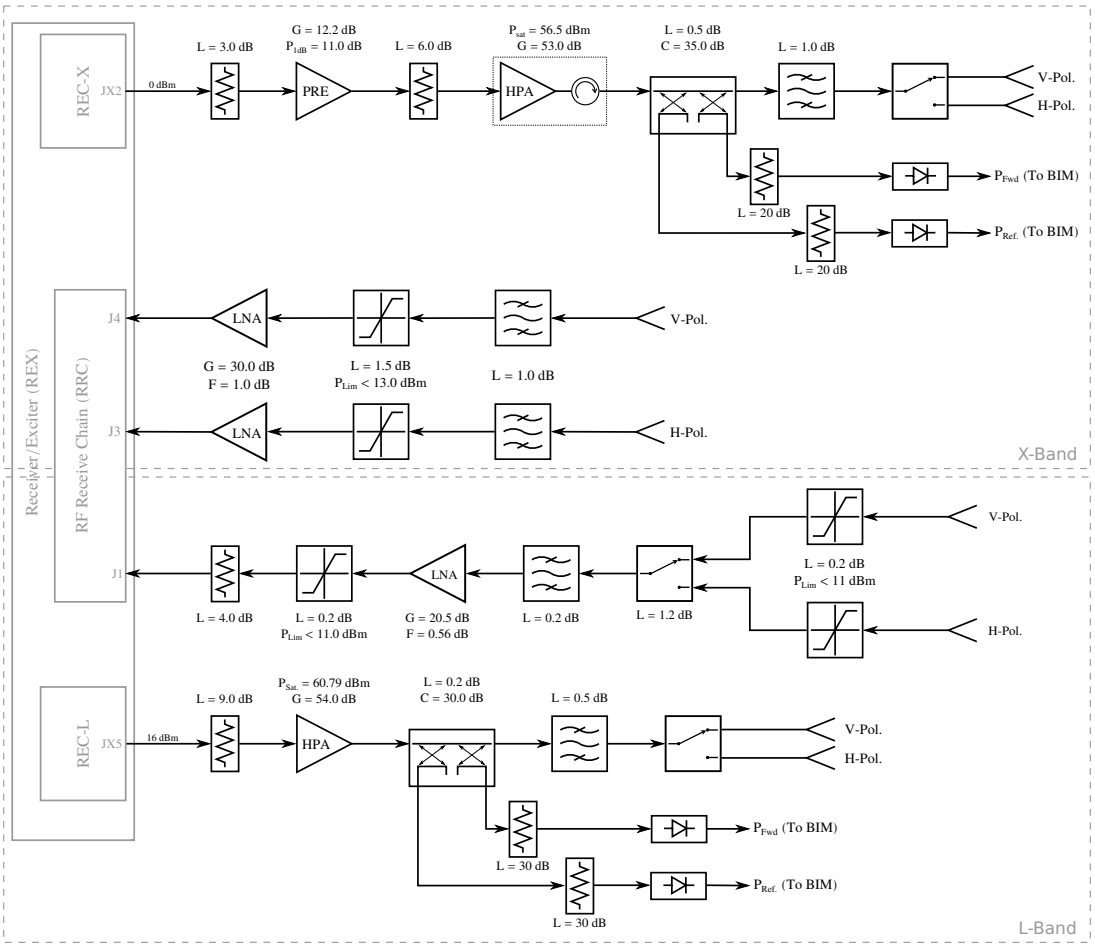

Figure 3.11: Revised front end design with reduced functionality for initial system build.

Chapter 4

System Analysis

In this chapter we investigate the signal levels through the system to ensure that they fall within the design limits. This includes an analysis of the RF front end, and the SNR from the receiver input to the REX IF output. A *SystemVue* model is also constructed for design verification.

4.1 Front End Analysis

This section looks at the hardware performance, specifically the power levels as the signal passes through the various stages of the RF front end.

4.1.1 Transmitter Performance

Using the final transmitter front end designs described in Section 3.3, it was necessary to trace the signal power levels through the various components in order to determine the expected power level at the input to the transmit antenna. This is important for determining overall system performance, as is done in Section 4.2. Furthermore, this cascade analysis is useful for verifying that none of the components are operated outside of their specified limits.

The cascade analysis was based on the typical component specifications provided in the respective datasheets. Where specifications were not provided, assumptions were made based on available information.

4.1.1.1 L-Band Transmitter

For the L-band Tx front end cascade analysis, shown in Figure 4.1, we start with an input power level of 16 dBm ±2 dB coming from the REX and going to the HPA via the attenuator. The ±2 dB variance is neglected due to the fact that the HPA is operated close to its saturation point, and the effect of this variance at the output is difficult to calculate due to the resulting non-linear HPA transfer function. It is, however, known that this variance will decrease at the HPA output.

For the output filter the insertion loss is assumed to be 0.5 dB. This is a reasonably modest value, considering the fact that the RRS band pass filter (BPF) for the Rx front end has an insertion loss of 0.2 dB. This value therefore provides a reasonable amount of leeway for the student who will be developing this filter.

Coaxial cables are assumed to be short enough such that the losses are negligible. The exception to this is the antenna feed cable, where a Huber & Suhner SUCOFLEX 406 cable having attenuation of 0.16 dB/m at 1.3 GHz is used. The length of this cable is assumed to be 1.5 m.

Finally, the polarisation switch was omitted since it does not form part of the first revision.

Based on this cascade analysis, the expected transmitter output power was found to be $P_t = 59.85$ dBm, which is 0.94 dB below the typical HPA output power level, due to system losses. Total gain through the front end was found to be $G = 43.85$ dB.

4.1.1.2 X-Band Transmitter

For the X-band front end we follow the same principles as with L-band. A number of assumptions are also made for components which do not have full specifications available.

The X-band HPA is supplied with an external isolator for protecting its output port. The third port on this isolator is connected to a dedicated port on the HPA, likely a dummy load, which implies that the isolator is an integral part of the amplifier design. For this reason it is assumed that the manufacturers specified output power level includes losses in the isolator/circulator.

For the output filter the insertion loss is assumed to be 1.0 dB. Whilst this figure

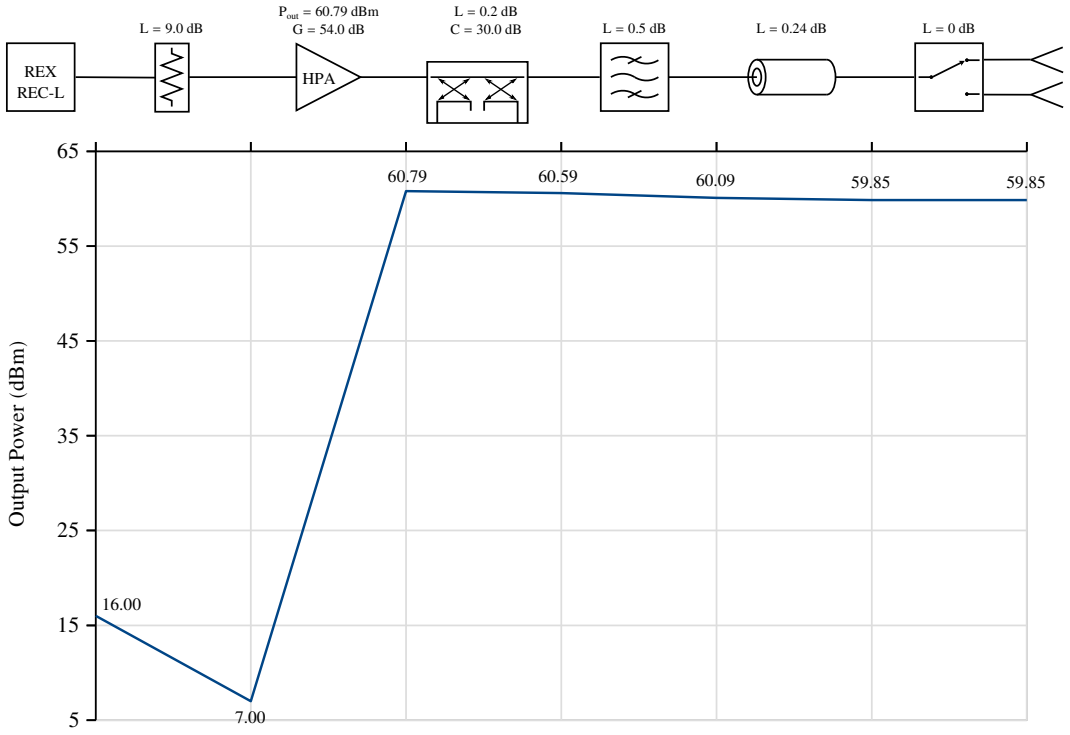

Figure 4.1: Cascaded L-band transmitter front end power levels.

is larger than that for L-band, it is also considered more stringent since the lower HPA output power level means that we need to keep system losses to a minimum.

For the antenna feed cables we assume a 1.5 m length of SUCOFLEX 406, which at 8.5 GHz has an attenuation per unit length of 0.44 dB/m.

The polarisation switch is excluded for the same reasons as before.

The results from the cascade analysis, shown in Figure 4.2, reveal that the expected transmitter output power level is $P_t = 54.34$ dBm. This is as a result of the 2.16 dB of loss between the HPA and the antenna. This is a significant reduction in power (approximately 39 %), which is difficult to improve upon due to the higher system losses at higher frequencies. This also shows the importance of obtaining a filter design with the lowest achievable insertion loss. Total gain through the front end was found to be $G = 54.34$ dB

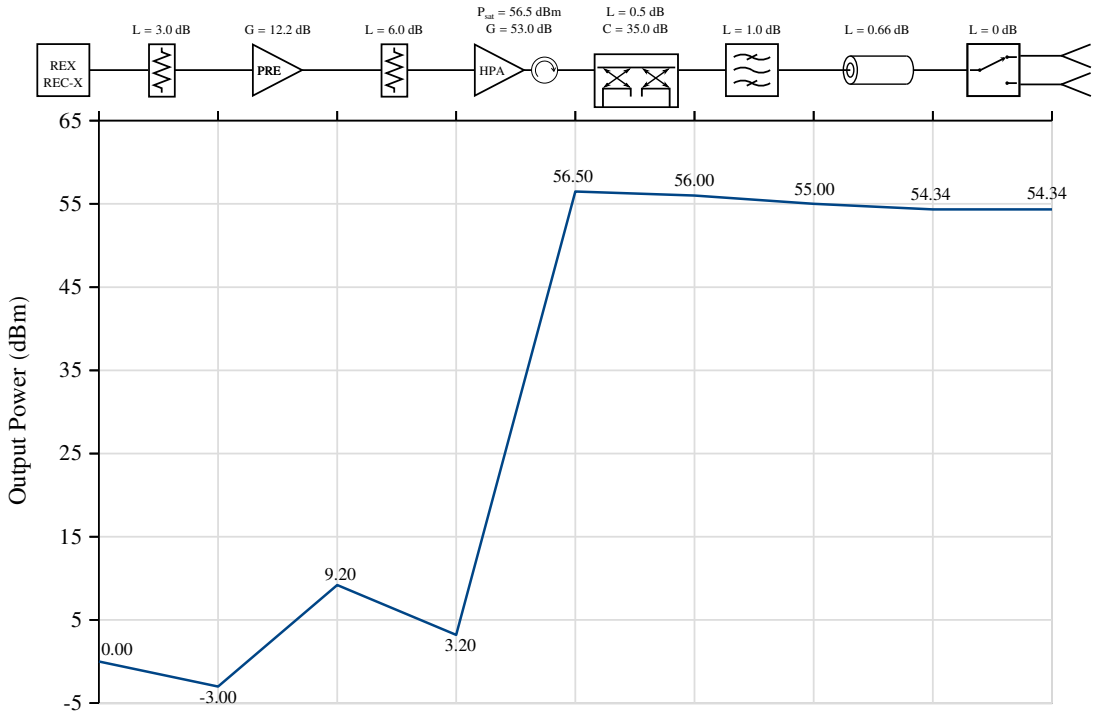

Figure 4.2: Cascaded X-band transmitter front end power levels.

4.1.2 Receiver Performance

For the receiver we need to consider three separate power levels within the RF front end chain. These are:

1. The gain of a large input signal from the antenna
2. The gain of a small input signal from the antenna
3. The noise power through the front end chain

A large signal is defined as any signal which would drive the front end components beyond their linear operating region, resulting in gain compression through the chain. Specifically, we want to consider the effects of the limiters when the input signal is larger than the limiter leakage value, as this allows us to determine if the signal entering the REX is below the maximum acceptable signal level.

For the small signal gain we use a signal small enough so as not to drive any of the receiver front end components out of their linear operating region, while simultaneously being large enough so as not to be lost below the noise floor. This gives us the total front end gain expected under normal operating conditions.

The noise power level through the system is important as it has implications on the target detectability, since the target return generally needs to remain above the noise floor in order to be detected by the receiver. It is therefore necessary to look at the noise power at each individual stage of the receiver, as well as at the output.

The calculation of the noise power is done by first determining the input noise power from the feed antenna, using [18]:

$$N_i = kT_aB \tag{4.1}$$

where T_a is the noise temperature seen by the antenna, B the antenna bandwidth, and k Boltzmann's constant. The antenna noise temperature depends on where the antenna is pointed, but for an antenna pointed towards the earth's surface this number can be assumed to be $T_a = T_0 = 290\,\mathrm{K}$ [21],[28].

Once the input noise has been determined, the cascaded noise figure, F, is calculated with [18]:

$$F = F_1 + \frac{F_2 - 1}{G_1} + \frac{F_3 - 1}{G_1G_2} + ... \tag{4.2}$$

where the subscript indices indicate the respective component stages in the cascade. The equivalent noise temperature, T_e, is calculated using the equation [18]:

$$T_e = (F - 1)T_0 \tag{4.3}$$

The final output noise power is then calculated by:

$$N_o = k(T_a + T_e)BG \tag{4.4}$$

with B representing the bandwidth of the receiver chain, and G the total gain through the chain.

4.1.2.1 L-Band Receiver

For the L-band receiver an antenna bandwidth of 100 MHz was used for the calculations, as this was considered a good representation of a worst-case scenario for antenna noise power (since the antenna bandwidth was specified in Section 3.1.5 as being $< 100\,\mathrm{MHz}$). Coaxial feed cables are assumed to be identical to those used in the transmitter, but with the feed cable located between the LNA and

final limiter instead.

For the large signal and small signal analysis, an input of +20 dBm and −20 dBm was used, respectively. The front end noise figure, determined using Equation 4.2, was found to be $F = 2.20\,\text{dB}$, while the total small signal gain was found to be $G = 15.46\,\text{dB}$. The maximum output power level in limiting mode was found to be $P_{max} = 8.50\,\text{dBm}$.

Antenna noise power, calculated using Equation 4.1, was found to be $N_i = -93.98\,\text{dBm}$, while the output noise power at the end of the front end (into the REX) was found to be $N_o = -76.32\,\text{dBm}$ (calculated using Equation 4.4).

The full cascade analysis is shown in Figure 4.3. The relevant component specifications used for the analysis are shown at each stage. This diagram tracks the signal and noise levels all the way through to the output of the REX, which was treated as a black box with $F = 20\,\text{dB}$ and gain set to $G = 0\,\text{dB}$, in accordance with its specifications. Note that this is a highly simplified representation of the REX, used for analysing the performance in linear operating modes only, but its gain and noise figure values were taken from its specifications sheet [4].

4.1.2.2 X-Band Receiver

For the X-band receiver, the antenna and filter bandwidth were both assumed to be 100 MHz. Coaxial cable losses are again assumed to be negligible, with the exception of the 1.5 m long SUCOFLEX 406 cables placed between the LNA and the REX.

Large signal gain was done using a +20 dBm input, while small signal gain was done with a −30 dBm input. The results, shown in Figure 4.4, include the signal path through the REX. For the RF front end section the analysis produced a noise figure of $F = 3.50\,\text{dB}$, small signal gain of $G = 26.84\,\text{dB}$, RF front end input and output noise power levels of $N_i = -93.98\,\text{dBm}$ and $N_o = -63.64\,\text{dBm}$, and a maximum signal output power level of $P_{max} = 16.34\,\text{dBm}$ in limiting mode.

4.1.3 Verification Modelling

In order to get a more accurate indication of expected system performance, and to verify the preceding design calculations, a model of the RF front end was

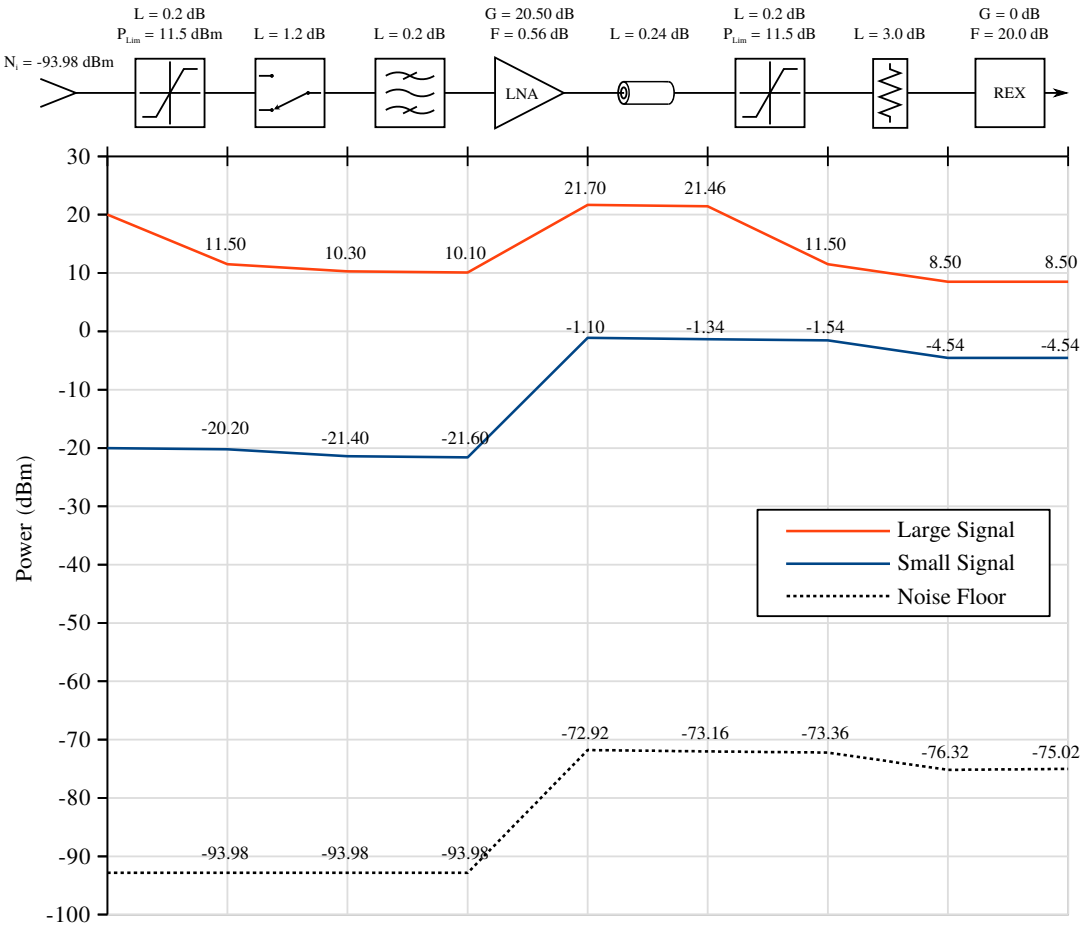

Figure 4.3: Cascaded L-band receiver front end power levels. A bandwidth of 100 MHz is used for components prior to the REX, which reduces to 50 MHz from the REX onwards.

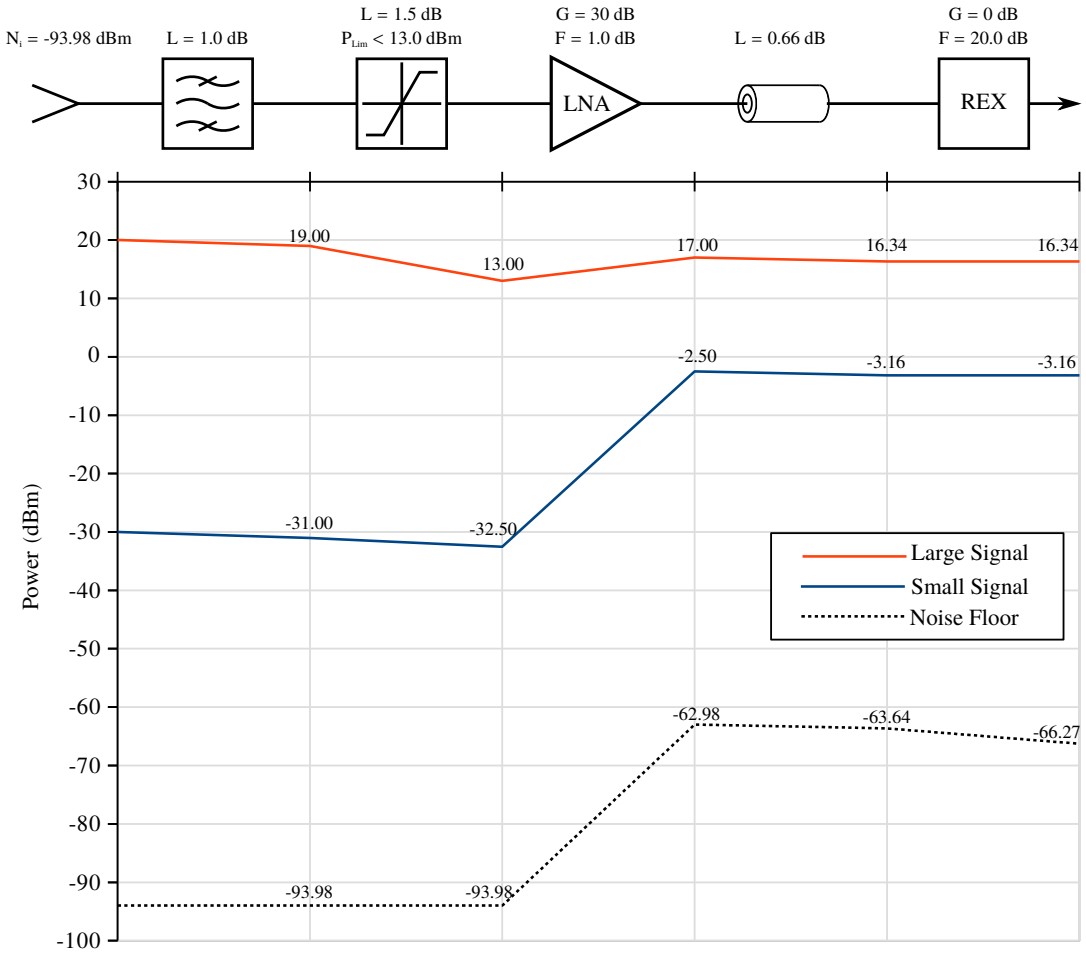

Figure 4.4: Cascaded X-band receiver front end power levels. A bandwidth of 100 MHz is used for components prior to the REX, which reduces to 50 MHz from the REX onwards. This results in the noticeable reduction in noise power at the REX output.

created using *SystemVue* Electronic System-Level Design Software. This allowed for a more detailed analysis of system performance, since non-linear effects and the interaction of harmonics are easily included in the simulation — something which is not easily achievable using a spreadsheet. Another benefit is the ability to quickly change components or parameters and view the effects these changes have on the system, particularly into the future when upgrades may take place.

While it is possible to model the entire *NeXtRAD* system, the focus here was purely on the signal levels through the front end due to the presence of components operating in non-linear modes.

Each of the four front ends were modelled separately using the same specifications as in the preceding calculations, obtained from the respective component datasheets. One caveat was that *SystemVue* appeared unable to calculate noise power for different bandwidths within the same component chain, as it relied on a globally defined measurement bandwidth for thermal noise analysis. This meant that in order to accurately view the noise power at each stage from the antenna through to the REX output, the simulation had to be run twice — once with the thermal noise bandwidth set to the RF front end bandwidth ($B = 100\,\text{MHz}$), and once with the bandwidth set to 50 MHz to match the REX IF bandwidth.

The results of the front end models are shown in Figures 4.5 – 4.8. For the Rx front ends the REX is included as the last stage of the chain, but due to the simulation bandwidth problem the noise power at the REX output in these figures is not correct and should be disregarded.

As a result of the simulation, it was found that the X-band HPA drive level was likely to be too low to push it into saturation. By reducing the attenuation between the pre-amp and the HPA from 6 dB to 3 dB the simulation indicated an HPA output power level of 56.01 dBm, which more closely matched the datasheet value of 56.50 dBm. This was left to be confirmed through lab testing, along with the L-band HPA which had a simulated output of 60.20 dBm — 0.59 dB less than the datasheet value.

Total Tx power delivered to the antennas was found to be $P_{t_L} = 59.25\,\text{dBm}$ and $P_{t_X} = 53.69\,\text{dBm}$. For the Rx front ends there was close correlation between the cascade analysis and the simulation, with small signal gain $G_L = 15.45\,\text{dB}$ and $G_X = 26.83\,\text{dB}$. Noise power at the output of the front end was $N_{o_L} = -75.21\,\text{dBm}$ and $N_{o_X} = -63.59\,\text{dBm}$.

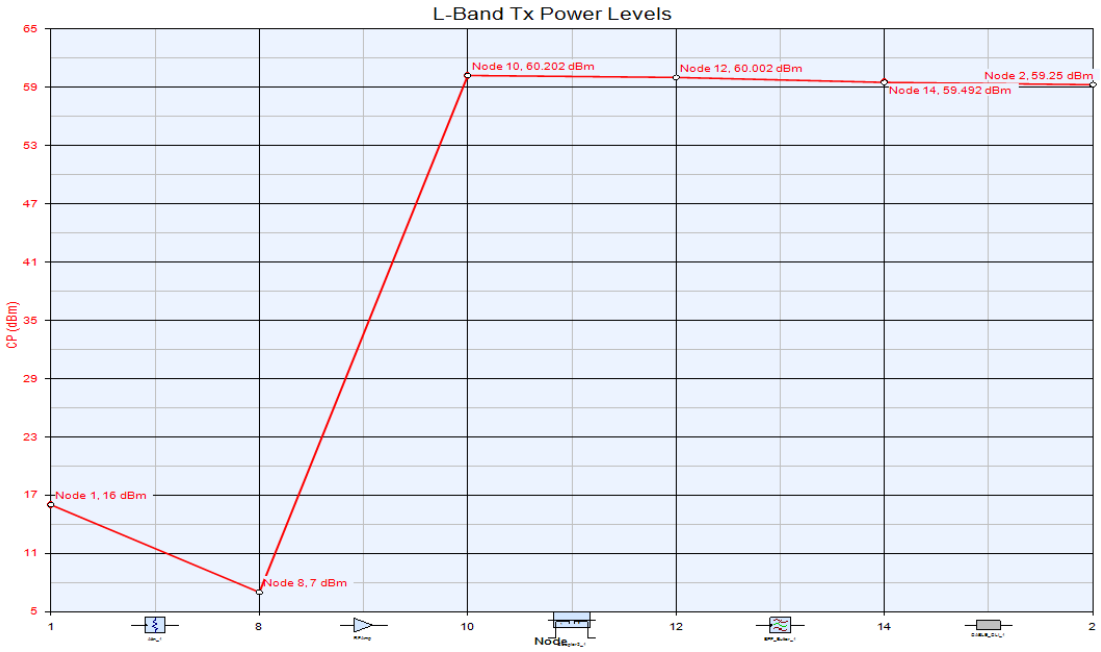

Figure 4.5: *SystemVue* simulation of L-band transmitter RF front end power levels.

These results are discussed further in Chapter 6.

4.2 Signal Analysis

This section discusses the signal integrity as it moves through the individual stages of the RF front end. Section 4.1 looked at the signal levels from a hardware perspective. In this section we look at external factors, namely the antennas and target, and combine these with the hardware effects in order to determine the expected signal levels in real-world operation.

4.2.1 Target RCS

In a typical radar system the dynamic range of the target RCS is very large since targets of interest could include anything from humans to large warships. For the *NeXtRAD* system we expect to look primarily at smaller targets such as swimmers and small boats. We therefore need to consider what the RCS of such targets would be, as well as determine a range of RCS values to use to investigate the expected SNR range at the receiver.

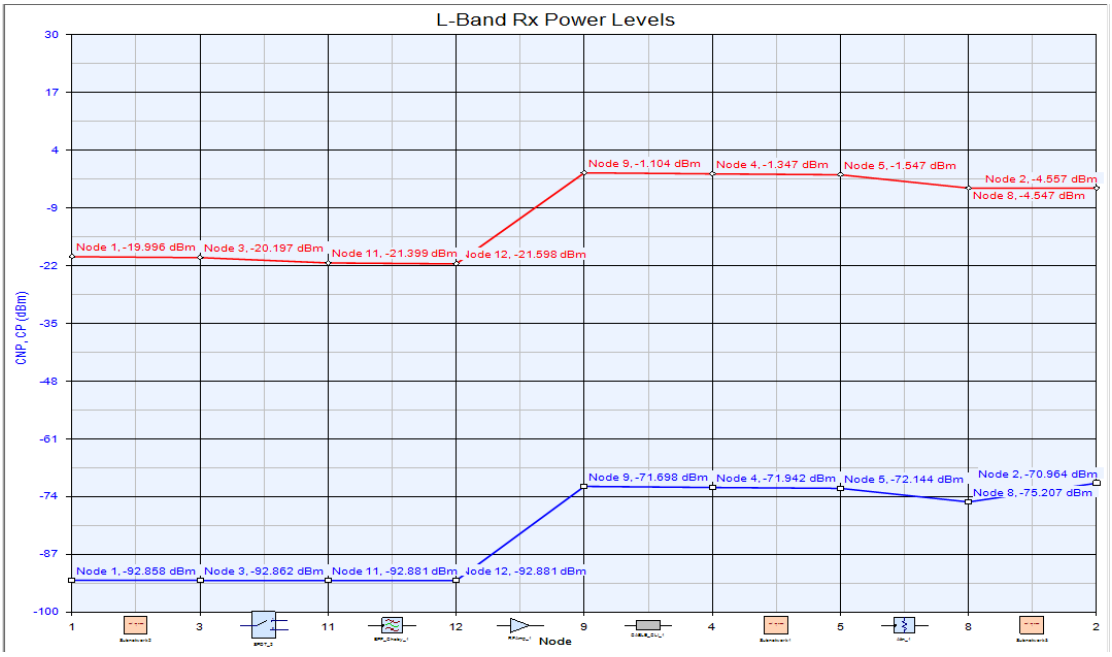

Figure 4.6: *SystemVue* simulation of L-band receiver RF front end signal and noise power levels with small signal input of −20 dBm.

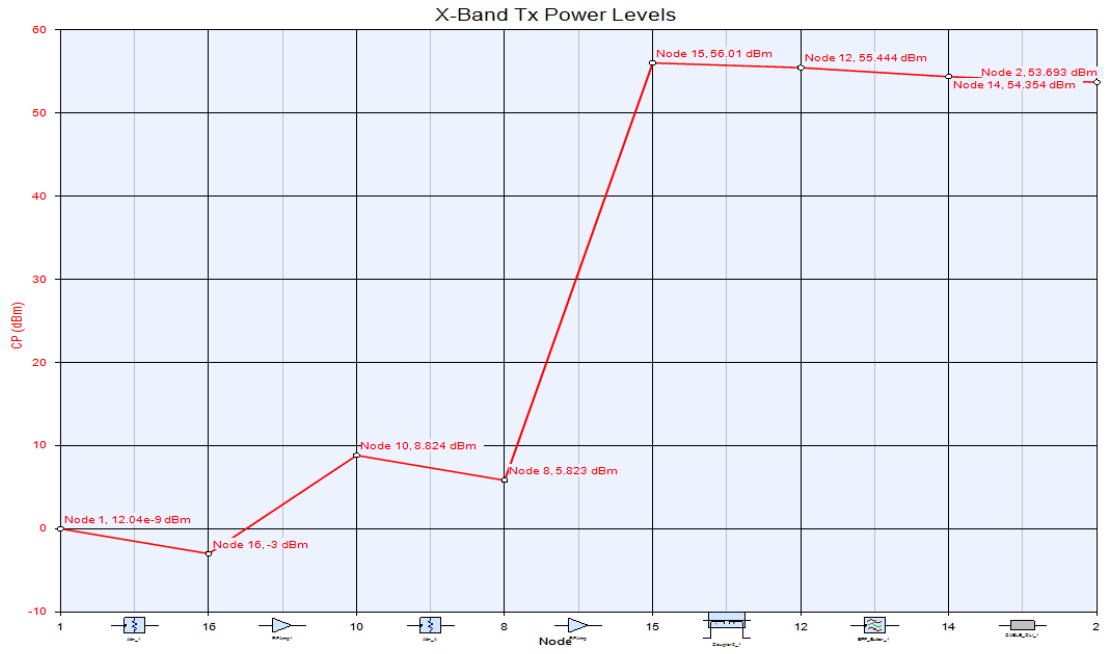

Figure 4.7: *SystemVue* simulation of X-band transmitter RF front end power levels.

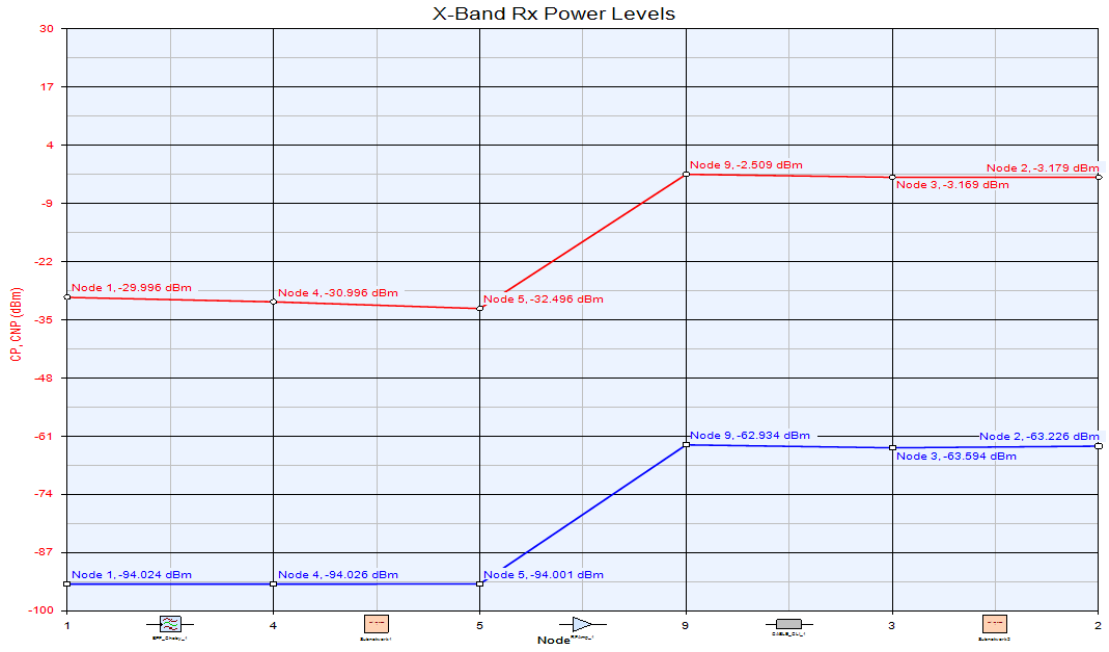

Figure 4.8: *System Vue* simulation of X-band receiver RF front end signal and noise power levels with small signal input of −30 dBm.

For the case of a known target RCS, it was decided to use a simplified approximation of the upper part of an outboard motor used on a small boat. This was considered to be a cylindrical shape of radius $r = 0.6\,\text{m}$ and height $h = 0.6\,\text{m}$. The RCS of a cylinder with these dimensions is calculated by [13]:

$$\sigma = \frac{2\pi r h^2}{\lambda} = \frac{0.432\pi}{\lambda}$$

Note that for this to hold true, the curved surface of the cylinder needs to be normal to the antenna boresight. For the L-band system operating at 1.3 GHz we have a wavelength of $\lambda_L = \frac{c}{f} = \frac{3\times10^8}{1.3\times10^9} = 0.23\,\text{m}$, giving an RCS of:

$$\sigma_L = \frac{0.432\pi}{0.23} = 5.88\ m^2$$

Similarly, for the X-band system operating at 8.5 GHz we have a wavelength of $\lambda_X = \frac{3\times10^8}{8.5\times10^9} = 0.035\,\text{m}$, and subsequently an RCS of:

$$\sigma_X = \frac{0.432\pi}{0.035} = 38.45\ m^2$$

This gives us what we will consider to be the typical or nominal target RCS for both operating bands, and serves as a reference target for use during SNR

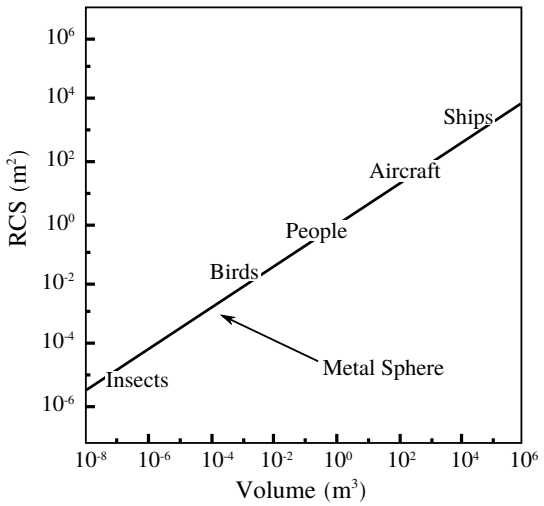

Figure 4.9: Table of approximate RCS values for various target sizes (adapted from [19]).

calculations. Furthermore, we also need to consider a range of RCS values that may be encountered by the system so as to ensure that the receiver dynamic range is capable of measuring all targets of interest.

Figure 4.9, adapted from [19], was used as a very crude guide for determining a range of RCS values across which to evaluate the system performance. Due to the significant variation possible with a given target type's RCS, the graph merely provides an approximate range of possible values to expect, without taking into account the electrical length of the targets. From this graph it is evident that an RCS of between 100 – 1000 m^2 corresponds to a reasonably large target such as an aircraft or medium-sized boat. With *NeXtRAD* focussing on smaller maritime targets, an RCS of 500 m^2 was chosen as the maximum value for use as this should correspond to, or exceed, the typical size of a boat which may be used during the measurement campaigns.

4.2.2 Received Power

Due to the combination of the target RCS and the fact that $P_r \propto \frac{1}{R^4}$ [13], the radar receiver is required to have high dynamic range in order to detect small and large targets at short and long ranges, without saturating the receiver or having the power level of the returned echo less than the receiver sensitivity. The $\frac{1}{R^4}$ factor in the radar equation is the biggest contributor to the dynamic range problem, but one way to overcome this is through a technique known as sensitivity time control

(STC) [13]. STC exploits the fact that the target range is directly proportional to the time elapsed since the pulse was transmitted. Thus by placing a variable gain amplifier (VGA) within the receiver chain and sweeping its gain as a function of time, you are able to remove the range dependency of the received power prior to its arrival at the ADC. In simple terms this means that a target with a given σ will appear to produce the same target return regardless of its range. This, of course, does not compensate for effects such as glint, scintillation, etc. seen in more complex targets, or the antenna gain variation as the target moves around within the main lobe.

Due to *NeXtRADs* intended multistatic configuration, the STC function, which would have been implemented within the IF receive chain (IRC) of the REX, was converted to a manual gain controller. This allows for the selection of a gain value within the range 1 – 31 dB ±2 dB. When combined with the 0 ± 2 dB gain in the preceding RRC we have a total REX receiver gain range of 1 – 31 dB ±4 dB. Since this is a manual gain control, the gain setting needs to be pre-selected based on the targets within the scene of interest, and the input to the ADC will remain range-dependant.

In order to analyse the performance of the receiver, it is required to have an idea of expected target return power levels for typical targets within the systems anticipated operating environment. This requires that the received power level be calculated as a function of both range and target size. A range of $0.15 \leq R \leq 20\,\text{km}$, and an RCS of $0.1 \leq \sigma \leq 500\,\text{m}^2$ was selected for a typical scene of interest. The values for the target range were chosen based on the systems minimum blind range, as defined in Section 3.1.6, and maximum likely radar horizon using a 4/3 Earth model, defined as [13]:

$$R'_h = \sqrt{2(4/3)ah_t} \tag{4.5}$$

with $a = 6\,371\,\text{km}$ the radius of the earth, and $h_t = 20\,\text{m}$ the assumed maximum height of the transmitter above the surface. This produces a radar horizon of $R'_h = 18.43\,\text{km}$, which was rounded to 20 km for the analysis. Note that this range falls outside of the systems minimum unabiguous range of $R_a = \frac{c}{2PRF} = 15\,\text{km}$ [13], which occurs when PRF = 10 kHz.

Table 4.1: Summary of constants and variables for calculating received power, P_r, and receiver gain, G_{Rx}.

	L-band	X-band	Units
Transmitted Power, P_t	59.85	54.34	dBm
Antenna Gain, G	19.65	23.37	dB
Wavelength, λ	0.231	0.035	m
System Losses, L_s	0	0	dB
Target RCS, σ	0 – 500		m^2
Target Range, R	150 – 20000		m

From the radar equation, the received power is given by [13]:

$$P_r = \frac{P_t G^2 \lambda^2 \sigma}{(4\pi)^3 L_s R^4} \tag{4.6}$$

where P_t is the transmitter power (in Watts), G is the antenna gain (unitless) and is assumed to be identical for both transmit and receive antennas, λ is the wavelength (in metres), σ is the radar cross section of the target (in m^2), L_s is the system losses (unitless), and R is the range to the target (in metres).

For these calculations we define P_t as the power at the input port of the transmitting antenna. The value P_r can then be defined as the power at any point within the receive chain, provided that L_s includes all the losses between the output port of the receiving antenna and the point at which P_r is chosen to be.

Typically, the interest is in knowing the power levels at the final IF output, where it gets sampled by the ADC. For this analysis though, we simply define P_r as the power at the output of the Rx antenna. System losses can therefore be omitted from the calculation as there are no hardware components between the defined points P_t and P_r, except for the antennas which are accounted for in the antenna gain variable G. If the power levels at other points within the receiver are needed, the calculated value for P_r can simply be combined with the cascade analyses from Section 4.1.2.

Using the system parameters summarised in Table 4.1, plots were generated to determine the received power as a function of range for targets of varying RCS. This is shown in Figure 4.10 and includes curves for the small boat proposed as a reference target in Section 4.2.1, with $\sigma_L = 5.88\,m^2$ and $\sigma_X = 38.45\,m^2$. From this analysis it was confirmed that the received power fell below the front end

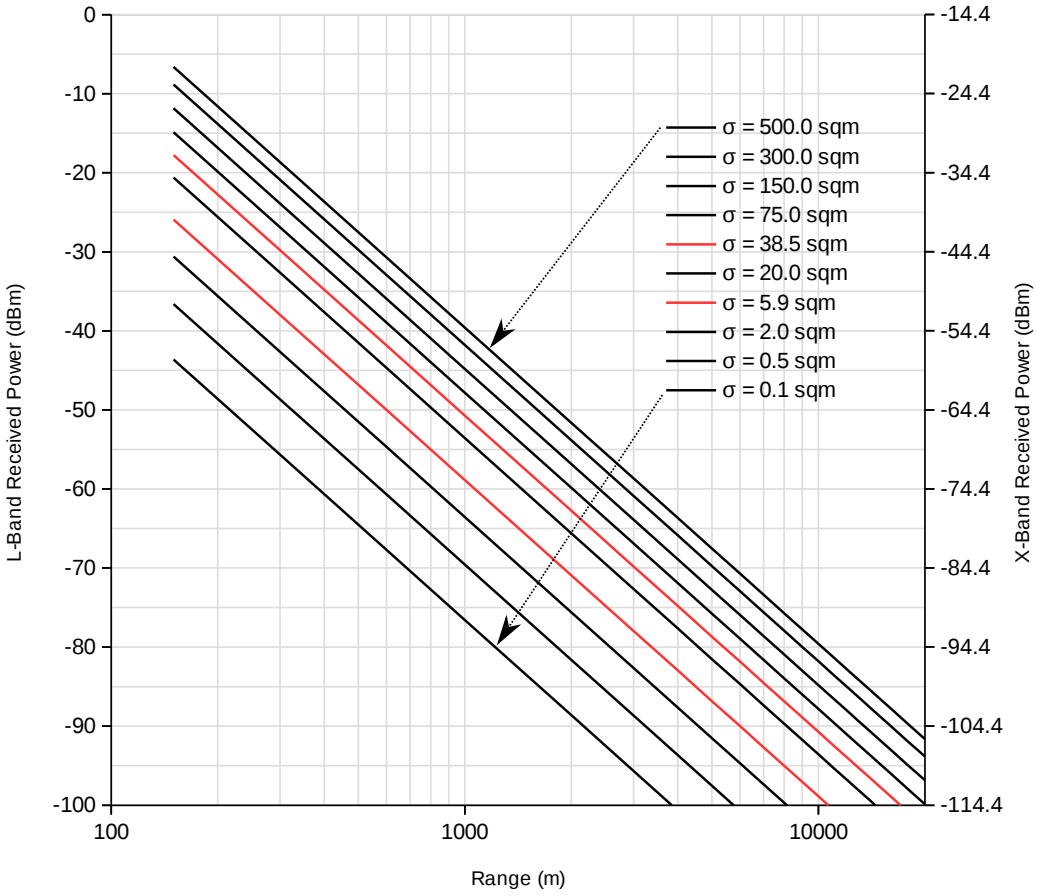

Figure 4.10: Plot of received power levels, as a function of range, for different sized targets. L-band power levels are indicated on the left axis, and X-band power levels on the right. The red curves represent the reference target.

maximum input power level limits for all values of target range and RCS. For the the two operating bands the maximum received power levels were found to be $P_{R_L} = -6.63\,\text{dBm}$ and $P_{R_X} = -21.0\,\text{dBm}$, which was less than the large signal input level used for the cascade analyses.

Continuing with the target returns through the Rx front ends, we wish to have a nominal power level of around $P_o \approx 0\,\text{dBm}$ at the input to the REX (and subsequently its IF output as well, due to the internal REX gain of 0 dB). The linear RF front end gain values were previously found to be $G_L = 15.46\,\text{dB}$ and $G_X = 26.84\,\text{dB}$ respectively, which meant that we required $P_{R_L} \approx -15.46\,\text{dBm}$ and $P_{R_X} \approx -26.84\,\text{dBm}$ to achieve an IF power level $P_{IF} \approx 0\,\text{dBm}$. These values are achievable only for targets approximately 150 m from the radar (i.e. at the system's minimum blind range) and with $\sigma_L \gtrapprox 75\,\text{m}^2$ and $\sigma_X \gtrapprox 150\,\text{m}^2$.

Since most targets would fall outside of these range and RCS values, the internal VGA in the REX needs be used to achieve an additional gain of up to 31 dB to increase the amplitude of the echo. This would extend the range for which $P_{IF} \approx 0\,\text{dBm}$ would be achievable to $R_L \approx 1\,500\,\text{m}$ and $R_X \approx 1\,250\,\text{m}$, dependant on the target RCS.

For distant or small targets producing an IF output signal below 0 dBm (after using the internal REX VGA), detection is still possible but as this signal gets weaker and approaches the noise floor detectability degrades until the SNR is eventually too low to detect anything meaningful.

4.2.3 Signal to Noise Ratio

As has just been illustrated, not all targets will produce a sufficiently large return to meet the desired $P_{IF} \approx 0\,\text{dBm}$, and these returns would also vary significantly due to the nature of the target and scene of interest. The SNR is therefore more valuable than absolute power level as it describes how easily a target return can be distinguished from noise as it passes through the receiver.

The equation for SNR is a combination of the previously discussed noise power and target returns, and since pulse compression waveforms are used, it also incorporates the time-bandwidth product or pulse compression gain, τB. It is formally

Table 4.2: System parameters used for calculating the SNR as a function of range, as seen at the receiver IF output.

Parameter	L-band	X-band	Units
Transmitted Power, P_t	59.85	54.34	dBm
Antenna Gain, G	19.65	23.37	dB
Wavelength, λ	0.231	0.035	m
Target RCS, σ	0 – 500		m^2
Receiver Noise Figure, F	6.51	3.88	dB
Pulse Width, τ	10	10	μs
IF Bandwidth, B	50	50	MHz
System Losses, L_s	0	0	dB
Target Range, R	150 – 20000		m

defined as [13]:

$$SNR = \frac{P_t G^2 \lambda^2 \sigma}{(4\pi)^3 R^4 k T_0 F B L_s} \tau B = \frac{P_t \tau G^2 \lambda^2 \sigma}{(4\pi)^3 R^4 k T_0 F L_s} \tag{4.7}$$

where the variables are the same as used in Equations 4.6 and 4.4, but for system losses we let $L_s = 0\,\text{dB}$ since losses have previously been accounted for in P_t.

For a radar observing a scene using a given pulse width τ, the SNR is a function of two variables: target RCS σ, and target range R. It is therefore necessary to evaluate the SNR as a function of both σ and R to understand the expected real-world performance of the system. In particular, we are interested in the SNR at the final IF output port, and as such the receiver parameters for the combined front end and REX, as shown in Table 4.2, are taken into account for the calculations.

A graph of the SNR as a function of range, at the IF output, for the same set of discreet RCS values as used for the received power calculations is shown in Figure 4.11. Whilst the receiver signal processing is beyond the scope of this dissertation, it was necessary to determine a minimum SNR for target detection in order to do the performance analysis. In [13] it is shown that for a probability of detection $P_d = 0.8$, an SNR = 10 dB corresponds to a probability of false alarm $P_{FA} = 10^{-4}$ (for a coherent detector with single pulse). This was considered an acceptable combination of P_d and P_{FA}, thus SNR $\geq$ 10 dB was selected for detection (this value is also suggested in [29]). Using this threshold we can see from the graph in Figure 4.11 that a target as small as $\sigma = 0.1\,\text{m}^2$ would be discernible up to $R = 6\,\text{km}$ at L-band and $R = 3\,\text{km}$ at X-band. For the previously defined

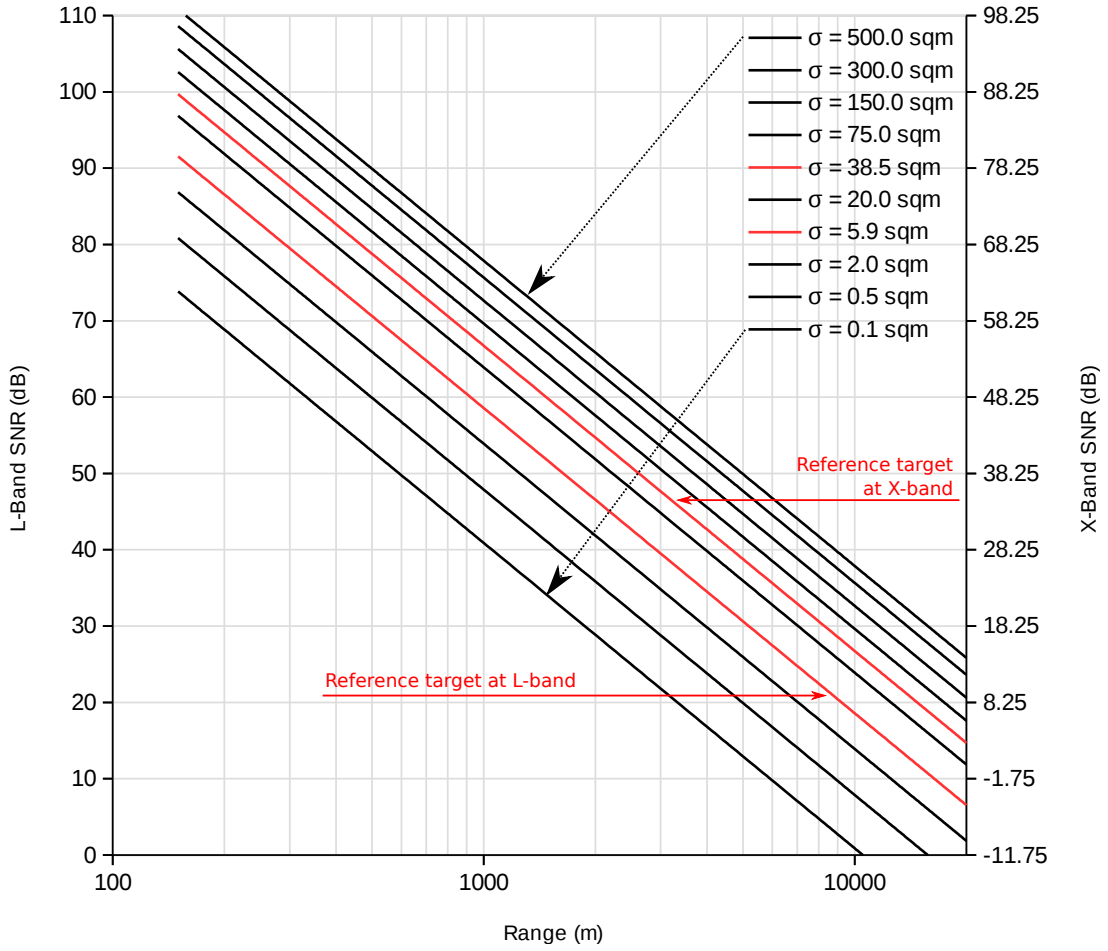

Figure 4.11: Plot of SNR at the IF output of the REX for targets of different sizes in both frequency bands. Red curves represent the reference target in the two different frequency bands ($\sigma_L = 5.88\,\mathrm{m}^2$ and $\sigma_X = 38.5\,\mathrm{m}^2$).

reference target we see detection up to $R \approx 16\,\mathrm{km}$ at L-band, and $R \approx 13\,\mathrm{km}$ at X-band, as a result of the 3.59 dB higher SNR at L-band.

4.3 Summary

The front end design was analysed through the use of a cascade analysis in order to check the power levels at each stage through the chain. Using this process, the transmitter output power level was predicted to be 59.85 dBm at L-band and 54.34 dBm at X-band.

Analysis of the receiver chains included calculations of the expected front end noise figure and gain. Here the L-band front end noise figure was calculated as

2.20 dB and the small signal gain 15.46 dB. The maximum output power level in limiting mode, based on the component selection and design, was determined to be 8.50 dBm. Similarly for X-band, the analysis yielded a front end noise figure of 3.50 dB, a small signal gain of 26.84 dB and a maximum output power level of 16.34 dBm in limiting mode.

The front end design was also implemented in *SystemVue* in order to do a more accurate design verification. Here it was found that the X-band transmitter input power level would be too low, and the attenuation at the input port would need to be reduced by 3 dB. Analysis of the rest of the chains revealed an expected X-band transmitter output power level of 53.69 dBm and L-band output of 59.25 dBm.

Signal integrity through the front end was also considered. Using the antenna gain values for the antennas designed for the system, and the approximated RCS of a boat used as a reference target, the target return at L-band was shown to have a 3.59 dB higher SNR at the IF output of the receiver than for the X-band return from the same target. This reference target was also determined to be detectable up to a range of approximately 16 km at L-band and 13 km at X-band, due to the larger electrical size of the target at X-band. This applied for an assumed minimum SNR of 10 dB.

The successful completion of this phase indicated that the design met the requirements set out in Section 3.1, with the exception of those which could not be achieved within the project budget. The components could thus be acquired and the front end built and tested.

Chapter 5

Testing and Integration

All components for the RF front end were individually tested in order to verify that they were in conformance with the specifications published in the datasheets. Once each components performance had been verified, it was integrated into the RF subsystem in order to evaluate the overall performance and compare it with that of the subsystem model.

Since most of the components used for the RF front end were COTS units, minimum and typical performance specifications were readily available in the product datasheets. Unfortunately these values do not provide insight into the true performance of the specific units delivered. More importantly, since the design bandwidth of the components may be significantly wider than the operational bandwidth of the system, it is possible that the performance within the operational bandwidth may be better than specified in the datasheets.

For this reason all components were lab tested to verify their performance, particularly within the system bandwidth, in order to more accurately predict the system performance. For the small number of components which were supplied with certificates of conformance (CoC), these tests were repeated, where possible, in order to eliminate any variation in the test setup used by the manufacturer. This is important in the case where functionally equivalent components were supplied by different manufacturers (as a result of the dual band requirement), since acceptance test procedures (ATPs) may differ from manufacturer to manufacturer.

5.1 Component Testing

Component testing was limited to those parameters which were of importance to the system design. Test results therefore contain data for only certain parameters and not all parameters specified in the datasheets. The basic test procedure is described in each components respective section.

As discussed in Section 3.3, budgetary restrictions resulted in a need to modify the system design in order to obtain a working system, albeit with a reduced functionality set. This resulted in a reduction in the number of components required for the initial system configuration, but since the intention is to upgrade the system to achieve full functionality once additional funding becomes available, all components which were procured, regardless of whether or not they are used in the initial configuration, were tested. Where more than one of the same component exists, the test results in the tables reflect the worst of the batch.

5.1.1 Power Detectors

The power detectors form part of the HPA performance monitoring system, with the primary intention being to measure the peak transmitted and reflected power levels. This, however, could be extended to perform some degree of pulse characterisation (discussed further in Section 5.1.3) *in situ*, rather than taking the system offline to perform testing with a peak power meter — a device which UCT does not possess. It was therefore decided that part of the test procedure for the power detectors would include the measurement of the HPA pulse envelope to confirm its suitability for such implementation in future.

Testing of the power detectors involved determining its transfer function in order to map the detected power levels to the corresponding output voltage for sampling by an ADC in the monitoring system. This was done by injecting a CW RF signal of known amplitude and measuring the detector output voltage using an oscilloscope set to $1M\Omega$ input impedance.

The results of the tests, conducted at room temparature, showed that in the linear region the output voltage V was related to the input power $P(dBm)$ by the equations:

- $P_L(dBm) = \frac{V-1.02}{-0.0240}$ for L-band ($f_0 = 1.3\,\text{GHz}$)

- $P_X(dBm) \approx \frac{V-1.44}{-0.0234}$ for X-band ($f_0 = 8.5\,\text{GHz}$)

This deviates slightly from the datasheet, where the slope is given as $-0.025\,\text{V}$ up until 8.0 GHz. In contrast, at 8.5 GHz the deviation is to be expected since the power detector is not specified for operation at this frequency. Note that at $f_0 = 8.5\,\text{GHz}$ the detector response is non-linear and the above equation is therefore an approximation only.

The power detectors contain a temperature output pin to allow for temperature compensation, but without an environmental test chamber, determining the effect of temperature variation cannot be done reliably. Referring to the datasheet, it was found that the output voltage could vary by approximately 10 mV across the detectors operational temperature range spanning $-40\,^\circ\text{C}$ to $+85\,^\circ\text{C}$. This translates to a worst case error of 0.41 dB if temperature compensation is not done. The datasheet contains graphs to illustrate the effects of temperature on the output voltage, but interpolating and extrapolating the effects for the specific frequencies of interest cannot be done to a sufficient level of accuracy to warrant inclusion in the transfer function. The equations therefore apply at $25\,^\circ\text{C}$.

Figure 5.1 shows the error resulting from the use of the above derived X-band equation for power measurements at $f_0 = 8.5\,\text{GHz}$. The X-band equation can be modified slightly to minimize the error at the input power level corresponding to the output level at the coupled port during normal operation i.e. for a peak HPA output power level of 56.5 dBm, the measured output power as a result of the coupler and attenuator would be 1.5 dBm, thus the equation should be modified to minimise the error at an input power level of 1.5 dBm.

The transfer function could be investigated further to obtain a more accurate second order function, but it is suggested that the monitoring system implement a lookup table instead, in order to reduce the computational complexity. Since development of the monitoring and control system is beyond the scope of this project, the implementation method is not considered further.

Results of the HPA pulse envelope measurements using the detectors are shown in Section 5.1.3.

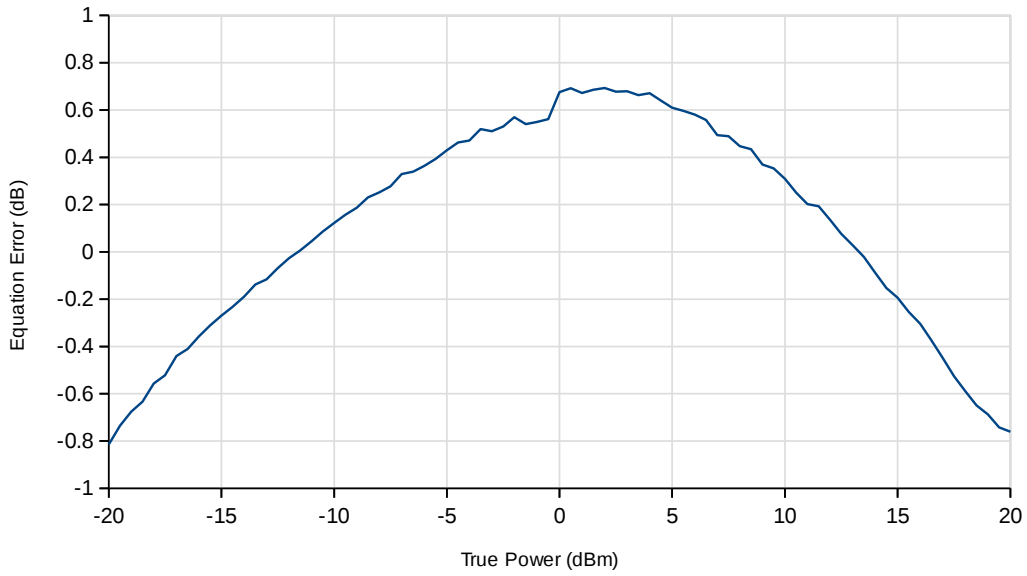

Figure 5.1: Measurement error resulting from derived voltage-power relationship equation for *Mini-Circuits* power detectors at 8.5 GHz.

5.1.2 Dual-Directional Couplers

For the coupler testing we refer to the input and output ports of the direct (or 'through') line as P1 and P2, and the forward and reverse coupled ports as P3 and P4 respectively. Insertion loss is then measured between P1 and P2, forward coupling between P1 and P3, and reflected or reverse coupling between P2 and P4.

The L-band coupler (*ATM* CHP273-30F-30R) was tested from 1.2 – 1.4 GHz, and X-band (*ATM* CH235H-35) tested from 8.4 – 10.6 GHz. Using a network analyser, the insertion loss, return loss and coupling was measured. Isolation and directivity are not of critical importance to this application, and were thus not evaluated. Figure 5.2 shows the port numbers and how the S-parameters relate to them.

For this application the most critical specification for the coupler is the insertion loss, as this determines how much power is lost between the input and output ports, and thus the reduction in power delivered to the antenna as a result of the use of the directional coupler for monitoring.

For the L-band coupler shown in Table 5.1, a marginal improvement in the insertion loss was observed, while the return loss had a more significant improvement

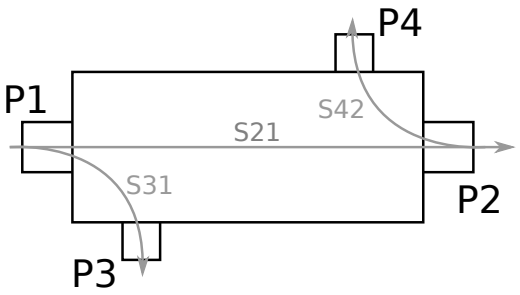

Figure 5.2: Test setup for dual-directional couplers, showing coupler port numbers as used for S-parameters.

Table 5.1: Comparison of manufacturer specifications and test results for L-band dual-directional coupler.

	Specification	Test Result	Units
Applicable Frequencies	1.0 – 2.0	1.2 – 1.4	GHz
Insertion Loss (max.)	0.20	0.11	dB
Input VSWR (max.)	1.20	1.07	:1
Fwd Coupling	30.0 ± 1.0	28.75 ± 0.13	dB
Rev. Coupling	30.0 ± 1.0	29.62 ± 0.10	dB

Table 5.2: Comparison of manufacturer specifications and test results for X-band dual-directional coupler.

	Specification	Test Result	Units
Applicable Frequencies	4.0 – 18.0	8.4 – 10.6	GHz
Insertion Loss (max.)	0.5	0.38	dB
Input VSWR (max.)	1.45	1.17	:1
Fwd Coupling	35.0 ± 1.5	35.96 ± 0.33	dB
Rev. Coupling	35.0 ± 1.5	35.67 ± 0.35	dB

of 3 dB (VSWR of 1.07:1 instead of 1.20:1). Coupling factors are specified as being 30.0 ± 1.0 dB, but test results show them to be lying just outside this range. This is of little consequence to the system configuration. In both cases there was an improvement in the flatness of the coupling factor, with a maximum measured variation of < 0.13 dB across the narrower measurement bandwidth.

The X-band coupler also exhibited good improvements in the narrower measurement bandwidth, with S_{21} showing an improvement of 0.12 dB — which will make a good contribution towards increased transmitter output power. Full results are shown in Table 5.2.

5.1.3 High Power Amplifiers

The HPAs are arguably the most critical components in the RF front end. Their performance, and in particular their peak output power, contribute significantly to the systems detection capabilities. It is thus important to ensure that the verification tests are done carefully in order to obtain accurate test results and to avoid damage to these costly units. Whilst the amplifiers have protection measures built in to prevent any damage occurring due to fault conditions at the RF ports, the effects of faults at the power and control ports are not documented, and as such should be treated as potential points of critical failure in the event of any power or input signal not falling within specification.

In order to avoid such a failure occurring, the power supplies were carefully tested and adjusted to ensure they fell within the permissible voltage ranges and, once connected to the HPAs, special care was taken to ensure that the correct power sequencing (as discussed in Section 3) was followed.

Ideally the HPAs should be tested under all possible operating conditions, which would include variation of the PRF, duty cycle, supply voltage, ambient temperature, input power levels, etc. However, due to time and, primarily, equipment constraints it was deemed impossible to perform an exhaustive verification test procedure on the HPAs, and testing was thus limited to those parameters which could be reliably verified using the equipment on hand.

For a pulsed system there exists a number of pulse parameters which are typically measured in order to assess the systems performance. These parameters, in minimalistic form, are shown in Figure 5.3 and are described as [30]:

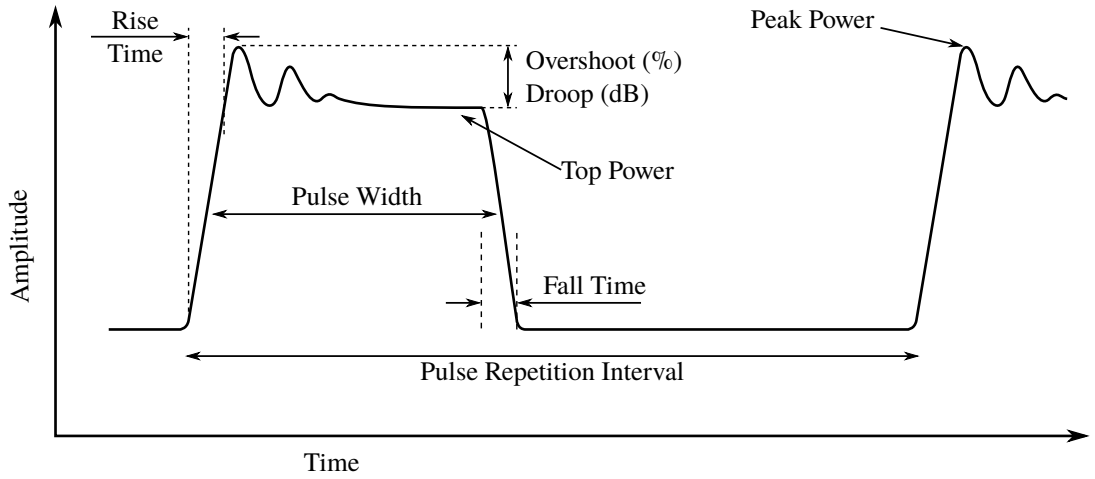

Figure 5.3: Graphical depiction of typical pulse parameters evaluated in a pulsed radar system (adapted from [30]).

- **Rise Time**: time taken for the pulse to transition from 10 % to 90 % of its top power value (power in linear units).
- **Fall Time**: time taken for the pulse to transition from 90 % to 10 % of its top power value (power in linear units).
- **Pulse Width**: the period over which the pulse is above 50 % of its top power value.
- **Top Power**: flat part of the pulse envelope after overshoot and prior to start of the off transition period.
- **Peak Power**: the maximum value attained by a pulse, typically occurring during overshoot.
- **Overshoot**: the difference between the peak power and top power values, given as a percentage of the top power value.
- **Droop**: the difference between the peak and top power, given in dB.

A more extensive discussion on pulse characteristics and parameters can be found in [30], but for the purposes of this system the aforementioned parameters are of most significance.

The full test setup consisted of an RF signal generator for the source, along with an RF peak power meter (obtained from the Institute for Maritime Technology, a division of Armscor SOC) for the measurements. The HPAs were tested with the

output coupler and attenuator in place, as per the front end system diagram, due to the high power levels involved. Whilst the test procedures for the two amplifiers are fundamentally the same, they are discussed separately in order to clarify the subtle differences and performance results.

5.1.3.1 L-Band High Power Amplifier

Lab testing of the L-band HPA required only the application of the +12 V and +50 V supplies. By default, the amplifier is biased when power is applied to it, and inhibiting the system is achieved by applying a TTL low signal to the 'on/off control' pin. In the final system the amplifier will be placed into standby mode between pulses, but for lab testing this was deemed unnecessary.

The output port of the coupler was terminated using a dummy load with power rating of 5 kW peak, 25 W average. Dummy loads usually specify a maximum pulse duration for the peak power rating, commonly 5 μs, however the load in question did not provide this information. In order to avoid damaging the load it was assumed that a 5 μs pulse with peak power of 5 kW would not do any damage to it. From this, the pulse energy for the given pulse width was calculated [31]:

$$E = \tau \times P_{pk} = 5\ \mu s \times 5\ kW = 0.025\ J$$

where τ is the pulse width and P_{pk} is the peak pulse power. For the L-band HPA, the maximum pulse width which would result in the same amount of pulse energy being absorbed by the load, with an assumed $P_{pk} = 1\,600$ W, was determined to be:

$$\tau = \frac{E}{P_{pk}} = \frac{0.025\ J}{1\,600\ W} = 15.625\ \mu s$$

The pulse width was therefore kept below 15 μs for the first few tests, with the duty cycle kept extremely low (approximately 0.1 %) in order to stay below the maximum average power rating of 25 W (assuming a peak power of 1 600 W, a duty cycle of 0.1 % results in an average power of only 1.6 W). Testing was also done with a minimal number of 100 μs pulses in order to ascertain the performance at maximum anticipated pulse width.

A power sweep was conducted in order to determine the HPA gain and compression points. This involved sweeping the input power from −10 dBm to +10 dBm and measuring the corresponding output power level. The results of this power

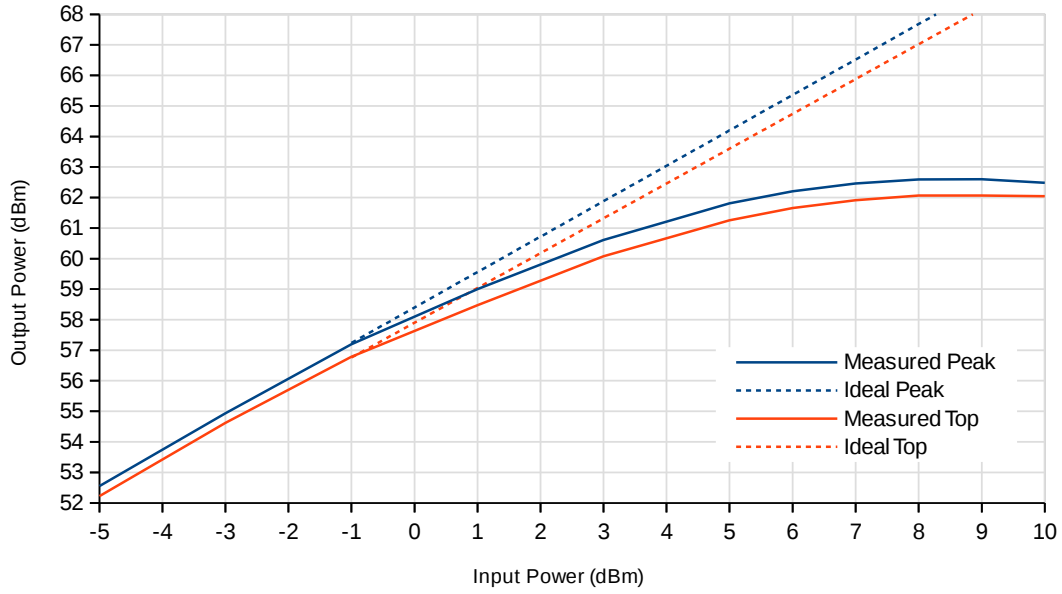

Figure 5.4: L-band HPA gain compression curves, showing peak power and pulse-top amplitude.

sweep are shown in Figure 5.4. From the measurements, and with reference to the curve plotted in Figure 5.4, it was found that the HPA had a peak gain of $G = 58.40\,\text{dB}$ with a peak 1 dB compression output $P_{1dB} = 62.02\,\text{dBm}$ and peak saturated output power $P_{sat} = 62.60\,\text{dBm}$. The separate pulse-top amplitude curve revealed a pulse-top $G = 57.9\,\text{dB}$, $P_{1dB} = 61.64\,\text{dBm}$ and $P_{sat} = 62.06\,\text{dBm}$. From the peak power curve it is also noted that at the recommended input power level of 7 dBm the HPA is operated in compression, with a peak output power level of 62.46 dBm ($\approx 1\,763\,\text{W}$). This output power level significantly exceeds the typical value of 1 200 W specified in the datasheet.

The HPA output pulse envelope for an input pulse of $\tau = 100\,\mu\text{s}$, $P_{in} = 7\,\text{dBm}$ is shown in Figure 5.5. The pulse envelope was obtained using the *Mini-Circuits* power detector, with power levels confirmed using the peak power meter. The resultant pulse characteristics are summarised in Table 5.3.

5.1.3.2 X-Band High Power Amplifier

Testing of the X-band HPA focused primarily on the power levels due to the fact that the pulse rise and fall times were too small to measure with the power detectors. The test setup consisted of the HPA and coupler (as per the system diagram) with a dummy load terminating the output, precisely as was done for

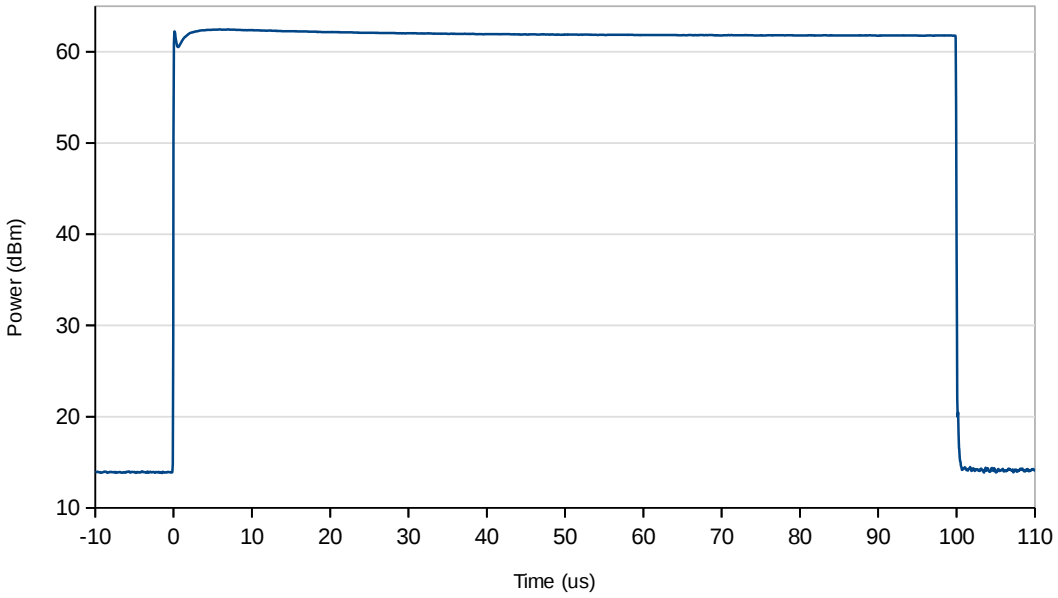

Figure 5.5: Output pulse envelope for the L-band HPA, measured with the *Mini-Circuits* power detector, with $P_{in} = 7\,\text{dBm}$, $\tau = 100\,\mu\text{s}$.

Table 5.3: L-band HPA pulse test results, showing typical manufacturer specification (over HPA bandwidth) compared with measured results (over system bandwidth) with $P_{in} = 7\,\text{dBm}$, $\tau = 100\,\mu\text{s}$.

	Specification	Test Result	Units
Peak Power ($P_{in} = 7\,\text{dBm}$)	60.79	62.46	dBm
Pulse Droop (max)	0.50	0.56	dB
Small Signal Gain (min)	54.00	58.40	dB
Rise Time	200	52.50	ns
Fall Time	200	not tested	ns

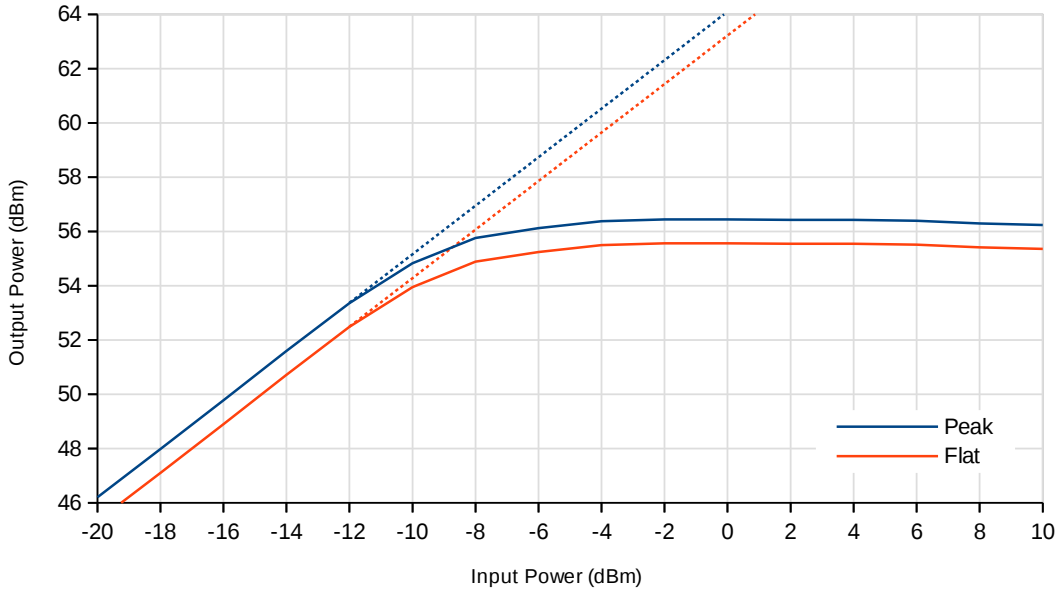

Figure 5.6: X-band HPA gain compression curves, showing peak power and pulse-top amplitude.

the L-band HPA. The availability of a suitable load for the X-band tests meant that 100 μs pulses and duty cycles up to 10 % could be used.

A power sweep from −20 dBm to +10 dBm was done in order to determine the amplifier gain, 1 dB compression and saturation points. The results of this power sweep, shown in Figure 5.6, revealed the small signal gain to be significantly larger than specified, whilst the 1 dB compression and saturation levels were within specification. These values, summarised in Table 5.4, reveal that for maximum output power the input power level should be at 0 dBm, and not +3 dBm, as determined during the design phase. The front end was thus modified by removing the pre-amp and attenuators preceding the HPA.

Due to the fast rise and fall time of the HPA, it was also not possible to get an accurate measurement of the pulse overshoot using the peak power meter. The pulse envelope shown in Figure 5.7 therefore may not be a true reflection of the overshoot and peak power of the HPA.

5.1.4 Limiters

Limiters were tested using a vector network analyser (VNA) for insertion loss measurements in linear operation, and a signal generator and peak power meter

Table 5.4: X-band HPA pulse test results, showing typical manufacturer specification (over HPA bandwidth) compared with measured results (over system bandwidth) with $P_{in} = 0\,\text{dBm}$, $\tau = 100\,\mu\text{s}$.

	Specification	Test Result	Units
Small Signal Gain	≥ 53	≥ 65	dB
P_{1dB} Output	+55.5	+55.85	dBm
Saturated Output	+56.5	+56.45	dBm
Pulse Droop	Unspec.	0.88	dB

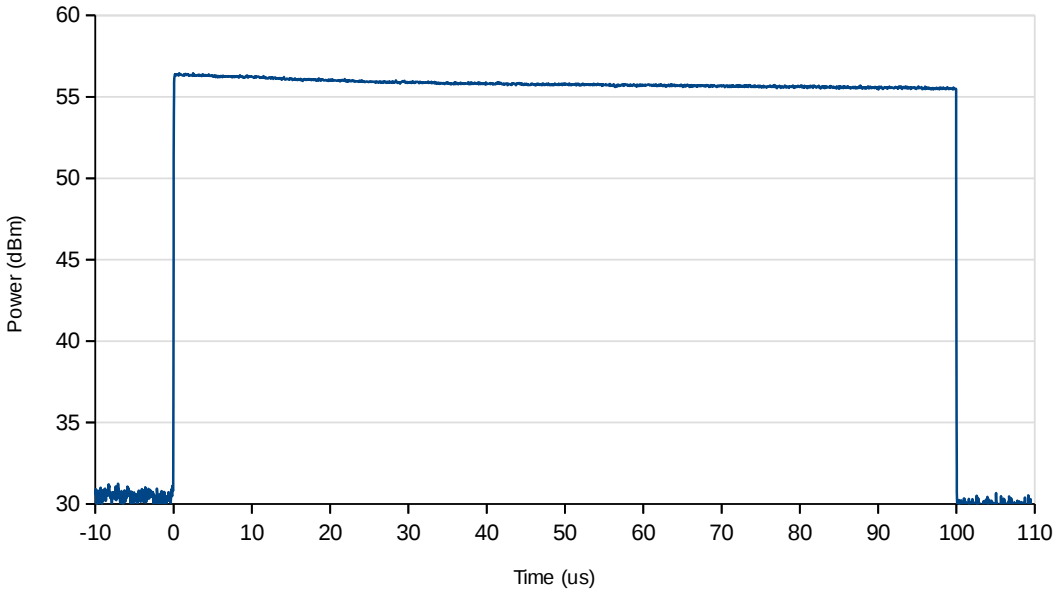

Figure 5.7: X-band HPA pulse envelope with $P_{in} = 0\,\text{dBm}$ and $\tau = 100\,\mu\text{s}$. Overshoot and peak power may not be accurate due to the rise time of the peak power meter and power detector being slower than the HPA.

Table 5.5: Comparison of manufacturer specifications and test results for limiters.

	L-Band		**X-Band**		
	Specification	Test Result	Specification	Test Result	Units
Applicable Freq.	1.2–1.4	1.2–1.4	8.0–12.0	8.4–10.6	GHz
Insertion Loss	0.22	0.30	1.50	1.80	dB
Input P_{1dB}	Unspec.	9.00	5.00 (typ.)	> 6.95	dBm
Flat Leakage	11.50 (typ.)	> 13.50	13.00	6.76	dBm

for leakage power in limiting and non-linear operation. A power sweep was done in order to determine the point at which compression begins, as well as the peak and flat leakage output power levels when using a pulsed input. A 100 μs pulse with maximum power level of 20 dBm was used, as well as a CW input for comparing flat leakage in pulsed and CW mode. The results for both L- and X-band limiters are provided in Table 5.5

A number of important observations were made. Most significantly, the L-band limiters failed to meet the manufacturer specifications, producing a leakage value in excess of 13.5 dBm at an input power of 23 dBm. This applied to all three of the units which were tested. Performance at the input limit of 34 dBm remained untested but was expected to further exceed the specification, which is evident from the input-output power relationship shown in Figure 5.8. This is a major point of concern, which requires further consultation with the manufacturer.

Testing of the X-band limiters showed a leakage value well below the specification. This was confirmed by the CoC, which indicated a CW leakage of 6.7 dBm (s/n: 0109) and 7.6 dBm (s/n: 0110) for an input of 33 dBm. Insertion loss, however, failed to meet the datasheet specification as well as the CoC at the upper end of the measured band of interest, producing a maximum of $S_{21} = -1.80$ dB at 10.57 GHz for limiter s/n: 0109 and $S_{21} = -1.64$ dB at 9.82 GHz for s/n: 0110. Inspection of the CoC graph suggested that a fewer number of frequency points may have been used by the manufacturer during measurements, possibly leading to the discrepancy. This does not create too much of a problem, as the insertion loss at 8.5 GHz falls within specification, and the system is not expected to operate at any of the higher frequencies in the immediately foreseeable future.

Pulse testing at lower power levels indicated the presence of a peak- and flat leakage value, but at higher power levels the flat leakage value approached the

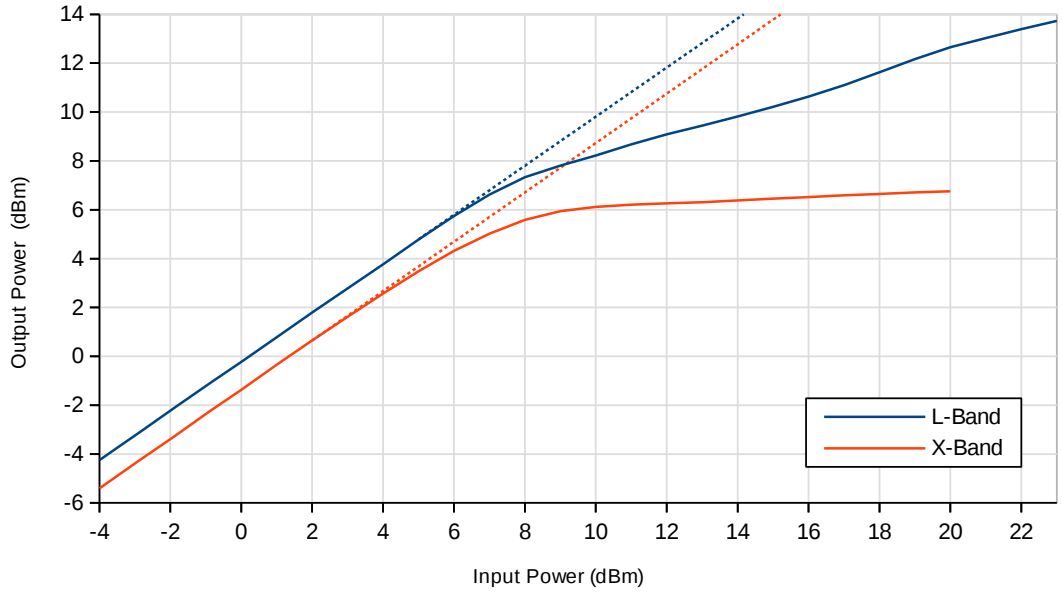

Figure 5.8: Plot of input vs. output power for L- and X-band limiters. Input levels above 20 dBm are unleveled/uncalibrated (due to limitations on the signal generator) and included only to indicate the non-compliance of the L-band units.

peak value, meaning that ratings applied to both peak and flat leakage.

5.1.5 Low Noise Amplifiers

Ideally, testing of the LNAs should, as a minimum, include measurements of gain as well as noise figure. Due to the very low noise figures of the LNAs in question (0.5 – 1 dB), testing had to be limited to measuring the amplifier gain only, since suitable equipment was not available for doing the noise figure analysis. For the X-band LNAs a CoC was supplied with each of them, thus the results of the CoCs were accepted as the true noise figure. For the L-band LNAs only the datasheet values were available.

Results of the LNA tests are shown in Tables 5.6 and 5.7.

5.1.6 Solid State Switch

The L-band solid state switch used for the receive chain was tested for insertion loss, return loss and isolation. The switching speed specified in the datasheet was

Table 5.6: Comparison of manufacturer specifications and test results for L-band *Mini-Circuits* ZX60-P162LN+ low noise amplifier.

	Specification	Test Result	Units
Applicable Frequencies	0.5 – 6.0	1.2 – 1.4	GHz
Gain	20.5 (typ.)	$\geq$ 18.45	dB
Noise Figure	0.56	Not Tested	dB
Input VSWR	1.23	1.19	:1
P1dB	19.70	22.57	dBm

Table 5.7: Comparison of manufacturer specifications and test results for X-band *Amplitech* low noise amplifier.

	Specification	Test Result	Units
Applicable Frequencies	8.5 – 10.5	8.4 – 10.6	GHz
Gain (min)	30.00	30.10	dB
Noise Figure (max)	1.00	0.94 (CoC)	dB
Input VSWR (max)	2.00	1.69	:1
P1dB (min)	15.00	17.00	dBm

35 ns which is significantly shorter than the minimum radar pulse width to be used, meaning that even if the switch falls outside of this specification, it would still have ample time to switch the receiver polarisation before the next pulse arrived. This very short switching time is also shorter than the rise time of the peak power meter (100 ns), which meant that this specification could not be tested.

The switch was tested as a 3-port device, with the common terminal designated as P1 and the two switching terminals as P2 and P3, as shown in Figure 5.9. Using these port designations, insertion loss is represented by the equivalent S-parameters S_{21} or S_{31} when the switch is set to position P2 or P3 respectively. Isolation is defined in two ways: isolation between the common port and the

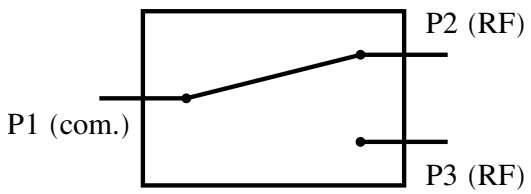

Figure 5.9: Port designations for the L-band solid state receive switch.

Table 5.8: Comparison of manufacturer specifications and test results for L-band solid state receive switch.

	Specification	Test Result	Units
Applicable Frequencies	0.5 – 6.0	1.2 – 1.4	GHz
Insertion Loss S_{21}, S_{31} (max.)	1.7	1.05	dB
Isolation, Com-RF S_{31}, S_{21} (min.)	55.0	60.71	dB
Return Loss, Open S_{22}, S_{33}	13.0 (typ.)	13.74 (min.)	dB

inactive RF port, i.e. in S-parameters S_{31} when P2 is connected to common, and S_{21} when P3 is connected to common; and isolation between the two RF ports, i.e. S_{32} or S_{23}. For this application we are only interested in S_{21} and S_{31}.

The test results, as provided in Table 5.8, reveal that the performance of the switch is significantly better within the band of interest than listed in the datasheet. The biggest benefit of the improved performance will come from the lower insertion loss figure. Since the SPDT switch is one of the first components after the receive antenna, its insertion loss influences the noise figure for the entire receive chain. The lower insertion loss thus results in a lower noise figure for the receive chain, which will improve overall receiver performance (SNR).

5.1.7 L-Band Receive Filter

The L-band filter, donated by RRS, was used for the receive filter due to its excellent insertion loss. The product specification claimed an insertion loss of 0.2 dB within the passband 1.235 – 1.365 GHz. Testing of the filter revealed an $S_{21} \geq -0.22\,\text{dB}$, and $S_{11} \leq -22.85\,\text{dB}$ within the passband. The filter response is shown in Figure 5.10.

5.1.8 Circulators

The circulators were not to be used in the initial system, but were tested anyway since they had been acquired and were to be used in future. Testing was conducted with a network analyser and involved measuring the insertion loss, isolation and VSWR at each of the pairs of ports (or individual ports, as applicable). Since this is a 3-port device, the S-parameter S_{nm} refers to the loss of power as the signal travels from port m to port n, where the direction of circulation is also

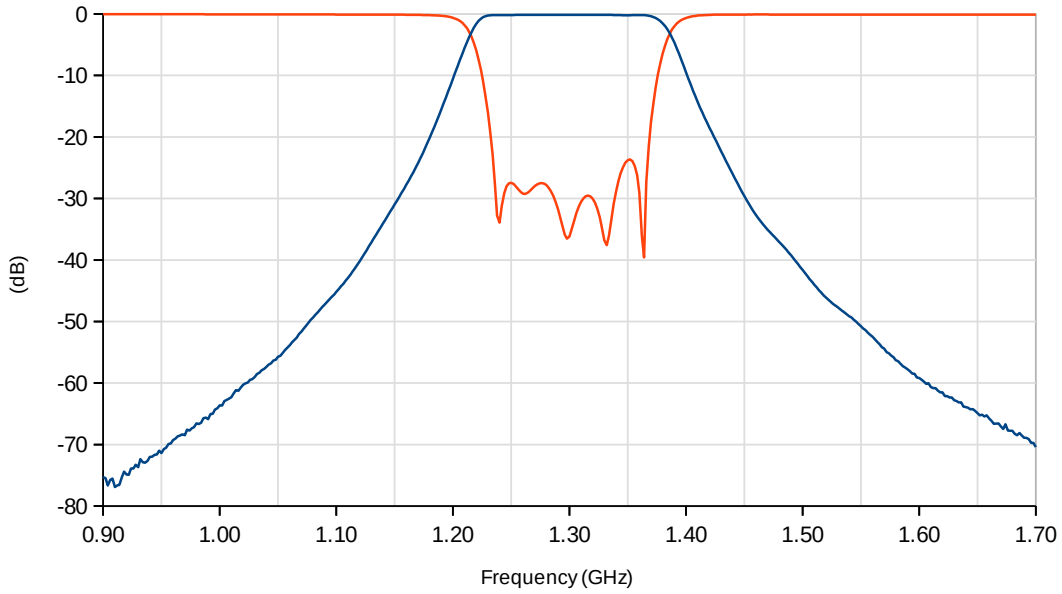

Figure 5.10: Response curve for L-band receive filter donated by RRS.

Table 5.9: Comparison of manufacturer specifications and test results for L-band circulators.

	Specification	Test Result	Units
Applicable Frequencies	1.2 – 1.4	1.2 – 1.4	GHz
Insertion Loss (max.)	0.40	0.30	dB
Isolation (min.)	20.00	23.97	dB
VSWR (max.)	1.25	1.12	:1

from port m to port n. Subsequently, isolation in S-parameter terms S_{mn} refers to the reduction in power at port m when the signal is applied to port n. This is depicted graphically in Figure 5.11.

Test results, as summarised in Tables 5.9 and 5.10, indicated an improvement in all specifications within the reduced bandwidth, with the exception of the VSWR at P3 of one of the X-band circulators, s/n: 122, which was found to be 1.33:1.

5.2 Integration Testing

In this section we measure the performance of the integrated components of the four individual front ends, specifically:

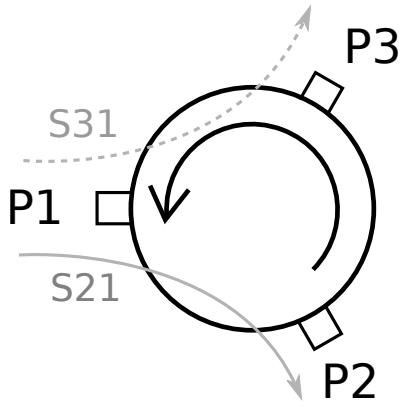

Figure 5.11: Example labelling and measurement convention used for circulator testing, showing the S-parameter equivalent of insertion loss, S_{21}, and isolation, S_{31}.

Table 5.10: Comparison of manufacturer specifications and test results for X-band circulators.

	Specification	Test Result	Units
Applicable Frequencies	7.0 – 11.0	8.4 – 10.6	GHz
Insertion Loss (max.)	0.50	0.43	dB
Isolation (min.)	18.00	19.07	dB
VSWR (max.)	1.30	1.33	:1

- L-band transmitter front end
- X-band transmitter front end
- L-band receiver front end
- X-band receiver front end

These tests focus on the power level at each stage through the front ends, at the systems intended operating frequencies of $f_{0_L} = 1.3\,\text{GHz}$ and $f_{0_X} = 8.5\,\text{GHz}$. Measurements are done between the REX and antenna ports of the various front ends, with the input and output ports as per the respective front end functions i.e. input at the antenna port for Rx front end, and output at antenna port for Tx front end. These measurements do not include cable losses from interconnecting cables, since the final *NeXtRAD* mechanical configuration needs to be determined before these cable lengths can be decided on, but they do include losses associated with adaptors, where applicable. For the majority of the interconnecting cables, this additional unmeasured loss would be small ($< 0.2\,\text{dB}$), with the exception being the antenna feed cables which are accounted for in the system model.

5.2.1 L-Band Transmitter Front End

For the L-band Tx front end, shown in Figure 5.12, we start with the 16 dBm input originating at the REX RF Exciter Chain. This is fed through the 9 dB attenuator to the HPA, followed by the coupler. At the coupler we obtain three output ports, as previously shown:

1. the coupled forward power port, followed by 30 dB attenuator into the power detector,
2. the through path, followed by the filter and polarisation switch,
3. the coupled reflected power port, followed by 30 dB attenuator into the power detector.

Each of these paths are tested separately from input to output. Note that since the L-band filter had not yet been completed, and the Tx polarisation switch not acquired due to cost, the measurement path only goes as far as the output port of the coupler. The power levels at each stage of the through and forward coupled

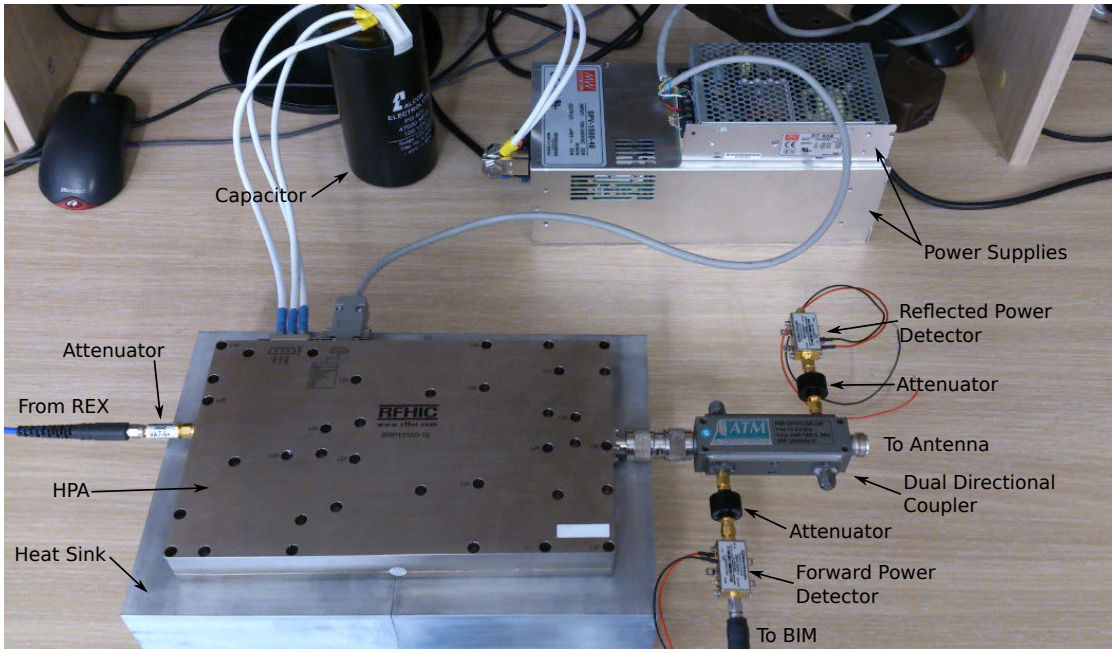

Figure 5.12: Integrated L-band transmitter front end components during lab testing.

paths are shown in Figure 5.13. The final output power level from the front end was found to be 62.16 dBm.

The reflected power path is not plotted since the input power level would be determined by the reflections at the antenna port — a value which is unknown. Testing of this path revealed a total coupling of 59.68 dB at 1.3 GHz, when including the 30 dB attenuator.

The addition of the filter at a later stage will result in a drop in output power level in accordance with its insertion loss, as would the addition of the Tx polarisation switch. In both cases it is recommended that the tests be repeated to verify performance.

5.2.2 X-Band Transmitter Front End

Testing of the X-band Tx front end, shown in Figure 5.14, followed the same philosophy as for L-band. Since testing of the HPA revealed that the maximum output power occurs with an input of $P_{in} = 0$ dBm, the pre-amp and attenuators were removed from the front end design so that the 0 dBm REX X-band RF exciter chain (REC-X) output could be connected directly to the input of the HPA. The cascaded gain and output power levels for the through and forward

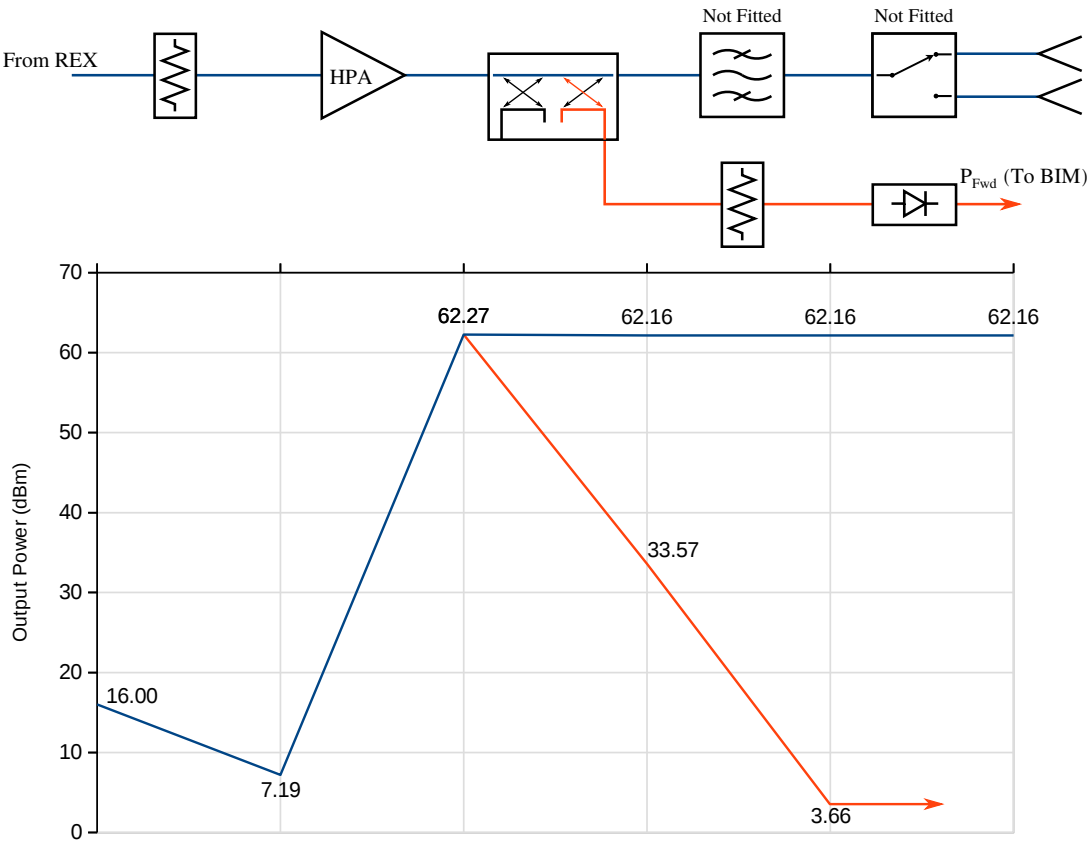

Figure 5.13: Diagram of power levels at consecutive stages through the L-band transmitter front end.

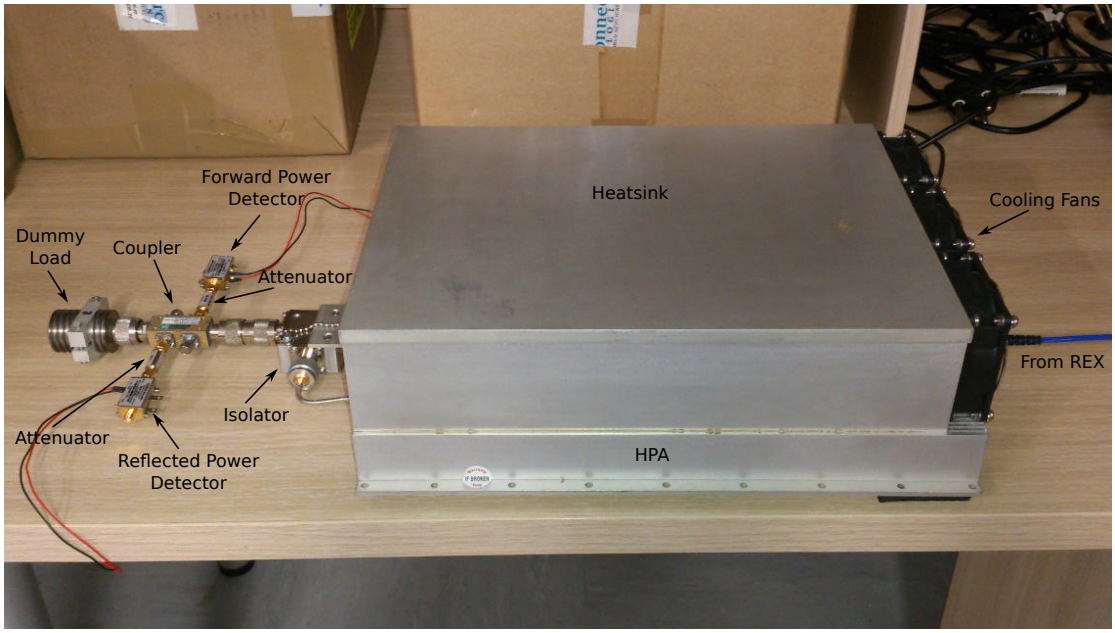

Figure 5.14: Integrated X-band transmitter front end components during lab testing, with a dummy load connected where the antenna feed cable would attach. Power supplies are not shown.

coupled power paths are shown in Figure 5.15. Transmitted power was found to be $P_t = 56.19\,\text{dBm}$. The reflected power port, not shown in the figure, showed a total coupling of 57.45 dB through the coupler and attenuator. As with L-band, the output filter and polarisation switch were not present and the transmit path thus stops at the output of the coupler.

5.2.3 L-Band Receiver Front End

The L-band receiver front end consists of two input paths and a single output path. For the integration testing it was treated as two separate paths, starting at either input (v-pol. or h-pol.) and terminating at the common output. The presence of limiters and the LNA meant that it was necessary to test the small signal and large signal gain, as was done in the simulations. For the small signal gain an input power level of $-20\,\text{dBm}$ was selected, as this was low enough to not cause any of the components to go into limiting or compression. For the large signal gain, a $+20\,\text{dBm}$ signal was used as this was high enough to force the first limiter in the receive chain into limiting mode. The integrated front end, as used for testing, is shown in Figure 5.16.

The results from these tests, shown in Figure 5.17, revealed that the maximum

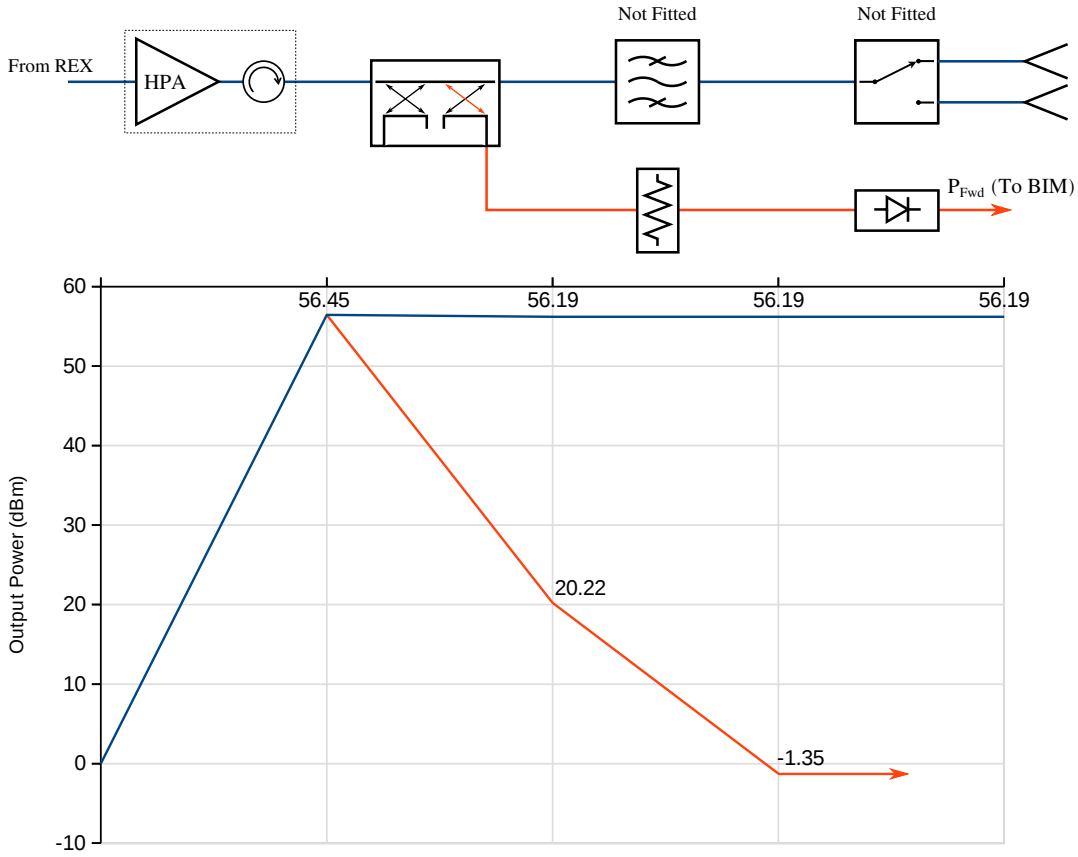

Figure 5.15: Diagram of power levels at consecutive stages through the X-band transmitter front end.

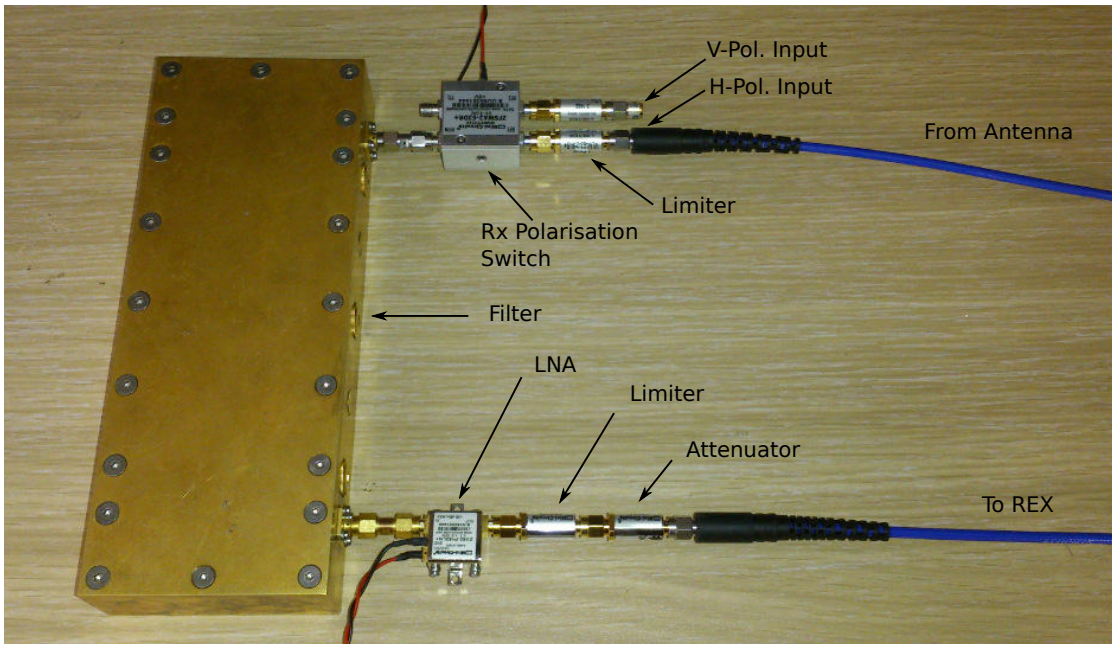

Figure 5.16: Integrated L-band receiver front end components during lab testing.

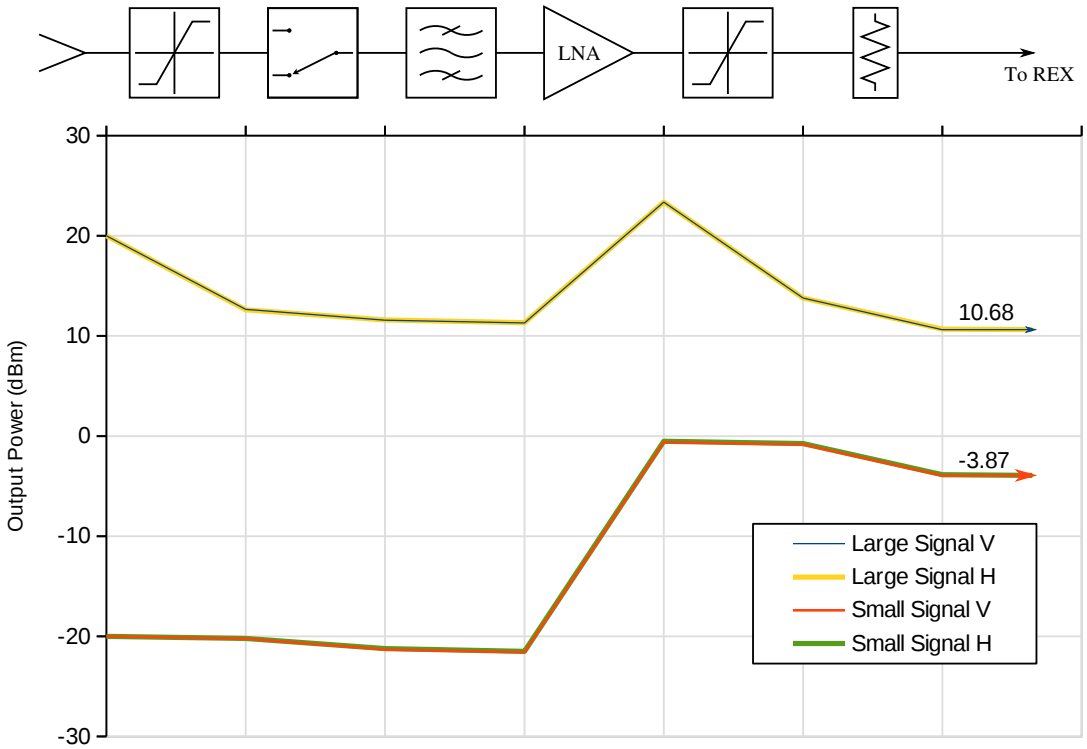

Figure 5.17: Power levels for small (−20 dBm) and large (+20 dBm) input signal through the L-band receiver front end.

output power level for a large signal input exceeded the acceptable REX specifications of 10 dBm. This was to be expected due to the fact that testing of the L-band limiters revealed they did not function within specification.

5.2.4 X-Band Receiver Front End

For the X-band Rx chain we have two separate paths from input to output. The design of the X-band filters were not complete at the time of integration testing and therefore the chain used for testing, shown in Figure 5.18, consisted only of the limiter and LNA for each path. Input power levels of −30 dBm and +20 dBm were used for testing the small signal and large signal gain respectively. The results for the two chains, shown in Figure 5.19, indicate that the maximum output power levels meet the requirements of the REX input.

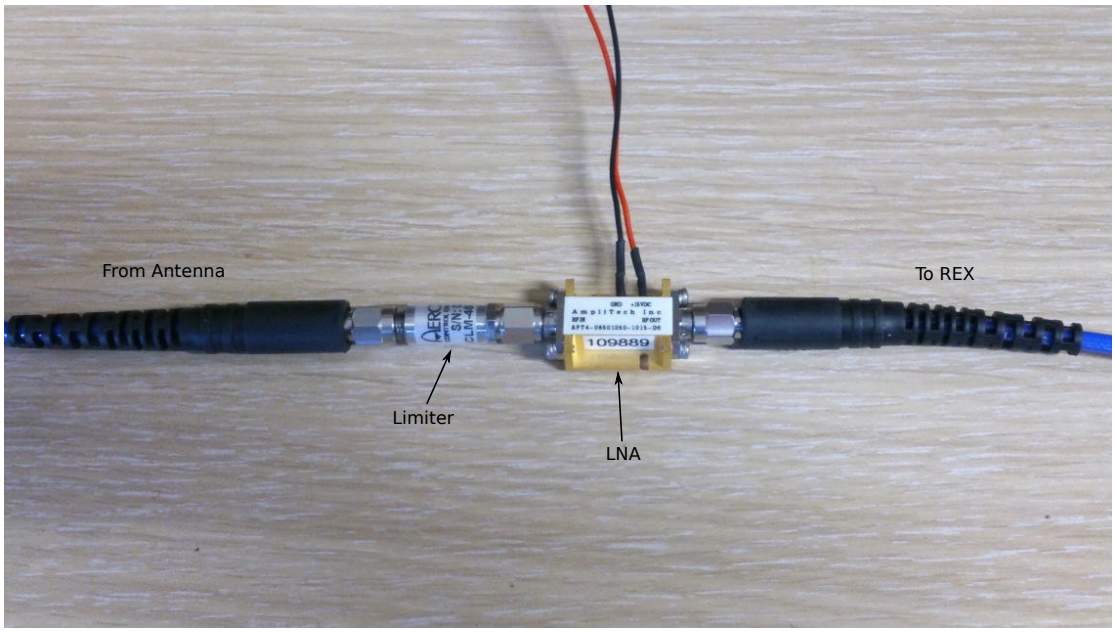

Figure 5.18: Integrated X-band receiver front end components as used during lab testing.

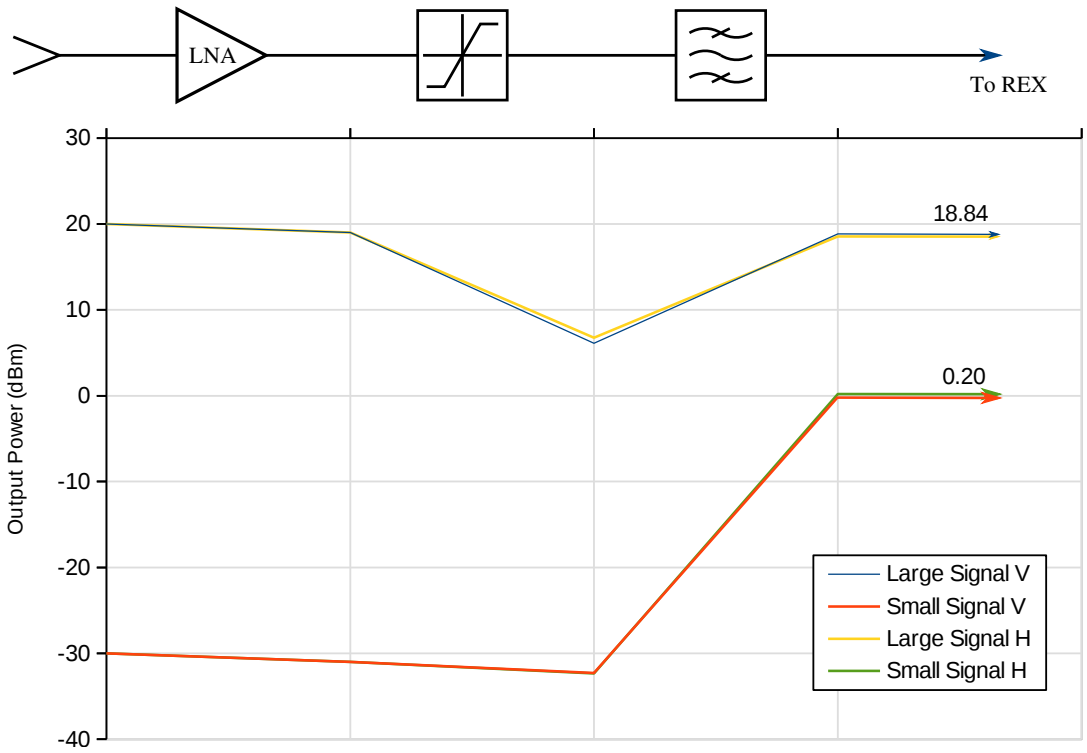

Figure 5.19: Power levels for small (−30 dBm) and large (+20 dBm) input signal through the X-band receiver front end.

5.3 Summary

Testing of individual components as well as the integrated front ends was conducted. This allowed for more accurate determination of component and subsystem performance within the operational bandwidth of the system. Here it was found that while most components exhibited a performance improvement in the reduced operational bandwidth of the system, the L-band limiters and dual directional coupler were outside of their specifications. The non-compliance of the coupler was acceptable as this was on the coupled ports and only required for monitoring. For the limiter, the non-compliance presented a problem as its function is essential for providing the required protection for the receiver.

For the integrated front end chains, a performance improvement was again observed as a result of the improved performance of the individual components. This resulted in a final L-band transmitter output power level of 62.16 dBm, and X-band transmitter output power level of 56.19 dBm. In both cases, this excluded losses resulting from the output filter, polarisation switch and antenna feed cables, since these components were not yet available.

The maximum output power level of the L-band receiver chain was found to exceed the REX input limit by an indeterminate amount due to the non-compliance of the L-band limiters. The X-band receive chains performed as expected, but the receive filter was not included in the measurements as its design had not yet been completed. For both bands the receiver noise figure could not be tested.

This provided the necessary information in order to do a performance comparison between the designed, simulated and actual system.

Chapter 6

Performance Comparison

The original design was done using typical component values based on datasheet specifications. It was therefore expected that the component and integration testing would yield different results to the design calculations. In this chapter a comparison is done between the designed, simulated and actual performance of the integrated front ends. Since the SNR could not be measured, it is recalculated using the results from the integration testing in order to more accurately determine the expected receiver SNR.

This comparison is done at the planned operating frequencies of the two bands ($f_{0_L} = 1.3\,\text{GHz}$ and $f_{0_X} = 8.5\,\text{GHz}$), and the results may therefore differ from those in Section 5, which generally covers the entire operational bandwidth in each frequency band.

6.1 Transmitter Performance

Testing of the Tx front ends revealed an improvement in the performance of most of the components when compared with their specifications. Most notable of these was higher output power for the L-band HPA. The combination of higher HPA output power and lower component losses resulted in a significant improvement in the transmitted power level for the physical system, when compared with the design and simulation. In the case of the L-band Tx front end, the final output power was found to be $P_t = 61.42\,\text{dBm}$ (including assumed filter and antenna feed cable losses), while the design calculations predicted $P_t = 59.85\,\text{dBm}$ and the simulation $P_t = 59.25\,\text{dBm}$. Figure 6.1 illustrates how the design and simulation

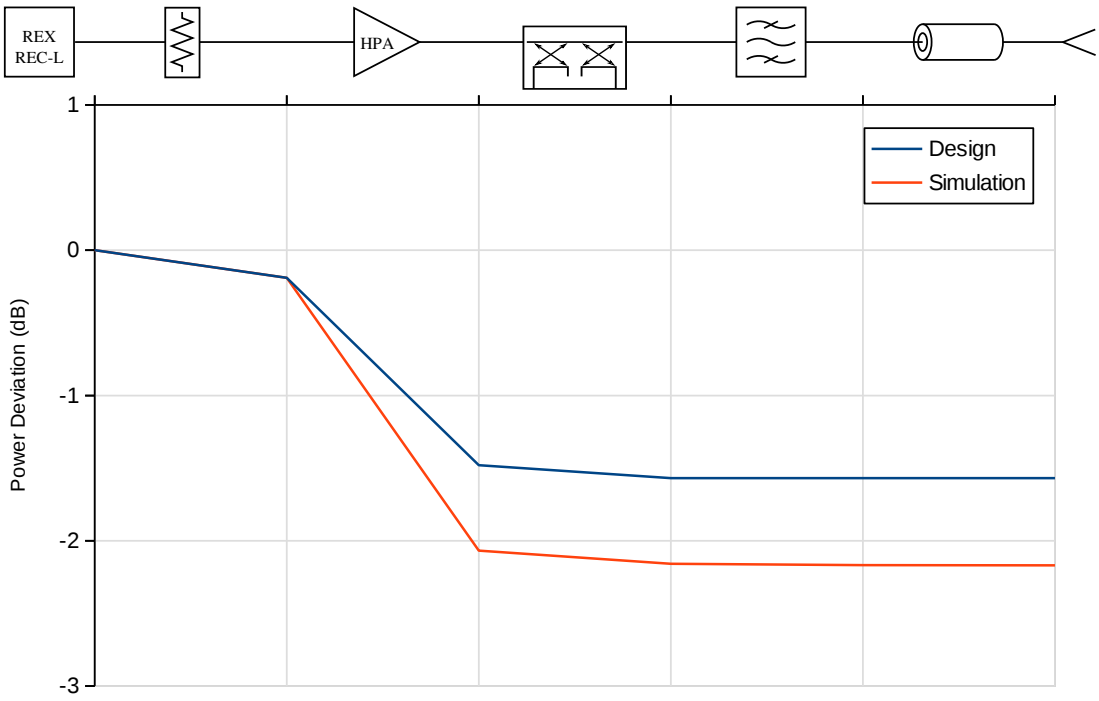

Figure 6.1: L-band transmitter front end design and simulation errors, with reference to the physical system, at respective stages through the front end chain.

power levels deviate from the physical system at each stage through the front end chain i.e. the Y-axis indicates the error (in dB) with reference to the real system.

For the X-band front end, testing revealed that the output power of the HPA was nearly identical to that specified in the datasheets, while the gain was significantly higher. Insertion loss of the coupler was found to be slightly lower than expected, resulting in an overall improvement in the transmitted power level, $P_t = 54.53\,\text{dBm}$ (including assumed losses for filter and antenna feed cable). In comparison, the design calculations and *SystemVue* simulation predicted transmitted power levels of 54.34 dBm and 53.69 dBm respectively. Figure 6.2 shows the deviation of the design calculations and *SystemVue* simulation, with respect to the true performance. Note that the pre-amp, which was removed after component testing, is included in the plot and therefore shows a large deviation due to the fact that it did not form part of the final system.

The accuracy of the simulations conducted during the design phase were dependant on the accuracy of the information provided in the component datasheets. Components performing outside of these specifications, or where specification limits are not provided, cannot be reliably modelled and simulated. This results

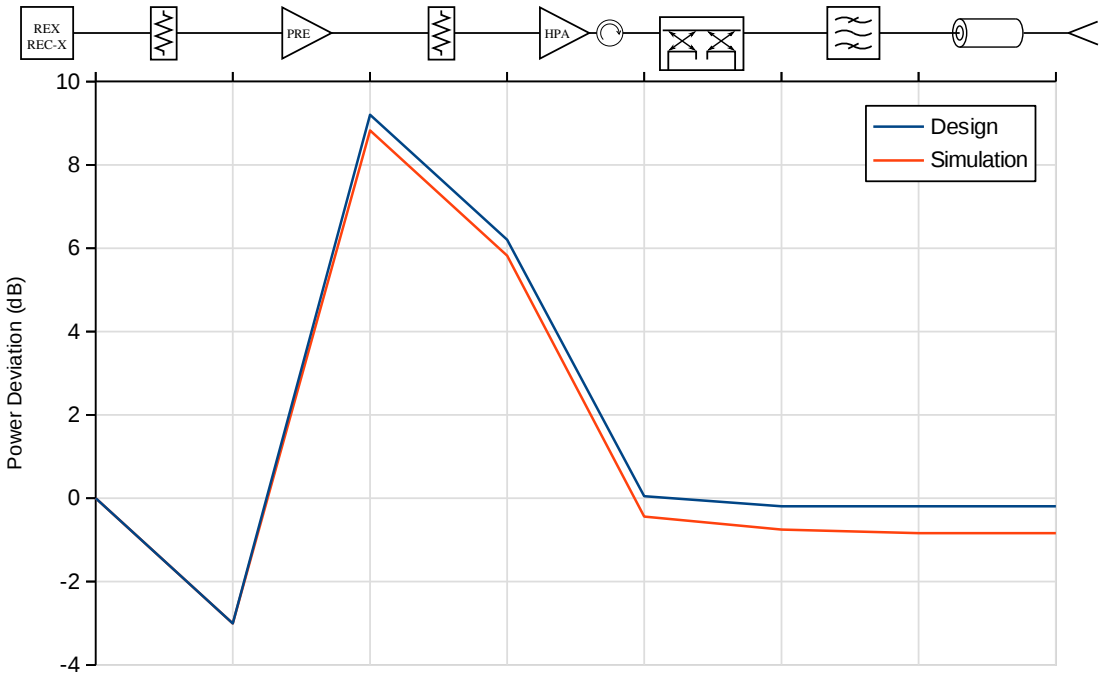

Figure 6.2: X-band transmitter front end design and simulation errors, with reference to the physical system, at respective stages through the front end chain. Removal of the pre-amp and attenuators in the final system (as a result of the higher than expected HPA gain) creates the large deviation seen between the REX and HPA stages.

in hard-to-predict system performance which could deviate significantly from the physical system. This is evident in the L-band HPA performance and resultant transmitter power levels shown above, since the HPA did not specify a maximum output power level and exceeded the typical power level by 1.5 dB.

Another source of inaccuracy in the system model results from the manner in which specifications in some datasheets are provided. Using the L-band HPA as an example again, typical values are provided for input power $P_i = 7\,\text{dBm}$, output power $P_o = 60.79\,\text{dBm}$ and power gain $G = 54\,\text{dBm}$. Using the input power and gain specifications, the corresponding output power should be $P_o = P_i + G = 7+54 = 61\,\text{dBm}$ if operating in the linear region. Since the HPA typically operates in (or just before) saturation mode, for the specified $P_o = 60.79\,\text{dBm}$ we would require $G \geq 54.79\,\text{dB}$ to operate the HPA in compression or saturation mode with a 7 dBm input. This highlights the inconsistencies in the manner in which datasheet specifications are determined, thus affecting the accuracy of the model when making use of these values.

Regardless of the aforementioned inaccuracies, the transmitter front ends were found to exceed their predicted power levels, thus providing an expected overall improvement in system performance.

6.2 Receiver Performance

For the receiver front ends a single chain, corresponding to the v-pol chain, was used for comparison due to the close matching between the two polarisation chains. Here it was found that the output power levels for the physical system exceeded that of the design and simulation. This was acceptable for the X-band front end, but with the L-band front end with a large signal input, the input to the REX was found to exceed the maximum acceptable signal level. This was as a direct result of the L-band limiters not performing acccording to specification.

At L-band a small signal input of $-20\,\text{dBm}$ produced an output of $P_o = -4.19\,\text{dBm}$, while the design and simulation predicted an output of $-4.54\,\text{dBm}$ and $-4.56\,\text{dBm}$ respectively. Note that the output from the physical system has been adjusted to include an expected cable loss of 0.24 dB, as was included in the calculations. The difference in the output power level arose from the fact that the LNA was found to have a higher gain value than specified.

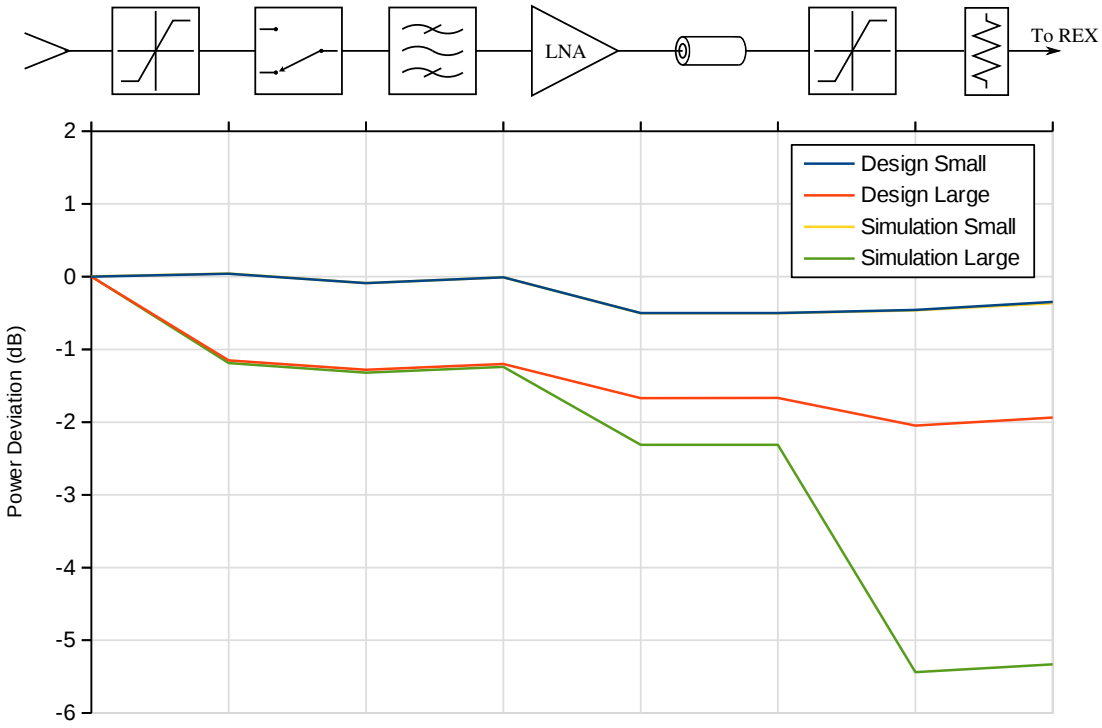

Figure 6.3: L-band receiver front end design and simulation errors, with reference to the physical system, at respective stages through the front end chain.

For the L-band front end with large signal input (+20 dBm), the final output was found to be $P_o = 10.44\,\text{dBm}$, while the predicted values were 8.50 dBm from the design, and 5.11 dBm from the simulation. This is a direct result of the non-compliance of the limiters. The reason for the lower output power from the final limiter in the simulation could not be explained, as the first limiter in the chain produced a leakage output of 11.46 dBm, but the second one produced a leakage power level of 8.11 dBm, even though the same model was used for both. The LNA was also found to produce a higher saturated output power level of $P_{sat} \approx 23.37\,\text{dBm}$ in the physical system — likely due to the fact that the predicted saturation value of 22 dBm, discussed in Section 3.2.2, was based on a supply voltage of 4 V, whilst the tests were conducted using a 5 V supply. Nonetheless, this should not have had any effect on the final output power level if the limiters were functioning within specification.

The L-band variation with respect to the physical system is shown in Figure 6.3.

For the X-band receiver the predicted performance matched the actual system reasonably closely, with a small signal output of $P_o = -0.93\,\text{dBm}$ and correspond-

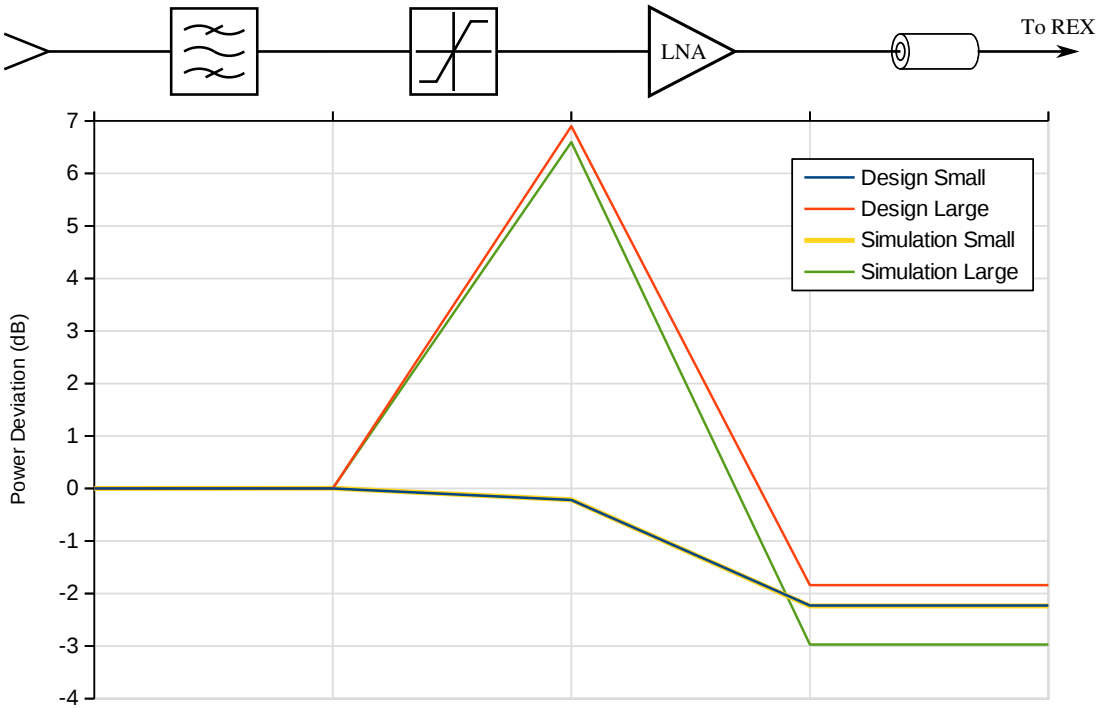

Figure 6.4: X-band receiver front end design and simulation errors, with reference to the physical system, at respective stages through the front end chain.

ing design and simulation results of $-3.16\,\text{dBm}$ and $-3.18\,\text{dbm}$ respectively. The source of this deviation was the LNA, which had a gain of $G \approx 32.5\,\text{dB}$ rather than the specified $G = 30\,\text{dB}$.

For the large signal input the test results also yielded a close match with the predicted values. The limiters, which had a lower leakage output than specified, had little effect on the system since the LNAs are driven into compression before the limiters. This meant that the maximum output power level of the receiver chain was directly related to the LNA saturation value. The result of this was a maximum front end output of $P_o = 18.18\,\text{dBm}$, while the predicted maximum was $16.34\,\text{dBm}$ from the design and $15.20\,\text{dBm}$ from the simulation. This falls below the maximum input level of $20\,\text{dBm}$ for the X-band channels of the REX.

The X-band receiver deviation is shown in Figure 6.4.

Table 6.1: Comparison of initial and revised SNR predictions, after conclusion of integration testing.

	Original		**As Tested**		
Parameter	L-band	X-band	L-band	X-band	Units
Centre Frequency, f_0	1.3	8.5	1.3	8.5	GHz
Wavelength, λ	0.231	0.035	0.231	0.035	m
Transmitted Power, P_t	59.85	54.34	61.42	54.53	dBm
Antenna Gain, G	19.65	23.37	19.65	23.37	dB
Target RCS, σ	5.88	38.45	5.88	38.45	m^2
Noise Figure, F	6.51	3.88	6.29	3.47	dB
IF Bandwidth, B	50	50	50	50	MHz
Pulse Width, τ	10	10	10	10	μs
System Losses, L_s	0	0	0	0	dB
Target Range, R	2 000	2 000	2 000	2 000	m
Signal-to-Noise Ratio, SNR	46.56	42.96	46.78	43.37	dB
SNR Improvement	–	–	0.22	0.41	dB

6.3 Signal-To-Noise Ratio

As a result of the difference between the predicted and tested hardware performance, it was necessary to evaluate how the SNR would be affected by this. Since it was not possible to test the SNR through the receiver, the calculations done in Section 4.2.3 were repeated using the results from Section 5, in order to more accurately determine the expected SNR for the system.

Component values were based on the test results at the intended operating frequency of each band ($f_{0_L} = 1.3\,\text{GHz}$ and $f_{0_X} = 8.5\,\text{GHz}$). In the case of noise figure, which could not be tested, CoCs or datasheets were used, as applicable.

A comparison of the SNR and the parameters used for calculating it is shown in Table 6.1. The SNR was evaluated using the same reference target used previously, but at a fixed range of $R = 2\,\text{km}$. As a result of the increased transmitter power level and decreased receiver noise figure in both bands, the resultant SNR improved by 0.22 dB at L-band and 0.41 dB at X-band. In real terms, this improvement is negligible and translates to an increase in detection range of our reference target by $\Delta R_L \approx 25\,\text{m}$ and $\Delta R_X \approx 48\,\text{m}$.

6.4 Summary

A comparison between the predicted system performance of the theoretical design, *SystemVue* simulation and physical system was presented. The theoretical design and simulation produced closely matched results as they were based on the same specifications provided in the datasheets. Where variations in the results existed, this was mostly due to the different manner in which the *SystemVue* simulation calculated its results.

For the physical system, test results revealed larger than predicted transmitter output power levels for both operating bands. This was due to the L-band HPA having a larger than expected peak power level, and the passive components for both bands having lower losses within the operational bandwidth of the system. For the receivers, the output power levels were also found to exceed their expected performance. For the X-band chain this was due to the slightly higher gain of the LNAs, but remained below the power limit for the receiver inputs. For the L-band chain this was due to the limiters not operating as per the manufacturer specifications, resulting in power levels exceeding the receiver input limits during large signal inputs.

Evaluating the SNR for the system it was found that there was an improvement of only 0.22 dB at L-band and 0.41 dB at X-band, due to the improved front end performance. This translated to a negligible real-world performance improvement, but confirmed that the system met design expectations.

Chapter 7

Conclusion and Recommendations

7.1 Conclusion

As a result of the work conducted in this dissertation, the following conclusions are drawn:

- An RF front end was designed to provide the required functionality for the *NeXtRAD* system. Due to cost constraints the design was modified to provide a reduced functionality set as a first build, with the expectation that the original design be implemented as additional funding becomes available.
- The components for the revised design were procured and tested, with integration testing revealing an overall improvement in performance within the operational bandwidth of the system when compared with the design prediction. Specifically, there was a 1.57 dB improvement in transmitted power at L-band, and 0.19 dB at X-band. Noise figures within the receivers could not be measured, but based on the measured performance of other component specifications and the provided CoC measurements (where applicable), the predicted improvement in SNR was a negligible 0.22 dB at L-band and 0.41 dB at X-band.
- Non-compliance of the L-band limiters meant that the maximum power levels within the receive chain could potentially exceed the maximum permissible input level of 10 dBm for the REX. This could temporarily be addressed

through increasing the attenuation between the limiter and the REX input, if deemed necessary, during system deployment.

- The chosen power supplies for the front end components were found to provide sufficient power for all components, including the HPAs, which required additional capacitors to support their large current requirements.
- Timing requirements for the control and monitoring of the front end components were derived in order to allow for the implementation of a control and monitoring system on a suitable microprocessor.
- The power level of the IF input signal to the REX was assumed to lie within the required limits, since this could not be tested due to ongoing development of the FPGA code. This would need to be confirmed once the digital back end is functional, and may necessitate the addition of amplifiers in the IF signal path in order to ensure that the results of the RF front end testing remain valid.

7.2 Recommendations

Based on the findings of this dissertation and the original *NeXtRAD* requirements and objectives, the following recommendations are made:

- An effort should be made to acquire the necessary components to implement the original front end design, in order to achieve the desired system functionality. This can be done done on a piecemeal basis, but implementation of the transmitter polarisation switches should be the first priority in order to achieve the dual-polarised transmitter functionality, which is an important requirement of the *NeXtRAD* system.
- Performance of the L-band limiters should be followed up with *Mini-Circuits* in order to address their non-compliance. Interim steps should be taken to ensure that L-band receiver power levels do not exceed the maximum input rating of the REX. The easiest way to accomplish this is to use a large attenuator between the limiter and the REX.
- Power levels of the IF signals need to be investigated to ensure they fall within the limits of the REX, ADC and DAC. If necessary, signal conditioning should be implemented.

- Monitoring and control of the front end components needs to be implemented on a suitable microprocessor. The timing requirements provided in Appendix B should be used as guidance for this implementation. Monitoring of the forward and reflected power levels should preferably be done using a lookup table in order to avoid the error present at X-band with the *Mini-Circuits* power detectors. Alternatively, the derived power detector equation should be adjusted to minimise the measurement error under normal operation, if the equations are used instead of a lookup table.

- The passive nodes for the multistatic configuration will require the implementation of a suitable RF front end. The receiver front ends used in this project are recommended for implementation at the passive nodes, with the addition of a variable attenuator to provide additional attenuation, when necessary, for forward scatter measurements. The proposed front end design is shown in Appendix C.

- Performance of the developed antennas used for the analysis of the system was found to be more than adequate. The SNR calculations provided in this dissertation should be taken into account if the decision is made to develop other antennas, as per the original project plan.

- The integrated RF front end and all supporting subsystems should be integrated into the final *NeXtRAD* system once a mechanical layout has been finalised.

Appendices

Appendix A

'As-Built' Front End with Power Distribution

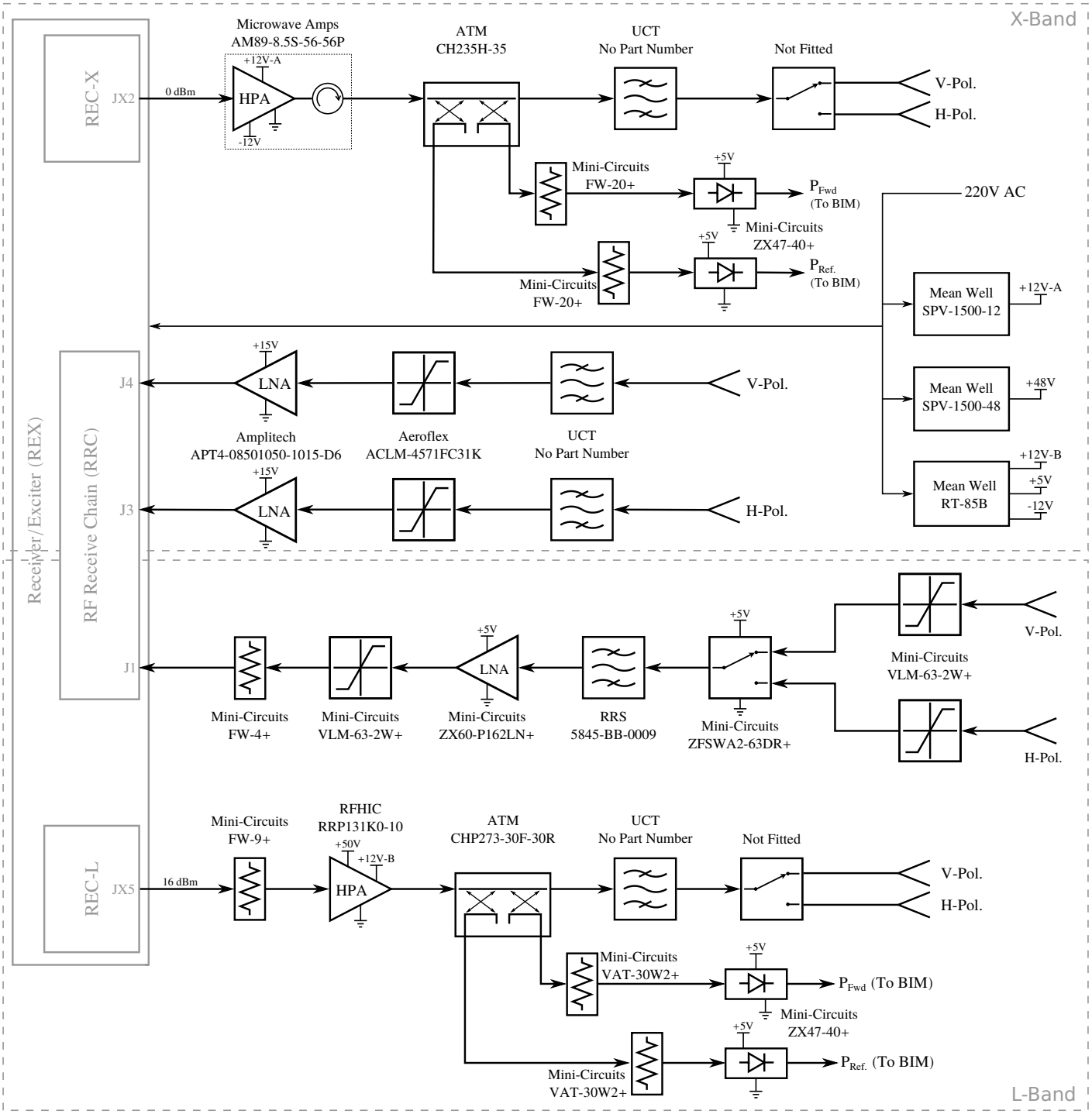
X-Band
REC-X
JX2
0 dBm
Microwave Amps
AM89-8.5S-56-56P
+12V-A
HPA
-12V
ATM
CH235H-35
UCT
No Part Number
Not Fitted
V-Pol.
H-Pol.
Mini-Circuits
FW-20+
+5V
P Fwd
(To BIM)
Mini-Circuits
ZX47-40+
P Ref.
(To BIM)
220V AC
Mean Well
SPV-1500-12
+12V-A
Mean Well
SPV-1500-48
+48V
Mean Well
RT-85B
+12V-B
+5V
-12V
Receiver/Exciter (REX)
RF Receive Chain (RRC)
J4
J3
+15V
LNA
Amplitech
APT4-08501050-1015-D6
Aeroflex
ACLM-4571FC31K
UCT
No Part Number
V-Pol.
H-Pol.
J1
Mini-Circuits
FW-4+
Mini-Circuits
VLM-63-2W+
Mini-Circuits
ZX60-P162LN+
RRS
5845-BB-0009
Mini-Circuits
ZFSWA2-63DR+
Mini-Circuits
VLM-63-2W+
REC-L
JX5
16 dBm
Mini-Circuits
FW-9+
RFHIC
RRP131K0-10
+50V
+12V-B
HPA
ATM
CHP273-30F-30R
UCT
No Part Number
Not Fitted
Mini-Circuits
VAT-30W2+
Mini-Circuits
ZX47-40+
Mini-Circuits
VAT-30W2+
L-Band

Appendix B

Guideline Timing & Control

Transmitter Power Up

	Event	Duration	Event Sequencing (not to scale)
1.0	L-band HPA into shutdown mode	1 µs	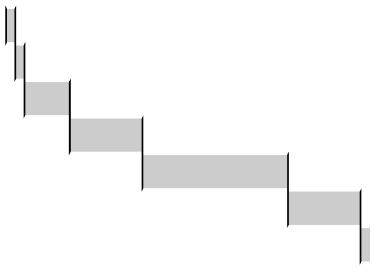
2.0	L-band HPA into standby mode	1 µs	
3.0	X-band HPA into standby mode	5 µs	
4.0	Apply HPA secondary supplies	1 s	
5.0	Apply HPA primary supplies	2 s	
6.0	Apply other front end power supplies	1 s	
7.0	L-band HPA out of shutdown mode	1 µs	

Transmitter Shut Down

	Event	Duration	Event Sequencing (not to scale)
1.0	L-band HPA into standby mode	1 µs	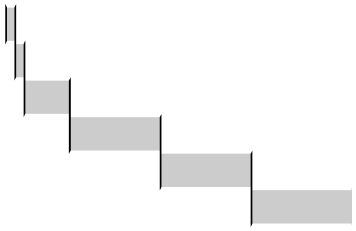
2.0	L-band HPA into shutdown mode	1 µs	
3.0	X-band HPA into standby mode	5 µs	
4.0	Remove HPA secondary supplies	5 s	
5.0	Remove HPA primary supplies	5 s	
6.0	Remove other front end power supplies	5 s	

L-Band Transmit/Receive

	Event	Duration	Event Sequencing (not to scale)
1.0	Set Tx switch to v-pol	TBD	
2.0	Set Rx switch to v-pol	50 ns	
3.0	HPA out of standby mode	1 µs	
4.0	Transmit RF	PW	
4.1	Measure peak power	PW	
4.2	Measure reflected power	PW	
5.0	Receive RF	PRI-PW	
5.1	HPA into standby mode	1 µs	
5.2	Measure HPA junction temperature	PW	
6.0	Set Rx switch to h-pol	50 ns	
7.0	Repeat steps 3–9		...
8.0	Set Tx switch to h-pol	TBD	
9.0	Repeat steps 3–9		...
10.0	Set Rx switch to v-pol	50 ns	
11.0	Repeat steps 3–9		...

X-Band Transmit/Receive

	Event	Duration	Event Sequencing (not to scale)
1.0	Set Tx switch to v-pol	TBD	
2.0	HPA out of standby mode	5 µs	
3.0	Transmit RF	PW	
3.1	Measure peak power	PW	
3.2	Measure reflected power	PW	
4.0	Receive RF	PRI-PW	
4.1	HPA into standby mode	5 µs	
4.2	Check for HPA over-temperature alarm	PW	
5.0	Set Tx switch to h-pol	TBD	
6.0	Repeat steps 2–8		...

Abbreviations:

PRI Pulse Repetition Interval

PW Pulse Width

TBD To Be Determined

Appendix C

Passive Node RF Front End

The proposed RF front end for implementation at the passive nodes of the multi-static setup is shown below. Components used are identical to those used for the active transceiver node front end, but with the addition of a *Mini-Circuits* ZX76-31R5-SP+ digital step attenuator inserted after the antenna. The addition of this attenuator is for use in forward scatter measurements, but it is recommended that it be moved to after the LNA if there is sufficient distance between the active and passive nodes such as not to saturate or damage the receiver front end. This would need to be calculated and decided on based upon the specific deployment, and is important for reducing the receiver noise figure.

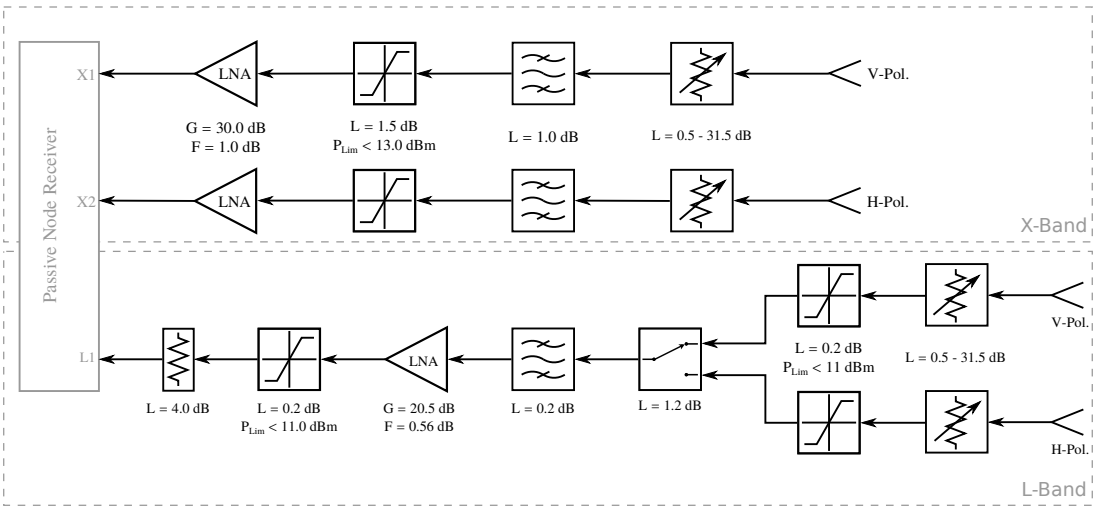

Appendix D

Component Datasheets

The following datasheets are included in this appendix:

- L-band limiter
- X-band limiter
- L-band low noise amplifier
- L-band RF switch
- Power supplies for high power amplifiers
- L-band high power amplifier
- X-band high power amplifier

Datasheets which have been excluded are due to confidentiality agreements or non-existence of official documentation.

+12 to +33dBm

Limiter

VLM-63-2W+

50Ω Broadband 30 to 6000 MHz

CASE STYLE: FF704

The Big Deal

- Protection against up to 2.5 W of unwanted input signals
- Wide frequency range, 30 MHz-6 GHz
- Very fast recovery time, 5 nsec typ.

Product Overview

The VLM-63-2W+ reacts almost instantaneously to protect sensitive devices from power surges and other unwanted signals at the device input. For inputs >12 dBm, the output power remains about 11.5 dBm, whereas lower-level input losses are only 0.4 dB typ. These units are housed in a patented, rugged unibody enclosure (1.43" x 0.410") specifically designed to function in tough environments such as manufacturing sites, train tunnels, weapon systems, or anywhere sensitive components, such as low noise amplifiers, need protection.

Feature	Advantages
High power handling, up to 2.5W max	Affords protection against peak voltages of multi-tone signals
Very fast recovery time, 5 nsec typ.	Back in operation almost instantaneously following signal spikes
Wideband, 30 MHz-6 GHz	Protection for a wide range of applications, from IF receivers to toll-booth operations

Mini-Circuits®
www.minicircuits.com P.O. Box 350166, Brooklyn, NY 11235-0003 (718) 934-4500 sales@minicircuits.com

+12 to +33dBm

Limiter

VLM-63-2W+

50Ω Broadband 30 to 6000 MHz

CASE STYLE: FF704

Connectors	Model	Price	Qty.
SMA	VLM-63-2W-S+	$51.95	(1-9)

+RoHS Compliant
The +Suffix identifies RoHS Compliance. See our web site for RoHS Compliance methodologies and qualifications

Maximum Ratings

Operating Temperature	-55°C to 100°C
Storage Temperature	-55°C to 100°C
RF Input Power	2.5W

Permanent damage may occur if any of these limits are exceeded.

Features

- wideband, 30 to 6000 MHz
- low insertion loss 0.4 dB typ.
- fast recovery time, 5nsec typ.
- excellent VSWR 1.05:1 typ.
- low leakage power, 11.5 dBm typ.

Applications

- protects low noise amplifiers and other devices from ESD or input power damage
- military, hi-rel applications

Coaxial Connections*

INPUT	SMA FEMALE
OUTPUT	SMA MALE

*Suggested Connections. For reverse connections, consult Mini-Circuits.

Outline Drawing

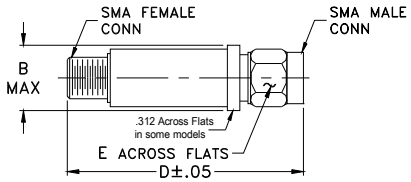

Outline Dimensions (inch / mm)

B	D	E	wt
.410	1.43	.312	grams
10.41	36.32	7.92	10.0

Electrical Specifications

Parameter	Condition	Min.	Typ.	Max.	Units
Frequency Range		30		6000	MHz
Insertion Loss in Linear Range	<+4 dBm Input	—	0.4	1.2	dB
VSWR	<+4 dBm Input	—	1.05	1.5	:1
Input Power Limiting Range		+12	—	+33	dBm
Output Power	In limiting range	—	+11.5	—	dBm
Recovery Time	1 watt pulse 50 µsec pw 1kHz duty cycle recovery to within 90% of final value.	—	5	—	nsec
Response Time	-30 to +33 dBm input 50 µsec, BW 1 kHz duty cycle	—	7	—	nsec
Limiting Δ Output/1dB Δ Input	Input Power Range (dBm) 12 to 20 20 to 25 25 to 33	 — — —	 0.3 0.5 0.6	 — — —	dB/dB

Typical Performance Data

Freq. (MHz)	I. Loss in Linear Range (dB)	VSWR in Linear Range (:1)	Power Output (dBm) +12dBm Input	+20dBm Input	+25 dBm Input	+33dBm Input	Δ Output 1dB Δ Input +12 to +20dBm Input	+20 to +25 dBm Input	+25 to +33 dBm Input
30.00	0.06	1.23	10.14	11.09	11.55	12.32	0.12	0.09	0.10
100.00	0.04	1.05	9.75	10.86	11.33	12.23	0.14	0.22	0.11
200.00	0.06	1.02	9.44	10.59	11.22	11.97	0.14	0.13	0.09
800.00	0.21	1.03	8.75	10.41	11.48	7.12	0.21	0.21	-0.55
1200.00	0.20	1.01	8.76	10.93	8.93	8.46	0.27	-0.40	-0.06
1600.00	0.24	1.01	8.72	8.29	6.22	9.42	-0.05	-0.41	0.40
2000.00	0.27	1.04	8.91	6.82	5.97	8.50	-0.26	-0.17	0.32
2400.00	0.30	1.07	8.83	5.65	6.02	8.87	-0.40	0.07	0.36
3000.00	0.35	1.10	7.59	2.42	6.54	7.06	-0.65	0.82	0.06
3600.00	0.38	1.11	7.61	1.42	6.40	8.13	-0.77	1.00	0.22
4000.00	0.40	1.12	5.75	2.04	6.60	8.39	-0.46	0.91	0.22
5000.00	0.45	1.07	-0.40	0.68	3.26	4.93	0.14	0.52	0.21
6000.00	0.53	1.11	-3.86	2.75	4.79	6.66	0.83	0.41	0.23

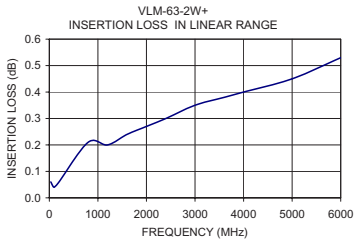

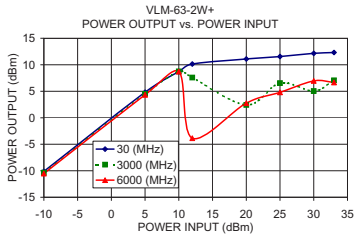

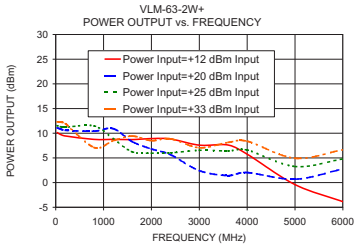

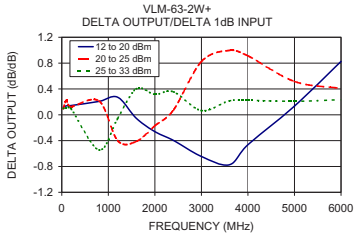

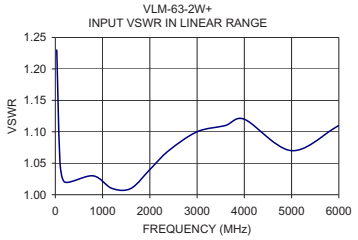

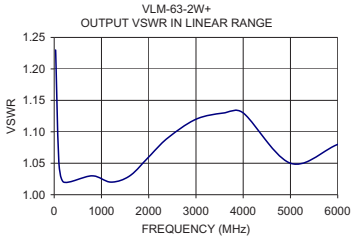

Notes
A. Performance and quality attributes and conditions not expressly stated in this specification document are intended to be excluded and do not form a part of this specification document.
B. Electrical specifications and performance data contained in this specification document are based on Mini-Circuit's applicable established test performance criteria and measurement instructions.
C. The parts covered by this specification document are subject to Mini-Circuits standard limited warranty and terms and conditions (collectively, "Standard Terms"); Purchasers of this part are entitled to the rights and benefits contained therein. For a full statement of the Standard Terms and the exclusive rights and remedies thereunder, please visit Mini-Circuits' website at www.minicircuits.com/MCLStore/terms.jsp

Limiters

Pin Diode Low Leakage Limiters

Low Leakage limiters are designed to have lower threshold and leakage levels than those of conventional limiters in order to protect more sensitive components. They incorporate input PIN diode limiters which are biased by a quasi-active driver. Most circuits include DC blocks, which are required for proper operation.

In some very low frequency models, it is not possible to include DC blocks. The application must be such that no low impedance DC path from the center conductor to ground exists outside the unit. The limiter threshold (1dB compression) is typically +5dBm.

Low Leakage limiters will also handle peak power levels above 100W (1usec pulse width, 0.001 duty cycle, and 1kHz repetition rate). Peak leakages are higher than CW leakages as they are with conventional limiters. This becomes exaggerated at frequencies below 2GHz.

Features

- Low Insertion Loss
- Low Leakage Power Circuit Protection
- High CW Power Handling
- Hermetically Sealed Modules
- Assorted Package Styles
- Custom Designs Available

PIN DIODE LOW LEAKAGE LIMITERS

Frequency Range (GHz)	Part Number	Peak Input Power (W)	CW Input Power (Watts)	Maximum Flat Leakage (CW Power) (+dBm)	Maximum Insertion Loss (dB)	Maximum VSWR	Standard Case Styles	Optional Case Styles
0.02 - 0.1	ACLM-4885F	100	1	15	0.5	1.7:1	C3	C36,C37,M10,M22
0.1 - 0.2	ACLM-4769F	100	1	11	0.5	1.7:1	C3	C36,C37,M10,M22
0.02 - 0.5	ACLM-4594F	100	3	13.5	0.4	1.3:1	C3	C36,C37,M10,M22
0.03 - 1	ACLM-4675F	100	3	13.5	0.3	1.3:1	C3	C36,C37,M10,M22
0.1 - 1	ACLM-4786F	100	2	13.5	0.3	1.3:1	C3	C36,C37,M10,M22
0.1 - 2	ACLM-4800F	100	2	13.5	0.5	1.3:1	C3	C36,C37,M10,M22
0.5 - 2	ACLM-4650F	100	2	13.5	0.5	1.4:1	C3	C36,C37,M10,M22
1 - 2	ACLM-4586F	100	2	13.5	0.5	1.3:1	C3	C36,C37,M10,M22
2 - 4	ACLM-4732F	100	2	13.5	0.6	1.4:1	C3	C36,C37,M22
0.5 - 6	ACLM-4700F	100	2	13.5	0.8	1.5:1	C3	C36,C37,M22
0.5 - 8	ACLM-4759F	100	2	13.5	1.0	1.7:1	C3	C36,C37,M22
2 - 8	ACLM-4504F	100	2	13	0.8	1.5:1	C3	C36,C37,M22
4 - 8	ACLM-4572F	100	2	13	1.0	1.8:1	C3	C36,C37,M22
0.4 - 12	ACLM-4727F	100	2	13	1.5	1.8:1	C3	C36,C37,M22
8 - 12	ACLM-4571F	100	2	13	1.5	1.8:1	C3	C36,C37,M22
1 - 18	ACLM-4618F	100	2	13	2.4	2.4:1	C36	C37,M22
2 - 18	ACLM-4619F	100	2	13	2.4	2.2:1	C36	C37,M22
6 - 18	ACLM-4616F	100	2	13	2.4	2.2:1	C36	C37,M22
8 - 18	ACLM-4797F	100	2	13	2.4	2.2:1	C36	C37,M22
18 - 26.5	ACLM-4809F	100	2	15	2.8	2.0:1	C36	C37,M22

01
2014/09/08
Adrian S.

NOTES

1. Typically CW leakage is measured at mid-band with 1W input.
2. Higher power handling available. Contact the factory to discuss specific requirements.
3. Power handling is linearly derated from full power at +25°C to zero power at +150°C.

SCREENING

Standard Screening:
Internal Visual per MIL-STD-883, Method 2017
Temperature Cycle: -65°C to +100°C, 10 cycles
Optional High-Rel Screening (Ref MIL-PRF-38534):
Internal Visual per MIL-STD-883, Method 2017
Stabilization Bake per MIL-STD-883, Method 1008
Temperature Cycle per MIL-STD-883, Method 1010
Constant Acceleration per MIL-STD-883, Method 2001
Burn-in per MIL-STD-883, Method 1015
Leak Test per MIL-STD-883, Method 1014
External Visual per MIL-STD-883, Method 2009

Pin Diode Low Leakage Limiters

OUTLINE CASE STYLE C3

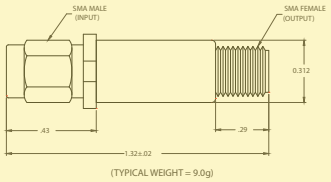

(TYPICAL WEIGHT = 9.0g)

OUTLINE CASE STYLE C37

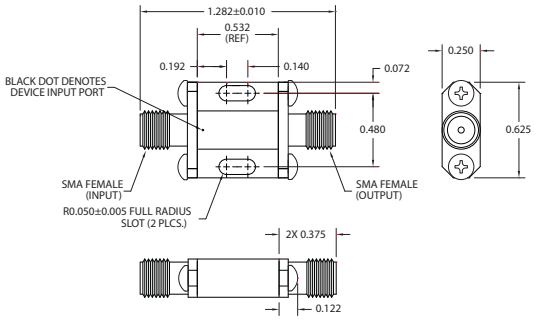

(TYPICAL WEIGHT = 13.0g)

OUTLINE CASE STYLE C36

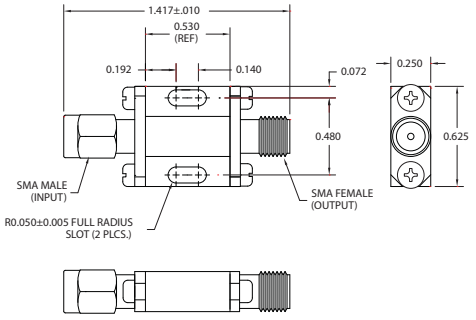

(TYPICAL WEIGHT = 13.0g)

OUTLINE CASE STYLE M22

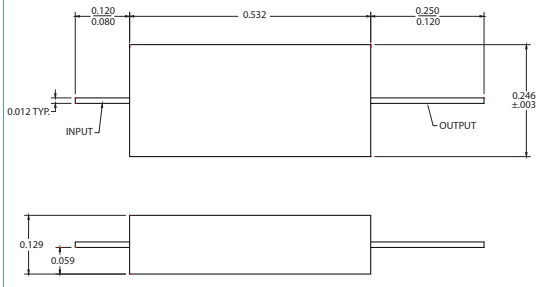

(TYPICAL WEIGHT =1.55g)

OUTLINE CASE STYLE M10

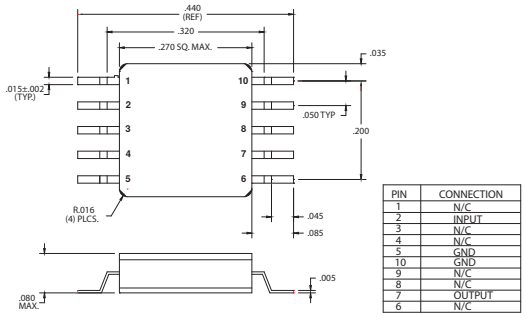

PIN	CONNECTION
1	N/C
2	INPUT
3	N/C
4	N/C
5	GND
10	GND
9	N/C
8	N/C
7	OUTPUT
6	N/C

(TYPICAL WEIGHT = 0.27g)

PART NUMBER ORDERING INFORMATION

Example:	ACLM-4504FC3R1K
ACLM-4504F:	Low Leakage limiter, 2 - 8GHz
C3:	Package type
R:	Reversed Connectors (Omit for standard configuration)
1K:	1kW peak power handling (Omit for standard 100W peak power handling)

Coaxial

Low Noise Amplifier

ZX60-P162LN+

50Ω 0.7 to 1.6 GHz

Case Style: GC957

The Big Deal

- Ultra Low Noise Figure, 0.5 dB typ.
- High Dynamic Range

Product Overview

The ZX60-P162LN+ (RoHS compliant) uses Mini-Circuits' E-PHEMT technology to offer ultra low noise figure over a broad frequency range and high IP3. Housed in a rugged, cost effective unibody chassis, this amplifier supports a wide variety of applications requiring moderate power output, low distortion and 50 ohm matched input/output ports.

Key Features

Feature	Advantages
Ultra Low Noise Figure, 0.5 dB at 1GHz	Outstanding world class noise figure performance.
High IP3 vs. DC power consumption 29.9 dBm typical at 1 GHz	Combining Low Noise and High IP3 makes this model ideal for use in Low Noise Receiver Front End (RFE)
Max. Input Power, +25 dBm	Ruggedized design operates to high input powers often seen at receiver inputs.
Very Small Size, 0.75" x 0.75"	The unique unibody size and construction enable the ZX60-P162LN+ to be used in extremely compact connectorized applications.

Coaxial

Low Noise Amplifier

ZX60-P162LN+

50Ω 0.7 to 1.6 GHz

Features

- Low Noise Figure, 0.5 dB at 1 GHz
- High IP3, 29.9 dBm typ. at 1 GHz
- High Pout, P1dB, +19.9 dBm typ. at 1 GHz
- High Gain, 22.5 dB typ. at 1 GHz

Applications

- Base station infrastructure
- Portable wireless
- GPS
- GSM
- Airborne radar

Case Style: GC957

Connectors	Model	Price	Qty.
SMA	ZX60-P162LN+	$54.95 ea.	(1-9)

+RoHS Compliant

The +Suffix identifies RoHS Compliance. See our web site for RoHS Compliance methodologies and qualifications

Electrical Specifications at 25°C and 4.0V unless noted

Parameter	Condition (GHz)	Min.	Typ.	Max.	Units
Frequency Range		0.7		1.6	GHz
Noise Figure	0.7		0.65	0.95	dB
	0.8		0.47		
	1.0		0.52		
	1.3		0.56		
	1.6		0.74		
Gain	0.7	20.9	24.1	24.5	dB
	0.8		23.8		
	1.0		22.5		
	1.3		20.5		
	1.6		18.5		
Output Power @ 1 dB compression	0.7	17.5	19.2		dBm
	0.8		19.9		
	1.0		19.9		
	1.3		19.7		
	1.6		19.5		
Output IP3	0.7	28.0	29.0		dBm
	0.8		29.8		
	1.0		29.9		
	1.3		30.2		
	1.6		29.6		
Input VSWR	0.7		2.18		dB
	0.8		1.63		
	1.0		1.19		
	1.3		1.23		
	1.6		1.39		
Output VSWR	0.7		1.57		dB
	0.8		1.42		
	1.0		1.38		
	1.3		1.65		
	1.6		2.11		
Directivity (Isolation-Gain)	0.7 - 1.6		8.0		dB
DC Supply Voltage		3.8	4.0	4.2	V
Supply Current		44	52	60	mA

ZX60-P162LN+

Maximum Ratings

Parameter	Ratings
Operating Temperature	-40°C to 85°C Case
Storage Temperature	-55°C to 100°C
DC Voltage	5.5 V
Input RF Power (no damage) Vd=4V	25 dBm
Power Consumption	0.55 W

Permanent damage may occur if any of these limits are exceeded.

Outline Drawing

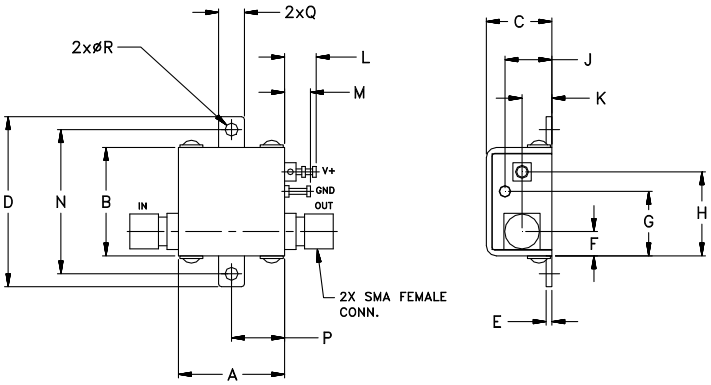

Outline Dimensions (inch / mm)

A	B	C	D	E	F	G	H	J	K	L	M	N	P	Q	R	wt
.74	.75	.46	1.18	.04	.17	.45	.59	.33	.21	.22	.18	1.00	.37	.18	.106	grams
18.80	19.05	11.68	29.97	1.02	4.32	11.43	14.99	8.38	5.33	5.59	4.57	25.40	9.40	4.57	2.69	23.0

Typical Performance Data/Curves **ZX60-P162LN+**

FREQUENCY (MHz)	GAIN (dB)	DIRECTIVITY (dB)	VSWR (:1)		POUT at 1dB COMPR. (dBm)	NOISE FIGURE (dB)	OUTPUT IP3 (dBm)
			IN	OUT			
700.00	24.09	13.78	2.19	1.58	19.2	0.7	29.0
800.00	23.78	13.74	1.64	1.43	19.9	0.5	29.8
900.00	23.17	14.08	1.35	1.37	20.0	0.6	30.2
1000.00	22.49	14.69	1.19	1.38	19.9	0.5	29.9
1100.00	21.81	15.35	1.09	1.44	19.9	0.6	30.3
1200.00	21.12	16.12	1.16	1.53	20.2	0.6	30.4
1300.00	20.46	16.65	1.23	1.65	19.7	0.6	30.2
1400.00	19.81	17.42	1.29	1.80	19.6	0.7	29.8
1500.00	19.16	18.07	1.34	1.95	19.3	0.6	29.8
1600.00	18.53	18.84	1.40	2.13	19.5	0.7	29.6

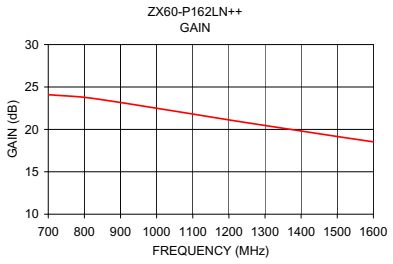

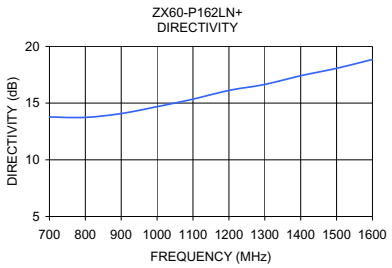

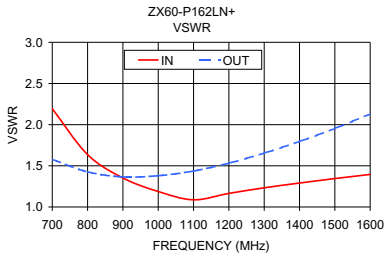

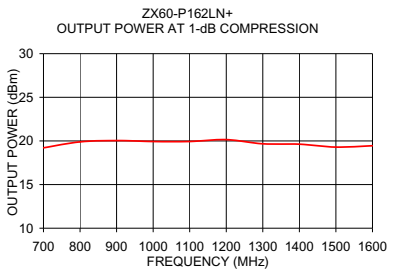

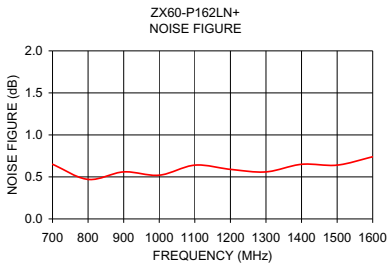

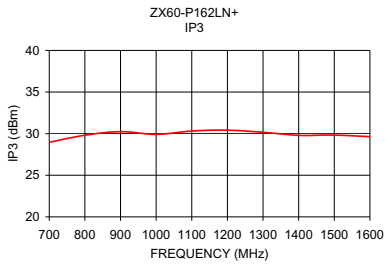

Notes
A. Performance and quality attributes and conditions not expressly stated in this specification document are intended to be excluded and do not form a part of this specification document.
B. Electrical specifications and performance data contained in this specification document are based on Mini-Circuit's applicable established test performance criteria and measurement instructions.
C. The parts covered by this specification document are subject to Mini-Circuits standard limited warranty and terms and conditions (collectively, "Standard Terms"); Purchasers of this part are entitled to the rights and benefits contained therein. For a full statement of the Standard Terms and the exclusive rights and remedies thereunder, please visit Mini-Circuits' website at www.minicircuits.com/MCLStore/terms.jsp

Absorptive SPDT Solid State RF Switch

ZFSWA2-63DR+

The Big Deal

- Wide bandwidth 500 to 6000 MHz
- Very high isolation, 65 dB at 1GHz
- Very fast switching, 35ns
- Rugged case with internal hermetically sealed ceramic semi-conductor module

Pricing: **$69.95** (QTY 1-9)

Product Overview

The ZFSWA2-63DR+ is a great general purpose SPDT solid state absorptive RF switch. With its broad frequency range, fast 35 ns switching time and excellent RF performance, the ZFSWA2-63DR+ is an excellent choice for many applications. In addition to it's versatility within system block diagrams, the ZFSWA2-63DR+ is designed for easy integration into your prototype design applications.

Key Features

Feature	Advantages
Designed for any environment	The ZFSWA2-63DR+ is equipped with a rugged shielded case, a hermetically sealed internal device with a wide operating temperature range (-55°C to 100°C) Suitable for many environments and applications the ZFSWA2-63DR+ offers excellent performance and value
Integrated CMOS Driver	-Operates from 3-5V -Low control current 5 µA allows compatibility with a variety of driver circuits -Internal Decoupling -Fast 35 ns Switching time
Excellent for a Variety of Applications From Bench to Integrated Systems	-High speed testers -Automated switching networks -Wireless Infrastructure -Military
Excellent RF Performance	-Wide bandwidth: 500 to 6000 MHz -Low Insertion Loss: 1.4 dB Typ -Low Supply current: 18 µA Typ -High Isolation: 65 dB Typ @ 1 GHz

Mini-Circuits®
www.minicircuits.com P.O. Box 35166, Brooklyn, NY 11235-0003 (718) 934-4500 sales@minicircuits.com

Coaxial

SPDT RF Switch

50Ω 500-6000 MHz

Absorptive RF Switch with Internal Driver
Single Supply Voltage, +3V to +5V

Product Features

- Wide bandwidth, 500 to 6000 MHz
- High Isolation, 65 dB typ. at 1 GHz
- Low Insertion loss, 1.4 dB typ.
- Internal CMOS driver
- Fast switching, Rise/fall time, 25 ns typ.
- Built rugged for tough environments
- Wide operating temperature, -55°C to 100°C

ZFSWA2-63DR+

CASE STYLE: ZZ1322

Connectors	Model	Price	Qty.
SMA	ZFSWA2-63DR+	$69.95 ea.	(1-9)
BRACKET (OPTION "B")		$5.00	(1+)

+RoHS Compliant
The +Suffix identifies RoHS Compliance. See our web site for RoHS Compliance methodologies and qualifications

Typical Applications

- Cellular
- ISM, WCDMA, WIMAX
- PCN
- Automated switching networks
- Military

General Description

The ZFSWA2-63DR+ is a 50Ω high isolation, absorptive SPDT RF switch designed for wireless applications, covering a broad frequency range from 500 to 6000 MHz with low insertion loss. The ZFSWA2-63DR+ operates on a single supply voltage in the range of +3V to +5V. This unit includes an internal CMOS driver. The switch consumes very low supply current, 18 µA typ. The ZFSWA2-63DR+ switch comes in a rugged built case for tough environments.

Schematic and Application Circuit

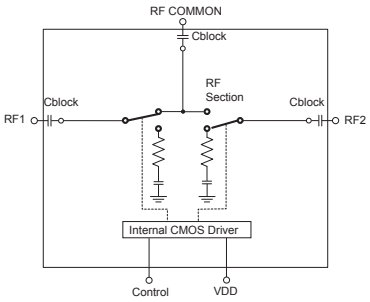

Mini-Circuits®
www.minicircuits.com P.O. Box 35166, Brooklyn, NY 11235-0003 (718) 934-4500 sales@minicircuits.com

SPDT RF Switch

ZFSWA2-63DR+

RF Electrical Specifications, 500 - 6000 MHz, T_{AMB}=25°C, V_{DD}= +3V to +5V

Parameter	Condition	Min.	Typ.	Max.	Units
Frequency Range		500		6000	MHz
Insertion Loss	500 MHz 1000 MHz 2000 MHz 4000 MHz 6000 MHz		1.0 1.15 1.4 1.7 2.0	1.3 1.5 1.7 2.1 2.4	dB
Isolation between Common port and RF1/RF2 Ports	500 to 2000 MHz 2000 to 4000 MHz 4000 to 6000 MHz	55 48 35	65 57 45		dB
Isolation between RF1 and RF2 ports	500 to 2000 MHz 2000 to 4000 MHz 4000 to 6000 MHz	50 43 35	60 50 45		dB
Return Loss (ON STATE)	500 to 2000 MHz 2000 to 4000 MHz 4000 to 6000 MHz		20 17 15		dB
Return Loss @ RF1/RF2 ports (OFF STATE)	500 to 2000 MHz 2000 to 4000 MHz 4000 to 6000 MHz		13 13 13		dB
Input IP3	V_{DD}=3V, 500 to 2000 MHz 2000 to 6000 MHz V_{DD}=5V, 500 to 2000 MHz 2000 to 6000 MHz		47 40 49 44		dBm
Input 1dB Compression (1)	V_{DD}=3V, 500 to 2000 MHz 2000 to 6000 MHz 2000 to 6000 MHz		24 24 27		dBm
DC Electrical Specifications					
VDD, Supply Voltage		3		5	V
Supply Current (2)	V_{DD}=5V		18		µA
Control Voltage Low		0		0.5	V
Control Voltage High (3)		2.7		V_{DD}	V
Control Current			5		µA
Switching Specifications					
Rise/Fall Time (10 to 90% or 90 to 10% RF)	V_{DD}=5V		25		nSec
Switching Time (50% CTRL to 90/10% RF)	V_{DD}=5V		35		nSec
Video Feed through (Control 0-5V, Frequency 1 MHz)	V_{DD}=5V		30		mV_{P-P}

Notes:
1. Note absolute maximum rating for input and dissipated power. At 5V, over 2000-6000 MHz, 0.2 dB compression.
2. Increases with switching repetition rate. See graph.
3. CMOS interface latch-up condition may occur when logic high signal is applied prior to power supply.

Absolute Maximum Ratings

Parameter	Ratings
Operating Temperature	-55°C to 100°C
Storage Temperature	-55°C to 100°C
V_{DD}, Supply Voltage	2.7 to 5.5V
Voltage Control	-0.2V Min. V_{DD} Max.
RF input power	1Watt
Dissipated Power at 25°C	370mW
ESD, HBM	Class 1A (250 to <500V) per JESD22-A114
ESD, MM	Class A (passes 50V) per JESD22-A115
ESD, CDM	Class III (500 to <1000V) per JESD22-C101

Mini-Circuits®
www.minicircuits.com P.O. Box 35166, Brooklyn, NY 11235-0003 (718) 934-4500 sales@minicircuits.com

SPDT RF Switch

ZFSWA2-63DR+

Truth Table *(State of control voltage selects the desired switch state)*

State of Control Voltage	Switch State - RF Common to	
	RF1	RF2
Low	ON	OFF
High	OFF	ON
ON- low insertion loss state OFF- Isolation State		

Coaxial Configuration

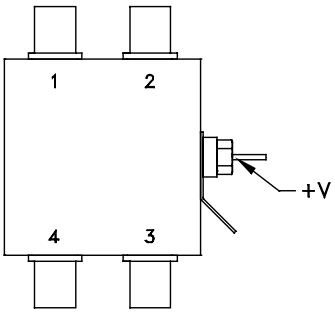

Coaxial Connections

Function	Port Number	Description
RF COM	1	RF Common/ SUM Port
RF1	4	RF Out #1/In Port #1
RF2	3	RF Out #2/In Port #2
Control	2	CMOS Control IN
VDD	V+	Supply Voltage
GND	Case	RF Ground

Mini-Circuits®
www.minicircuits.com P.O. Box 35166, Brooklyn, NY 11235-0003 (718) 934-4500 sales@minicircuits.com

SPDT RF Switch

ZFSWA2-63DR+

Outline Drawing (ZZ1322)

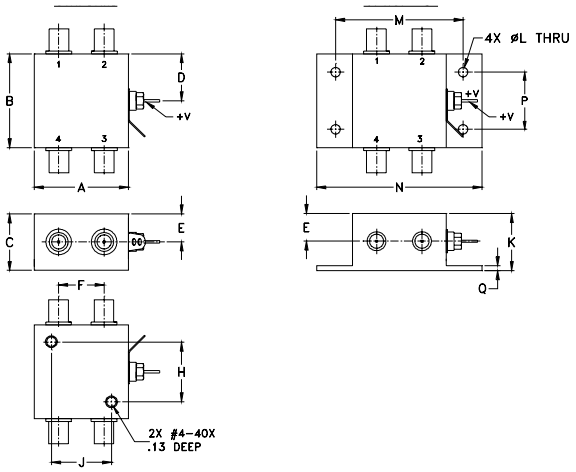

Outline Dimensions (inch / mm)

A	B	C	D	E	F	G	H	J	K	L	M	N	P	Q	wt
1.25	1.25	0.75	0.63	0.38	0.6	--	0.800	0.800	0.76	0.125	1.688	2.18	0.75	0.07	grams
31.75	31.75	19.05	16.00	9.65	15.24	--	20.32	20.32	19.30	3.18	42.88	55.37	19.05	1.78	85

Additional Detailed Technical Information

Additional information is available on our web site. To access this information enter the model number on our web site home page.

Performance data, graphs

Case Style: ZZ1322

Environmental Ratings: ENV28

Pricing & Availability Information

Mini-Circuits®
www.minicircuits.com P.O. Box 35166, Brooklyn, NY 11235-0003 (718) 934-4500 sales@minicircuits.com

MEAN WELL

85W Triple Output Switching Power Supply

RT-85 series

■ Features :

- Universal AC input / Full range
- Protections: Short circuit / Overload / Over voltage
- Cooling by free air convection
- LED indicator for power on
- 100% full load burn-in test
- All using 105℃ long life electrolytic capacitors
- Withstand 300VAC surge input for 5 second
- High operating temperature up to 70℃
- Withstand 5G vibration test
- High efficiency, long life and high reliability
- 3 years warranty

SPECIFICATION

MODEL		RT-85A			RT-85B			RT-85C			RT-85D		
OUTPUT	OUTPUT NUMBER	CH1	CH2	CH3	CH1	CH2	CH3	CH1	CH2	CH3	CH1	CH2	CH3
	DC VOLTAGE	5V	12V	-5V	5V	12V	-12V	5V	15V	-15V	5V	24V	12V
	RATED CURRENT	8A	3.5A	0.5A	8A	3.5A	0.5A	7A	3A	0.5A	6A	2A	1A
	CURRENT RANGE Note.6	2 ~ 10A	0.3 ~ 4A	0 ~ 1A	2 ~ 10A	0.3 ~ 4A	0 ~ 1A	2 ~ 10A	0.3 ~ 4A	0 ~ 1A	2 ~ 10A	0.3 ~ 2.5A	0.1 ~ 1A
	RATED POWER Note.6	84.5W			88W			87.5W			90W		
	RIPPLE & NOISE (max.) Note.2	80mVp-p	120mVp-p	100mVp-p	80mVp-p	120mVp-p	120mVp-p	80mVp-p	120mVp-p	120mVp-p	80mVp-p	150mVp-p	120mVp-p
	VOLTAGE ADJ. RANGE	CH1: 4.75 ~ 5.5V			CH1: 4.75 ~ 5.5V			CH1: 4.75 ~ 5.5V			CH1: 4.75 ~ 5.5V		
	VOLTAGE TOLERANCE Note.3	±2.0%	±5.0%	±6.0%	±2.0%	±5.0%	±6.0%	±2.0%	+3,-7%	±6.0%	±2.0%	±5.0%	±6.0%
	LINE REGULATION Note.4	±0.5%	±1.0%	±1.0%	±0.5%	±1.0%	±1.0%	±0.5%	±1.0%	±1.0%	±0.5%	±1.0%	±1.0%
	LOAD REGULATION Note.5	±1.0%	±3.0%	±6.0%	±1.0%	±3.0%	±6.0%	±1.0%	±3.0%	±6.0%	±1.0%	±3.0%	±6.0%
	SETUP, RISE TIME	500ms, 20ms/230VAC 1200ms, 30ms/115VAC at full load											
	HOLD UP TIME (Typ.)	100ms/230VAC 18ms/115VAC at full load											
INPUT	VOLTAGE RANGE	88 ~ 264VAC 125 ~ 373VDC (Withstand 300VAC surge for 5sec. Without damage)											
	FREQUENCY RANGE	47 ~ 63Hz											
	EFFICIENCY (Typ.)	76%			76%			77%			79%		
	AC CURRENT (Typ.)	2.5A/115VAC 1.5A/230VAC											
	INRUSH CURRENT (Typ.)	COLD START 40A/230VAC											
	LEAKAGE CURRENT	<2mA / 240VAC											
PROTECTION	OVERLOAD	110 ~ 150% rated output power											
		Protection type : Hiccup mode, recovers automatically after fault condition is removed											
	OVER VOLTAGE	CH1: 5.75 ~ 6.75V											
		Protection type : Hiccup mode, recovers automatically after fault condition is removed											
ENVIRONMENT	WORKING TEMP.	-25 ~ +70℃ (Refer to "Derating Curve")											
	WORKING HUMIDITY	20 ~ 90% RH non-condensing											
	STORAGE TEMP., HUMIDITY	-40 ~ +85℃, 10 ~ 95% RH											
	TEMP. COEFFICIENT	±0.03%/℃ (0 ~ 50℃)on +5V output											
	VIBRATION	10 ~ 500Hz, 5G 10min./1cycle, period for 60min. each along X, Y, Z axes											
SAFETY & EMC (Note 7)	SAFETY STANDARDS	UL60950-1, TUV EN60950-1 approved											
	WITHSTAND VOLTAGE	I/P-O/P:3KVAC I/P-FG:1.5KVAC O/P-FG:0.5KVAC											
	ISOLATION RESISTANCE	I/P-O/P, I/P-FG, O/P-FG:100M Ohms / 500VDC / 25℃/ 70% RH											
	EMC EMISSION	Compliance to EN55022 (CISPR22) Class B, EN61000-3-2,-3											
	EMC IMMUNITY	Compliance to EN61000-4-2,3,4,5,6,8,11, EN61000-6-2 (EN50082-2), heavy industry level, criteria A											
OTHERS	MTBF	215Khrs min. MIL-HDBK-217F (25℃)											
	DIMENSION	159*97*38mm (L*W*H)											
	PACKING	0.6Kg; 24pcs/15.4Kg/0.7CUFT											
NOTE	1. All parameters NOT specially mentioned are measured at 230VAC input, rated load and 25℃ of ambient temperature. 2. Ripple & noise are measured at 20MHz of bandwidth by using a 12" twisted pair-wire terminated with a 0.1uf & 47uf parallel capacitor. 3. Tolerance : includes set up tolerance, line regulation and load regulation. 4. Line regulation is measured from low line to high line at rated load. 5. Load regulation is measured from 20% to 100% rated load, and other output at 60% rated load. 6. Each output can work within current range. But total output power can't exceed rated output power. 7. The power supply is considered a component which will be installed into a final equipment. The final equipment must be re-confirmed that it still meets EMC directives. For guidance on how to perform these EMC tests, please refer to "EMI testing of component power supplies." (as available on http://www.meanwell.com) 8. Length of set up time is measured at cold first start. Turning ON/OFF the power supply very quickly may lead to increase of the set up time.												

File Name:RT-85-SPEC 2011-08-19

MEAN WELL

85W Triple Output Switching Power Supply

RT-85 series

■ Mechanical Specification

Case No. 901C Unit:mm

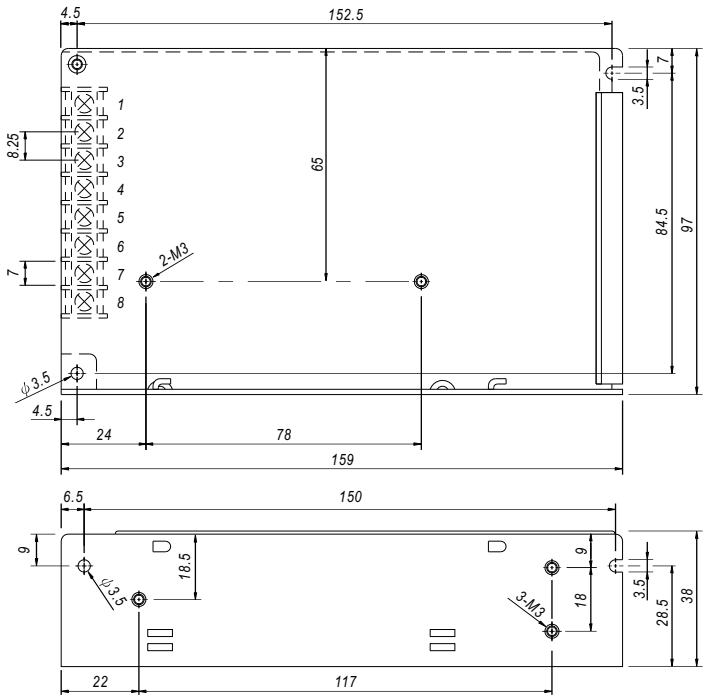

Terminal Pin No. Assignment

Pin No.	Assignment	Pin No.	Assignment
1	AC/L	5	DC OUTPUT V3
2	AC/N	6	DC OUTPUT +V2
3	FG ⏚	7	DC OUTPUT COM
4	NC	8	DC OUTPUT +V1

■ Block Diagram

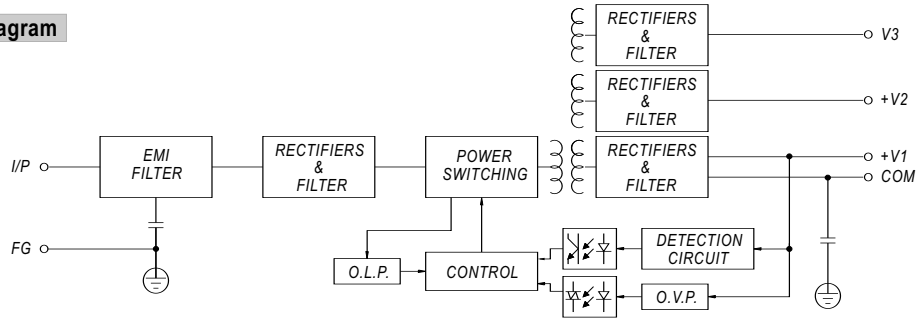

■ Derating Curve

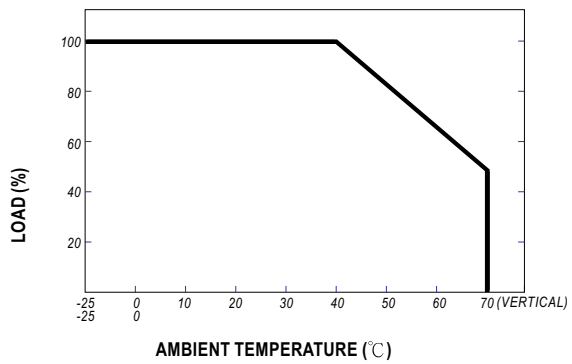

AMBIENT TEMPERATURE (℃)

■ Static Characteristics

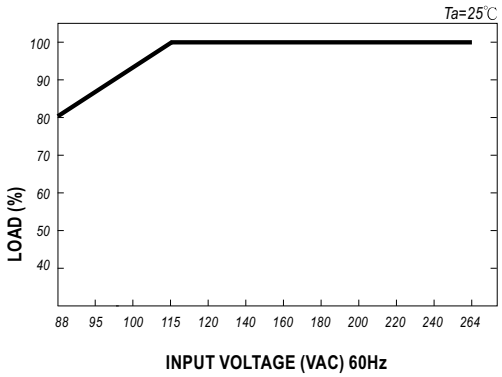

INPUT VOLTAGE (VAC) 60Hz

File Name:RT-85-SPEC 2011-08-19

MEAN WELL

1500W Single Output Power Supply

SPV-1500 series

■ Features :

- Universal AC input/Full range
- ZVS new technology
- AC input active surge current limiting
- Built-in active PFC function,PF>0.95
- Protections: Short circuit / Overload / Over voltage / Over temperature
- Forced air cooling by built-in DC ball bearing fan
- High power density 8.3W/inch^3
- Output voltage can be trimmed between 20% ~ 110% rated value
- Current sharing up to 4500W(2+1)
- Alarm signal output
- Built-in 12V/0.1A auxiliary output for remote control
- Built-in remote ON-OFF control
- Built-in remote sense function
- 3 years warranty

Parallel PFC c UL us CB CE

SPECIFICATION

MODEL		SPV-1500-12	SPV-1500-24	SPV-1500-48
OUTPUT	DC VOLTAGE	12V	24V	48V
	RATED CURRENT	125A	63A	32A
	CURRENT RANGE	0 ~ 125A	0 ~ 63A	0 ~ 32A
	RATED POWER	1500W	1512W	1536W
	RIPPLE & NOISE (max.) Note.2	150mVp-p	150mVp-p	200mVp-p
	VOLTAGE ADJ. RANGE	±5% typical adjustment by VR, 20% ~ 110% (typ.) adjustment by 1~6VDC external control signal		
	VOLTAGE TOLERANCE Note.3	±1.0%		
	LINE REGULATION	±0.5%		
	LOAD REGULATION	±0.5%		
	SETUP, RISE TIME	1500ms, 100ms at full load		
	HOLD UP TIME (Typ.)	10ms at full load	14ms at full load	16ms at full load
INPUT	VOLTAGE RANGE Note.5	90 ~ 264VAC 127 ~ 370VDC		
	FREQUENCY RANGE	47 ~ 63Hz		
	POWER FACTOR (Typ.)	0.95/230VAC 0.98/115VAC at full load		
	EFFICIENCY (Typ.)	86.5%	90%	90%
	AC CURRENT (Typ.)	17A/115VAC 8A/230VAC		
	INRUSH CURRENT (Typ.)	30A/115VAC 60A/230VAC		
	LEAKAGE CURRENT	<2.0mA / 240VAC		
PROTECTION	OVERLOAD	105 ~135% rated output power		
		Protection type : Constant current limiting, recovers automatically after fault condition is removed		
	OVER VOLTAGE	13.8 ~ 16.8V	30 ~ 34.8V	57.6 ~ 67.2V
		Protection type : Shut down o/p voltage, re-power on to recover		
	OVER TEMPERATURE	105℃ ±5℃ (TSW2) detect on heatsink of power transistor		
		Protection type : Shut down o/p voltage, recovers automatically after temperature goes down		
FUNCTION	AUXILIARY POWER(AUX)	12V@0.1A(Only for Remote ON/OFF control)		
	REMOTE ON/OFF CONTROL	Please see the Function Manual		
	ALARM SIGNAL OUTPUT	Please see the Function Manual		
	OUTPUT VOLTAGE TRIM	2.4 ~ 13.2V	4.8 ~ 28V	9.6 ~ 56V
ENVIRONMENT	WORKING TEMP.	-20 ~ +70℃ (Refer to "Derating Curve")		
	WORKING HUMIDITY	20~90% RH non-condensing		
	STORAGE TEMP., HUMIDITY	-40 ~ +85℃, 10 ~ 95% RH		
	TEMP. COEFFICIENT	±0.05%/℃ (0 ~ 50℃)		
	VIBRATION	10 ~ 500Hz, 2G 10min./1cycle, 60min. each along X, Y, Z axes		
SAFETY & EMC (Note 4)	SAFETY STANDARDS	UL60950-1, TUV EN60950-1 approved		
	WITHSTAND VOLTAGE	I/P-O/P:3KVAC I/P-FG:2KVAC O/P-FG:0.5KVAC		
	ISOLATION RESISTANCE	I/P-O/P, I/P-FG, O/P-FG:100M Ohms / 500VDC / 25℃/ 70% RH		
	EMC EMISSION	Compliance to EN55022 (CISPR22), EN61000-3-2,-3		
	EMC IMMUNITY	Compliance to EN61000-4-2,3,4,5,6,8,11, EN55024, light industry level, criteria A		
OTHERS	MTBF	109K hrs min. MIL-HDBK-217F (25℃)		
	DIMENSION	278*127*83.5mm (L*W*H)		
	PACKING	3.0Kg; 4pcs/13Kg/1.19CUFT		
NOTE	1. All parameters NOT specially mentioned are measured at 230VAC input, rated load and 25℃ of ambient temperature. 2. Ripple & noise are measured at 20MHz of bandwidth by using a 12" twisted pair-wire terminated with a 0.1uf & 47uf parallel capacitor. 3. Tolerance : includes set up tolerance, line regulation and load regulation. 4. The power supply is considered a component which will be installed into a final equipment. The final equipment must be re-confirmed that it still meets EMC directives. For guidance on how to perform these EMC tests, please refer to "EMI testing of component power supplies." (as available on http://www.meanwell.com) 5. Derating may be needed under low input voltages. Please check the derating curve for more details.		

MEAN WELL

1500W Single Output Power Supply **SPV-1500 series**

■ Mechanical Specification

Case No.943A Unit:mm

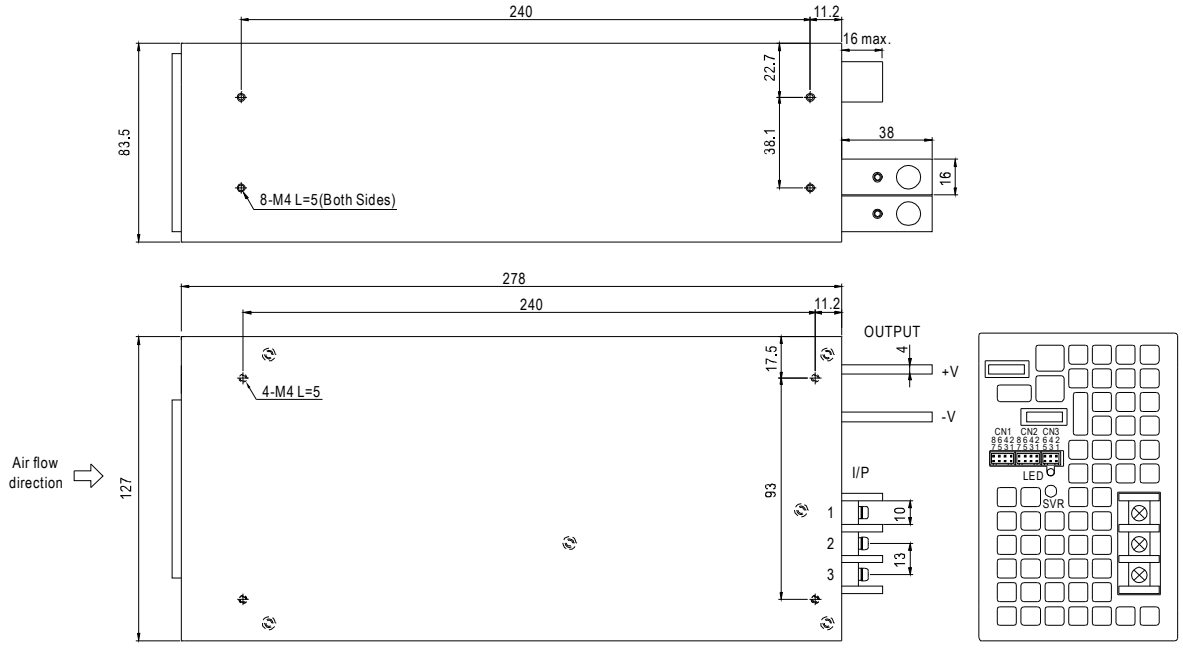

AC Input Terminal Pin No. Assignment

Pin No.	Assignment
1	FG ⏚
2	AC/N
3	AC/L

Control Pin No. Assignment(CN1,CN2) : HRS DF11-8DP-2DS or equivalent

Pin No.	Assignment	Pin No.	Assignment	Mating Housing	Terminal
1	RCG	5,7	-S	HRS DF11-8DS or equivalent	HRS DF11-**SC or equivalent
2	RC2	6	LS(Current Share)		
3	PV	8	+S		
4	PS				

RCG: Remote ON/OFF Ground -S: -Remote Sensing
RC2: Remote ON/OFF LS: Load Share
PV: Output voltage external control +S: +Remote Sensing
PS: Reference voltage terminal, PS and PV are connected when shipping

Control Pin No. Assignment(CN3) : HRS DF11-6DP-2DS or equivalent

Pin No.	Assignment	Pin No.	Assignment	Mating Housing	Terminal
1	P OK GND	4	AUXG	HRS DF11-6DS or equivalent	HRS DF11-**SC or equivalent
2	P OK	5	RC1		
3	RCG	6	AUX		

P OK GND: Power OK Ground AUXG: Auxiliary Ground
P OK: Power OK Signal RC1: Remote ON/OFF
RCG: Remote ON/OFF Ground AUX: Auxiliary Output

■ Block Diagram

PFC fosc : 70KHz
PWM fosc : 100KHz

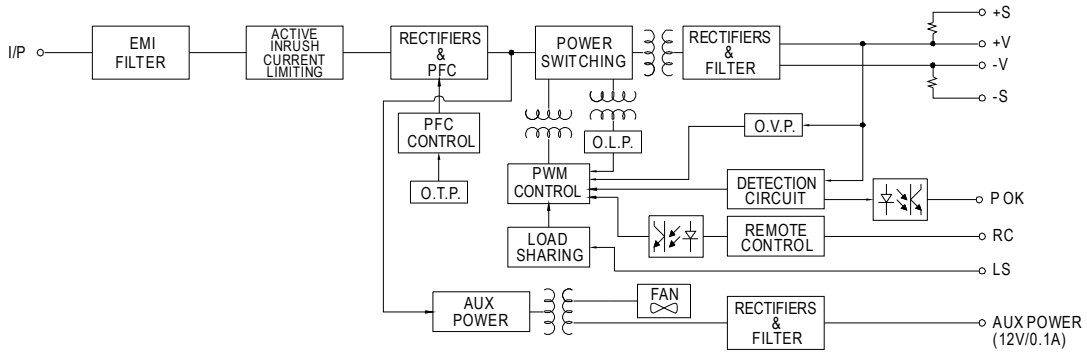

MEAN WELL 1500W Single Output Power Supply **SPV-1500 series**

■ Derating Curve

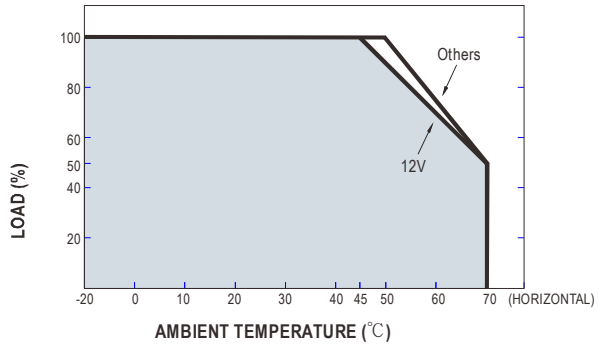

■ Static Characteristics

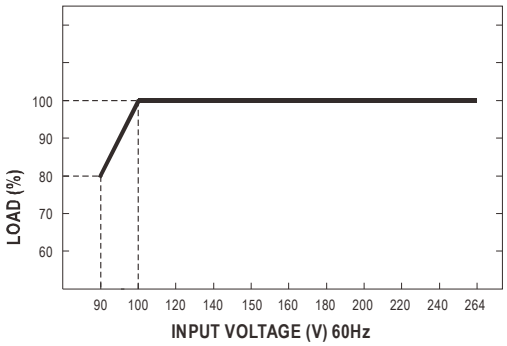

■ Function Manual

1.Remote ON/OFF

(1)Remote ON/OFF control becomes available by applying voltage in CN1 & CN2 & CN3

(2)Table 1.1 shows the specification of Remote ON/OFF function

(3)Fig.1.2 shows the example to connect Remote ON/OFF control function

Table 1.1 Specification of Remote ON/OFF

Connection Method		Fig. 1.2(A)	Fig. 1.2(B)	Fig. 1.2(C)
SW Logic	Output on	SW Open	SW Open	SW Close
	Output off	SW Close	SW Close	SW Open

Fig.1.2 Examples of connecting remote ON/OFF

(A)Using external voltage source

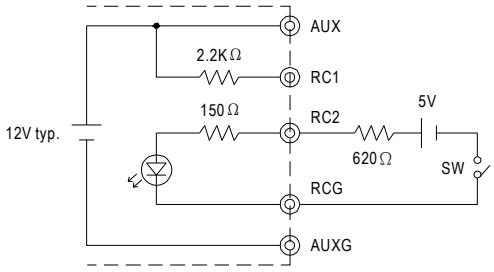

(B)Using internal 12V auxiliary output

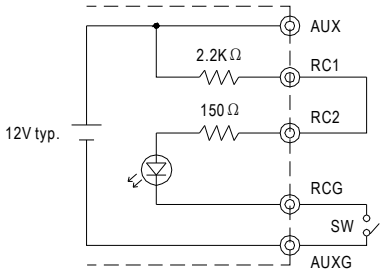

(C)Using internal 12V auxiliary output

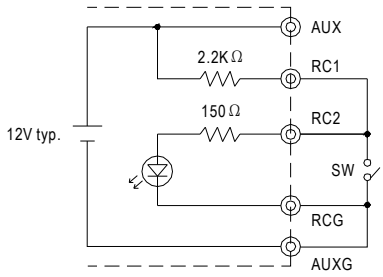

2.Alarm Signal Output

(1)Alarm signal is sent out through "P OK" & "P OK GND" pins
(2)An external voltage source is required for this function. The maximum applied voltage is 50V and the maximum sink current is 10mA
(3)Table 2.1 explains the alarm function built-in the power supply

Function	Description	Output of alarm(P OK)
P OK	The signal is "Low" when the power supply is above 15% of the rated output voltage-Power OK	Low (0.5V max at 10mA)
	The signal turns to be "High" when the power supply is under 15% of the rated output voltage-Power Fail	High or open (External applied voltage 10mA max.)

Table 2.1 Explanation of alarm function

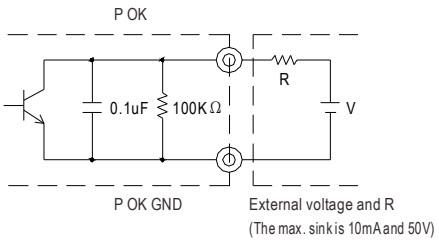

Fig. 2.2 Internal circuit of P OK (Open collector method)

3.External Voltage Control

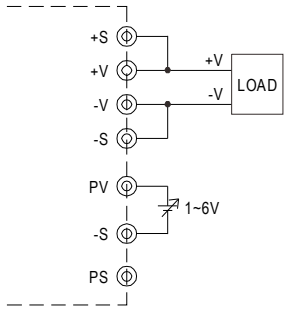

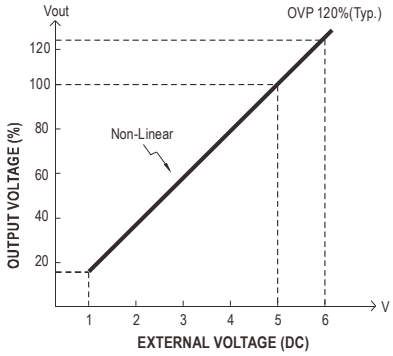

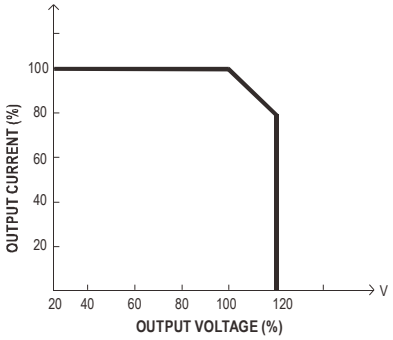

Note: (1)Reference voltage terminal, PS and PV are connected when shipping
(2)+S & +V, -S & -V also need to be connected on CN1 or CN2.

4.Current Sharing

(1)Parallel operation is available by connecting the units shown as below (+S,-S and LS are connected mutually in parallel):
(2)The voltage difference among each output should be minimized that less than 0.2V is required
(3)The total output current must not exceed the value determined by the following equation (Output current at parallel operation)=(The rated current per unit) x (Number of unit) x 0.9
(4) In parallel operation 3 units is the maximum, please consult the manufacturer for other applications
(5) When remote sensing is used in parallel operation, the sensing wire must be connected only to the master unit
Note : In parallel connection, maybe only one unit (master) operate if the total output load is less than 5% of rated load condition.
The other PSUs (slaves) may go into standby mode and their output LEDs will not turn on.
(6)Under parallel operation, the "output voltage trim" function is not available.

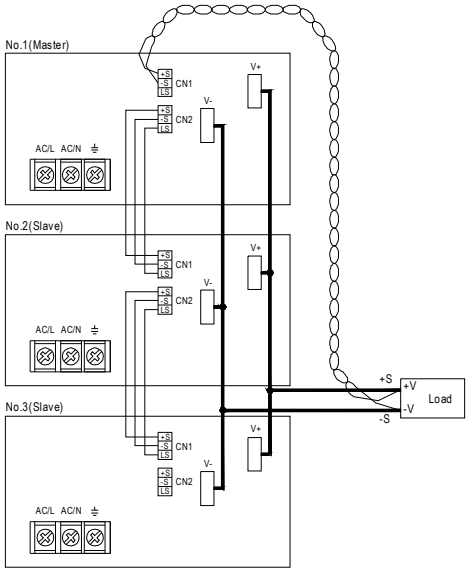

Pulse Amp Module RRP131K0-10

RFHIC

Product Features

- Frequency from 1.2 ~ 1.4GHz
- GaN HEMT
- 50 Ohm Input/Output impedance
- High efficiency

Applications

- Radar system

Description

The RRP131K0-10 is designed for Radar system application frequencies from 1.2 ~ 1.4GHz.
This module uses GaN HEMT technology which performs high breakdown voltage, wide bandwidth and high efficiency.

Electrical Specifications @ V_{DS} =50V, T=25°C, 50Ω System

PARAMETER	UNIT	MIN	TYP	MAX	SYMBOL
Operating Frequency	MHz	1200	-	1400	f_O
Operating Bandwidth	MHz	-	200	-	BW
Output Pulse Power	W	1000	1200	-	P_O
Input Pulse Power	dBm	-	7	10	P_I
Power Gain	dB	53	54	-	G_P
Gain Flatness	dB	-	-	±1.0	ΔG_P
Duty Cycle	%	-	-	20	DC
Pulse Width	us	-	-	500	PW
Efficiency	%	40	50	-	E_{ff}
Amplitude Pulse Droop	dB	-	0.5	1.0	Droop
Harmonics 1 to N	dBc	30	-	-	H_N
Spurious Level	dBc	60	-	-	Spur
Rise Time	ns	-	-	200	t_r
Fall Time	ns	-	-	200	t_f
Input VSWR	-	-	-	1.5:1	VSWR
Output VSWR	-	-	-	1.5:1	VSWR
Switching Time	us	-	0.5	1	t_{SW}
Phase Deviation	°	-20	-	20	Δφ

* Test Pulse conditions = 100us, 10%
* Above electrical specifications is measured by connecting electrolytic condenser 10,000uF to DC. Please make sure that electrolytic condenser is connected properly while testing the module.
* Custom design available

Absolute Maximum Ratings

PARAMETER	UNIT	RATING	SYMBOL
Operating Junction Temperature	°C	225	T_J
Operating Flange Temperature	°C	-30 ~ 75	T_C
Storage Temperature	°C	-30 ~ 125	T_{STG}

Pulse Amp Module RRP131K0-10

Operating Voltages

PARAMETER	UNIT	NOMINAL VOLTAGE	VOLTAGE ACCURACY	SYMBOL
Drain-Source Voltage	V	50	± 5%	$V_{DS}1$
Drain-Source Sub Voltage	V	12	± 5%	$V_{DS}2$
Shutdown Voltage	V	TTL Low(0V) : PA ON, TTL High(5V) : PA OFF		$V_{DC}1$
On/Off Control Voltage	V	TTL Low(0V) : PA ON, TTL High(5V) : PA OFF		$V_{DC}2$

Power Supply

PARAMETER	UNIT	MIN	TYP	MAX	SYMBOL
Drain-Source Current(AVG)	A	-	11	16	$I_{DS}1$
Drain-Source Sub Current(AVG)	A	-	0.12	0.2	$I_{DS}2$

* Duty Cycle 20%, Pulse Width 200us

Block diagram

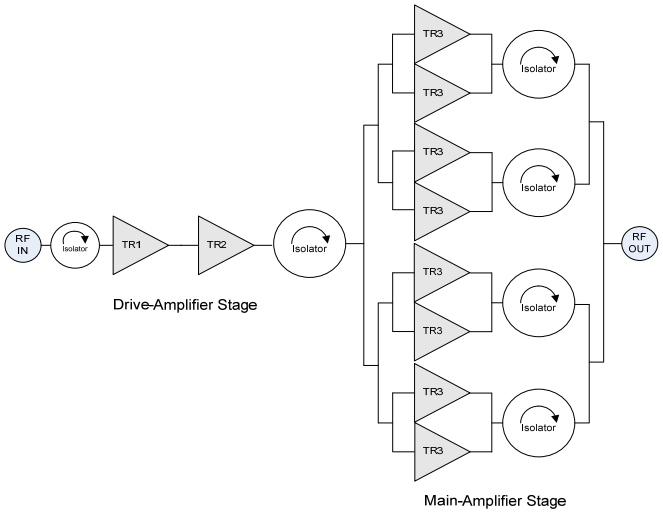

Mechanical Specifications

PARAMETER	UNIT	TYP
Mass	kg	1.3
Dimension	㎜	220 x 145 x 27
RF Connector	-	SMA Female : RF Input
		N-type Female : RF Output
DC Connector	-	3W3 connector : Supply
		9Pin D-Sub : Control

Pulse Amp Module RRP131K0-10

Outline Drawing

* Unit: mm[inch] | Tolerance ±0.2[.008]

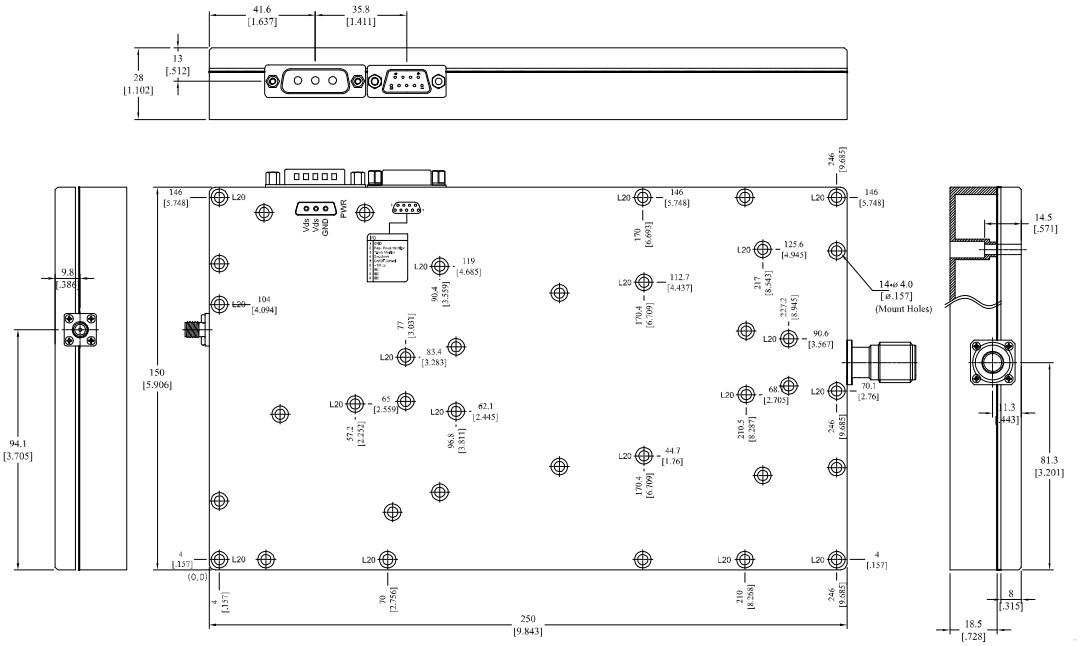

Pin Description

Supply : 3W3 Connector			
Pin No	**Description**	**Pin No**	**Description**
1 & 2	$V_{DS}1$ (+50V)	3	GND
Control : 9Pin D-Sub			
Pin No	**Description**	**Pin No**	**Description**
1	GND	6	$V_{DS}2$ (+12V)
2	Peak Power Monitor	7	NC
3	Temp Monitor	8	NC
4	Shutdown	9	NC
5	On/Off Control	-	-

Pulse Amp Module **RRP131K0-10** RFHIC

Revision History

Part Number	Release Date	Version	Modification	Data Sheet Status
RRP131K0-10	2012.12.28	1.0	Version update	-
RRP131K0-10	2012.9.6	0.1	-	Preliminary
-	-	-	-	-

AM89-06-001 RB
17-11-2011

Specification & Operating Instructions

Model AM89-8.5S-56-56P Pulsed Power Amplifier

Microwave Amplifiers Ltd
4 High Street
Nailsea
Bristol. UK
BS48 1BT

Tel: +44 (1275) 853196
Fax: +44 (1275) 858502
e-mail: sales@maltd.com

CONTENTS

1 Introduction.

The AM89 is a solid-state class A pulsed GaAS FET amplifier. It provides a minimum output of 400 Watts RF power over the bandwidth shown below. The amplifier may be operated only with pulsed inputs, and is gated for maximum efficiency and minimum heat generation

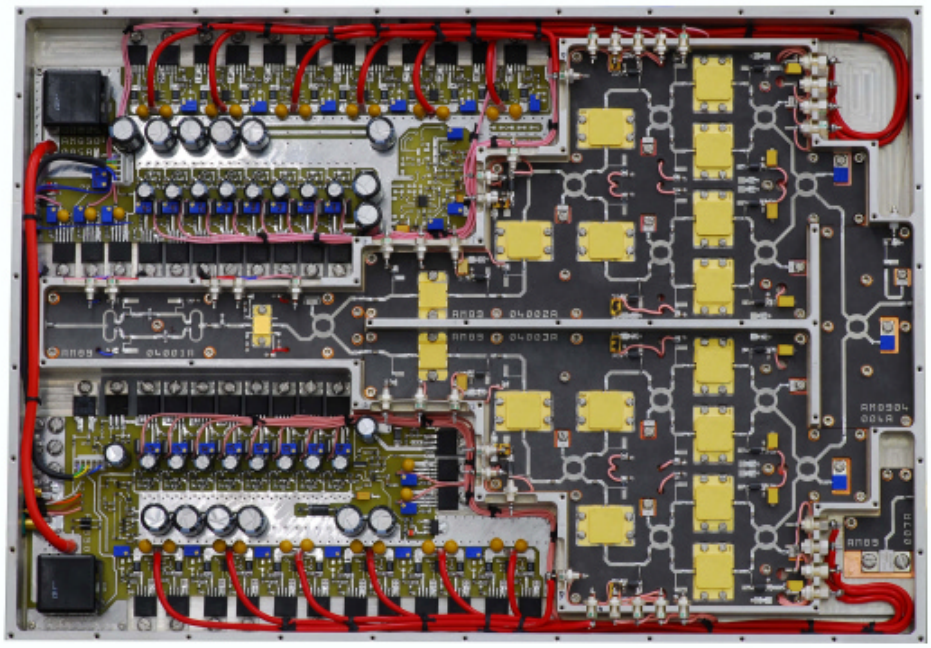

2 Specifications

2.1 Electrical

Frequency Range	8.4-8.5GHz
Small Signal Gain	53dB min
Gain Flatness	0.5dB p-p max
Maximum Input Power	+15dBm max
Maximum Duty Cycle	10% (see note 1)
Pulse Width	5uS nom
Pulse Repetition Frequency	1kHz nom
Output Power @ 1dB GCP	+55dBm min, +55.5dBm typ
Output Power Saturated	+56dBm min, +56.5dBm typ
Non-Harmonic Spurious	-80dBc min
Noise Figure @ 25C	8dB nom
Input Return Loss	14dB min, 17dB typ
Output Return Loss	14dB min, 17dB typ
TTL Pulse Control Rise Time	5uS max, 3uS typ (see note 3)
TTL Pulse Control Fall Time	5uS max, 4uS typ (see note 3)
TTL pulse control signal	TTL HIGH = amplifier biassed to class A (note 5)
RF Rise & Fall Times	50nS nom (note 4)
DC Detector	+5V min @ Pout +56dBm
Power Supply +Ve	+12V DC, +/-0.1V
Supply Current +Ve	140A peak nom @ max RF O/P (note 2)
Standby Supply Current	1500mA nom
Power Supply –Ve	-8 to -12V DC
Supply Current -Ve	1A peak nom (note 2)

NOTES

1 Duty Cycle

The amplifier duty cycle is limited to 10% at which the amplifier may be continuously operated. The pulse width and repetition frequency of the RF signal may be varied as required, but must not exceed the maximum rated duty. Built-in protection against excessive duty cycle in incorporated, which will automatically limit the RF output if this level is exceeded.

2 Power Consumption

The primary power input demand will be a function of the duty cycle. The +V supply voltage must not exceed +12V. The –V supply voltage must fall within the stated range.

3 Pulse Control Rise & Fall Time

This is the period of transition between standby & active states determined by measurement of the rise & fall time of a CW signal from 0-100% and from 100% to 0.
During the standby state the amplifier is disabled drawing minimal power, and can not amplify an RF signal. In response to a TTL (high) command, the amplifier switches to an active state with full DC bias, and is able to amplify a pulse. The duration of this transition is the *Pulse Control Rise Time.*
At the end of the pulse the amplifier may be reverted to the standby state. The duration of this transition is the *Pulse Control Fall Time*. Note that the application of RF signals during these transitions will result in a distorted output.

4 RF Rise & Fall Time

The RF rise/fall times are for a pulsed RF signal, with the amplifier stabilised in class A in response to TTL pulse-control signal.

5 TTL Pulse Control Signal

The TTL pulse control line is AC coupled to prevent accidental application of CW RF input signals.

2.2 Signal Interfaces

RF Input	SMA female panel jack
RF Output	N type female panel jack

A1	Ground
A2	+12V
1	Forward detector
2	Not connected
3	Overtemp alarm
4	TTL Pulse input
5	–8V supply

2.3 Mechanical

Module Dimensions (LWH)	400x300x123mm
Weight	10Kg nom

2.4 Controls & Indicators

2.4.1 TTL Pulse Control

A TTL high (+5v nom) signal activates the amplifier by applying class A bias to the RF power transistors. Input impedance 10K ohms.

2.4.2 Forward Power Detector

The forward detector comprises a shottky diode driven from a signal coupled from the RF output. DC output is approximately proportional to the level of RF output, with a diode non-linear response. The detector circuit is intended for RF status reporting, and not for use in ALC loops. The output is buffered, suitable for connection to circuits with >1k nominal impedance.

Detector voltage at max RF output	+5v nom
Dynamic range	15dB typ

2.4.3 Over Temp Alarm

The alarm circuit will disable the amplifier when the maximum permitted operating temperature is exceeded. The alarm will automatically reset when the permitted case operating temperature is restored.
Suitable for connection to circuits with >1k nominal impedance.

Alarm activation temperature (T_{act})	70C +/-5C
Alarm reset temperature	T_{act} –10C nom
Alarm output signal	+12V = ALARM, 0V = OK
Alarm output current	25mA max

2.4 Protection Features

Internal Bias Sequencing	Drain supply to the GaAs FET devices is prevented in the absence of Gate bias.
Output power limiter	Amplifier output is limited if average RF output power exceeds 10% duty.
Reverse Power Protection	Integral output isolator provides full power mismatch protection.
Over temperature protection	Monitors power module temperature, with automatic over temp shut-down, alarm output and auto reset. +12V alarm signal present at D-type connector under overheat condition.
CW Protection	The pulse control line is AC coupled to prevent CW operation.

2.7 Environmental

The amplifier is designed for operation within laboratory environments. The operating case temperature should be minimised for optimal performance and maximum life. A pattern of mounting holes for heatsink fitting is provided on the amplifier base.

Operating temperature range (case)	0 to +60C
Storage temperature range	-30 to +80C
Humidity (non-condensing)	95%

3.0 Technical Description

3.1 General

The amplifier is a solid state GaAs FET pulsed class A design
High power GaAs (Gallium Arsenide) transistors are controlled via a TTL command line to switch the bias levels so that the amplifier will be in a class A state for the duration of the RF pulse, but otherwise in a standby state. This design provides the superior performance possible from a class A design but without the disadvantages of high power consumption and heat generation, and offers significant advantages over conventional class C amplifiers as the amplitude variation and phase excursions caused by transistor junction heating are greatly reduced by the application of pre-pulse bias.

3.2 Main Features

GaAs FET design	-	*Utilises the latest state of the art devices*
Unconditional stability	-	*Will not oscillate with any I/P or O/P match*
Integral output isolator & dummy load	-	*Reverse power protection & improved O/P match*
Open & short cct protection	-	*Via output isolator unit*
O/temp protection (shut down with auto reset)	-	*Prevents overheat damage*
GaAs FET bias sequencing	-	*Essential FET operating precaution*

4.0 Power Supply Requirements

4.1 +12V DC Supply

This supply rail provides the drain bias to the GaAs transistors. The amplifier is internally regulated and so variations in the supply level will not effect the RF output level. Ensure that the rating of the power supply connected is appropriate to the DC demand in respect of the required duty cycle.

4.2 -8V DC Supply

This rail provides the gate bias to the GaAs transistors and is regulated within the module to the nominal –5V level required to maintain bias stability, and for the operation of the TTL control circuits.

4.3 Supply Rail Sequencing

The amplifier has internal bias sequencing which prevents the application of bias to the GaAs transistors in the wrong order. Even so, it is recommended that the –Ve supply rail is applied prior to the +Ve supply, with a delay of at least 1uS. Similarly, the +Ve rail must be removed prior to the –Ve supply, if the equipment is to be switched off. . Failure to ensure this may result in the destruction of the module if the internal sequencing circuits develop a fault.

THE +V SUPPLY SHOULD NOT BE PRESENT IN THE ABSENCE OF THE –V SUPPLY

5.0 Operating Instructions

5.1 Preparation

Ensure that the amplifier is correctly secured to its heatsink (for models without integral sink)
Ensure that the cooling fans are connected to a +12-15V DC supply

5.2 Pulsed Class A Operation

Connect, **but do not switch on**, the –8V supply to Pin 5 of D-type connector.

Connect, **but do not switch on**, +12V supply using connectors supplied with amplifier.

Connect TTL pulse control line to Pin 4 of D-type connector. Ensure suitable TTL ground connection.
This control line must be PULSED for pulsed operation.

As described in Section 2 note 3, an RF signal may be amplified only when a TTL command is applied at the pulse control connector.

5.3 Amplifying a Pulsed RF Signal

It is necessary to synchronise the RF pulse with the TTL pulse control signal. This is accomplished using two square wave pulse generators capable of the desired PRF, one as master the other as slave. The slave is configured to trigger a pulse from an RF source, the master to output the TTL pulse control signal to the amplifier and after the required delay (pulse control rise time), trigger the slave.

5.3.1 Fig 1 - using external pulse generators with an SMR20 Rohde & Schwarz source

For SMR20 specifications & function refer to the operating manual or to online information at:
http://www2.rohde-schwarz.com/file_3894/smr_20-40%20e03.pdf

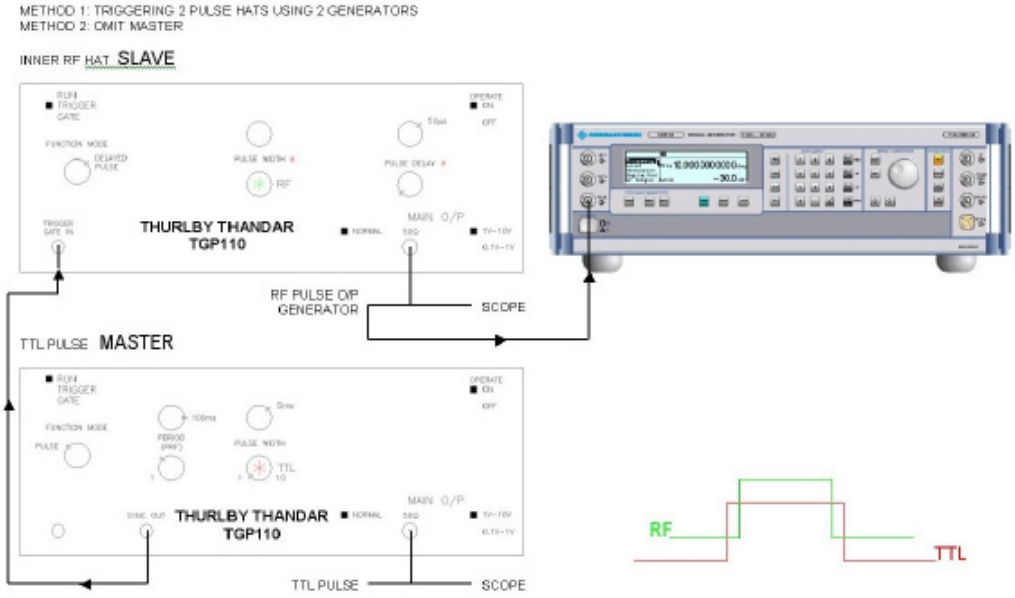

5.3.2 The timing sequence for a 5uS RF pulse should be as shown in Figure 2 below.

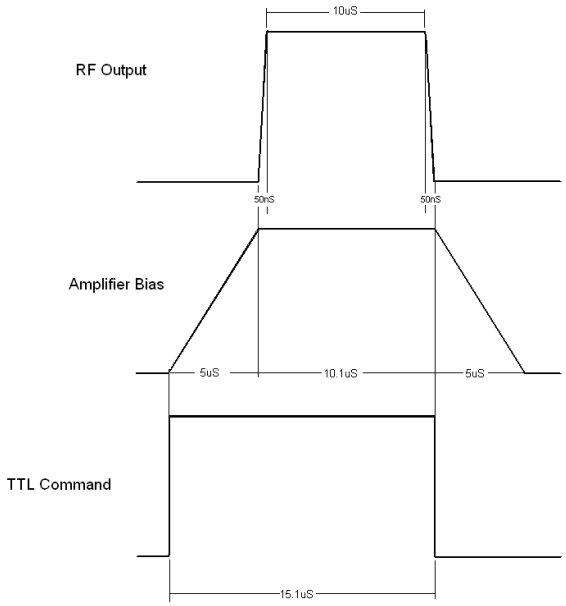

Connect RF input and RF output connectors. Ensure that the output load and cable rating is adequate for the intended power output which may exceed 80w. Ensure that the maximum RF input level does not exceed +15dBm. **Excessive overdrive will result in permanent damage to the amplifier.**

Set the input signal level to G-10dB, where G is the tested gain of the amplifier module.
Switch the cooling fans ON, unless the duty cycle is to be very low (<5%)

5.4 Switching the Amplifier ON

Switch ON the –8V supply.

THESE TWO OPERATIONS SHOULD BE DONE IN THIS ORDER

Switch ON the +12V supply.

The input drive to the amplifier may now be set at the desired level for the required output power.

The forward power may be monitored at pin 1 of the D-type connector.

5.5 Switching the Amplifier OFF

Switch OFF the +12V supply.

THESE TWO OPERATIONS SHOULD BE DONE IN THIS ORDER

Switch OFF the –12V supply.

6.0 Deliverables

Each amplifier is supplied packed in a purpose designed carton containing DC mating connectors and operating manual with test data.

7.0 Maintenance

There are no user serviceable parts within the amplifier. Each amplifier is factory tested and supplied with a set of test results. If degradation in performance to below the specified levels occurs, or a failure is suspected, then the complete unit should be returned to the manufacturer together with details of the fault.

8.0 Safety

There are no hazardous voltages within the module, however there may be radiated emissions at a harmful level – do not remove the amplifier lid.

THE CENTER CONDUCTOR OF THE RF OUTPUT CONNECTOR SHOULD NOT BE TOUCHED WHILST UNIT IS IN OPERATION. UP TO 250W RF POWER IS PRESENT WHICH CAN CAUSE SKIN BURNS

9.0 Warranty

Microwave Amplifiers Ltd warrants for 2 years from date of shipment that the goods supplied will be in full compliance with the agreed specifications and will be free from defects in material and workmanship. Any and all other warranties (except of title) express or implied, relating to fitness for particular purpose, merchantable quality or otherwise are expressly disclaimed. Seller will not be responsible for special or consequential loss or damages. Liability shall be limited to the repair or replacement of defective products subject to the return of the product intact, and un-tampered with by the buyer.

10.0 Amplifier Outline (fitted with heatsink & DC fans)

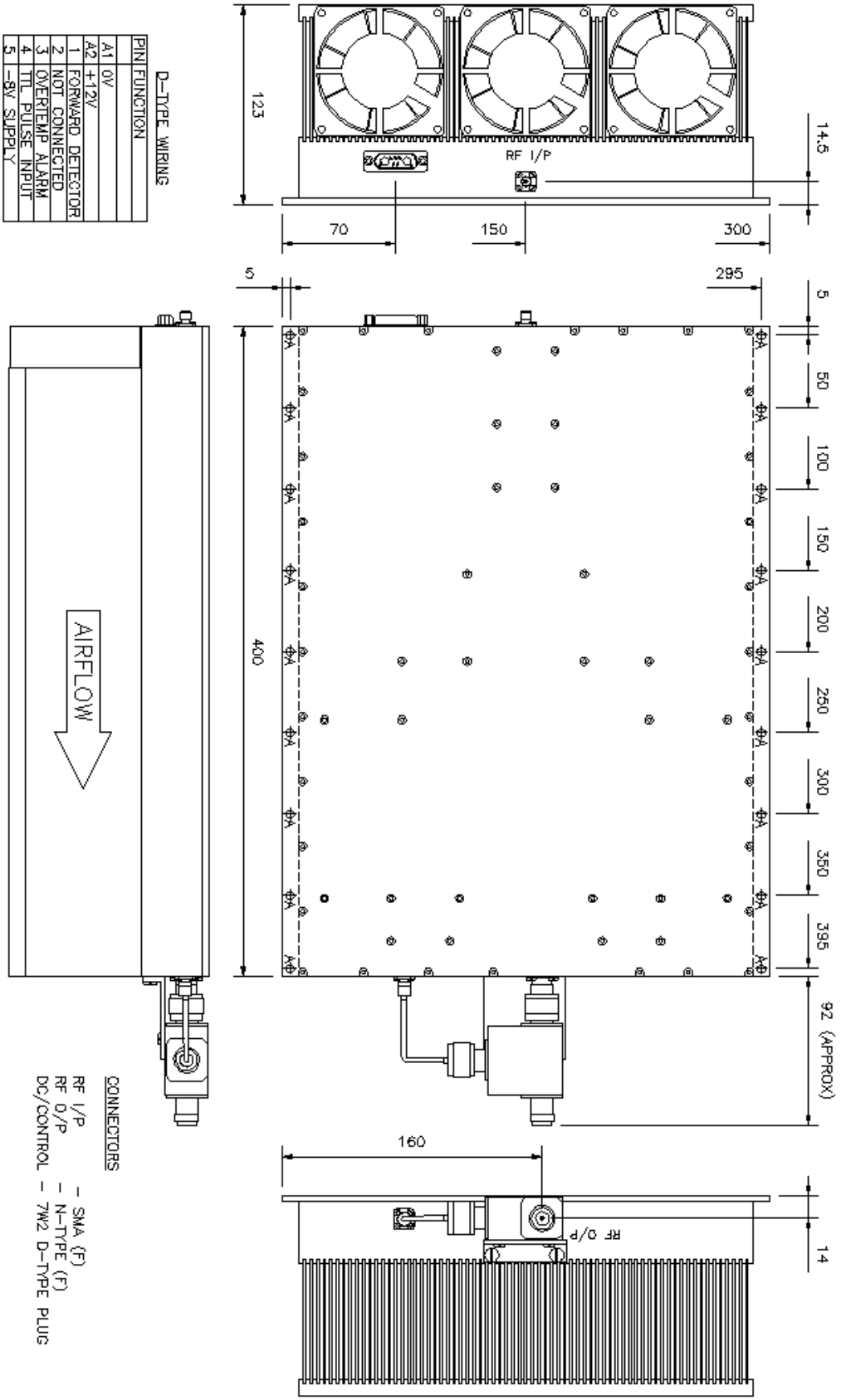

Appendix E

Ethics Assessment Form

EBE Faculty: Assessment of Ethics in Research Projects (Rev2)

Any person planning to undertake research in the Faculty of Engineering and the Built Environment at the University of Cape Town is required to complete this form before collecting or analysing data. When completed it should be submitted to the supervisor (where applicable) and from there to the Head of Department. If any of the questions below have been answered YES, and the applicant is NOT a fourth year student, the Head should forward this form for approval by the Faculty EIR committee: submit to Ms Zulpha Geyer (Zulpha.Geyer@uct.ac.za; Chem Eng Building, Ph 021 650 4791).
NB: A copy of this signed form must be included with the thesis/dissertation/report when it is submitted for examination

This form must only be completed once the most recent revision EBE EIR Handbook has been read.

Name of Principal Researcher/Student: *Adrian Dale Stevens* Department: *Electrical Engineering*

Preferred email address of the applicant: *stevens.adrian@gmail.com*

If a Student: Degree: *MSc (Eng) (Radar)* Supervisor: *Prof. Riana Geschke*

If a Research Contract indicate source of funding/sponsorship: n/a

Research Project Title: *Design and Implementation of an RF Front End for the NeXtRAD Radar System*

Overview of ethics issues in your research project:

Question 1: Is there a possibility that your research could cause harm to a third party (i.e. a person not involved in your project)?		NO
Question 2: Is your research making use of human subjects as sources of data? If your answer is YES, please complete Addendum 2.		NO
Question 3: Does your research involve the participation of or provision of services to communities? If your answer is YES, please complete Addendum 3.		NO
Question 4: If your research is sponsored, is there any potential for conflicts of interest? If your answer is YES, please complete Addendum 4.		NO

If you have answered YES to any of the above questions, please append a copy of your research proposal, as well as any interview schedules or questionnaires (Addendum 1) and please complete further addenda as appropriate. Ensure that you refer to the EIR Handbook to assist you in completing the documentation requirements for this form.

I hereby undertake to carry out my research in such a way that

- there is no apparent legal objection to the nature or the method of research; and
- the research will not compromise staff or students or the other responsibilities of the University;
- the stated objective will be achieved, and the findings will have a high degree of validity;
- limitations and alternative interpretations will be considered;
- the findings could be subject to peer review and publicly available; and
- I will comply with the conventions of copyright and avoid any practice that would constitute plagiarism.

Signed by:

	Full name and signature	Date
Principal Researcher/Student:	Adrian Dale Stevens	16 November 2016
This application is approved by:		
Supervisor (if applicable):		24/11/2016
HOD (or delegated nominee): *Final authority for all assessments with NO to all questions and for all undergraduate research.*		24/11/16
Chair : Faculty EIR Committee For applicants other than undergraduate students who have answered YES to any of the above questions.		

Bibliography

[1] M. Inggs, H. Griffiths, F. Fioranelli, M. Ritchie, and K. Woodbridge, "Multistatic radar: System requirements and experimental validation," in *2014 International Radar Conference*, pp. 1–6, Oct 2014.

[2] M. Inggs, H. Griffiths, F. Fioranelli, M. Ritchie, and K. Woodbridge, "Multistatic radar: System requirements and experimental validation," in *2014 International Radar Conference*, Oct 2014. Conference Presentation Slides.

[3] L. R. Danoon and A. K. Brown, "Modeling methodology for computing the radar cross section and doppler signature of wind farms," *IEEE Transactions on Antennas and Propagation*, vol. 61, pp. 5166–5174, Oct 2013.

[4] Reutech Radar Systems, a Division of Reutech (Pty) Ltd., "UCT receiver/exciter (REX) sub-system specification," tech. rep., Aug. 2014.

[5] Pentek, "Pentek model 71620 operating manual," operating manual 800.71620, Sept. 2014.

[6] U. K. Mishra, L. Shen, T. E. Kazior, and Y. F. Wu, "GaN-based RF power devices and amplifiers," *Proceedings of the IEEE*, vol. 96, pp. 287–305, Feb 2008.

[7] RFHIC Corporation, "Pulse amp module RRP131K0-10," datasheet, Dec. 2012. Rev. 1.0.

[8] "IEEE standard letter designations for radar-frequency bands," *IEEE Std 521-2002 (Revision of IEEE Std 521-1984)*, 2003.

[9] Microwave Amps Ltd, "Pulsed power amplifier AM89-8.5S-56-56P," datasheet AM89-06-001 RB, Nov. 2011.

[10] J. Kovatch, "5 steps to selecting the right RF power amplifier," whitepaper, AR Modular RF.

[11] S. T. Paine, "Design and implementation of a dual polarised l-band parabolic dish antenna for NeXtRAD," masters thesis, University of Cape Town, Rondebosch, South Africa, 2016.

[12] P.-K. Cheng, "NeXtRAD antenna design: X-band dual polarised conical horn antenna," masters thesis, University of Cape Town, Rondebosch, South Africa, 2016.

[13] M. A. Richards, J. Scheer, and W. A. Holm, *Principles of Modern Radar*. Raleigh, NC: SciTech Pub., 2010.

[14] Teledyne Coax Switches, "Series CCS-32/CS-32 high power DC – 12 GHz latching SPDT coaxial switch," datasheet, 2013.

[15] Mini-Circuits, "Mechanical switch extended life test report," appl. note AN-83-001, 2009.

[16] J. J. Carr, *Secrets of RF Circuit Design*. New York: McGraw-Hill, 3rd ed., 2001.

[17] W. L. Stutzman and G. A. Thiele, *Antenna Theory and Design*. Hoboken, NJ: Wiley, 3rd ed., 2013.

[18] D. M. Pozar, *Microwave and RF Design of Wireless Systems*. Hoboken, NJ: Wiley, 1st ed., 2000.

[19] M. Skolnik, *Radar Handbook*. McGraw-Hill, 3rd ed., 2008.

[20] Communications and Power Industries, Beverly Microwave Division, "Receiver protector technology," appl. note.

[21] D. M. Pozar, *Microwave Engineering*. Hoboken, NJ: Wiley, 4th ed., 2012.

[22] J. P. Heineberg, "Cooling solution for the NeXtRAD system," bachelors thesis, University of Cape Town, Rondebosch, South Africa, 2014.

[23] P. Horowitz and W. Hill, *The Art of Electronics*. New York, NY: Cambridge University Press, 1989.

[24] Fairchild Semiconductor Corporation, "Heat sink mounting guide," appl. note AN-4166, June 2014. Rev. 1.0.0.

[25] Electrolube, a division of H K Wentworth, "HTSP silicone heat transfer compound plus," datasheet, 2011.

[26] International Rectifier, "Heatsink characteristics," appl. note AN-1057.

[27] P. Bachman and R. Haiduk, "The effect of forced air cooling on heat sink thermal ratings," whitepaper, Crydom Inc., 2011.

[28] G. R. Curry, *Radar System Performance Modeling*. Norwood, MA: Artech House, 2nd ed., 2005.

[29] *Electronic Warfare and Radar Systems Engineering Handbook*. Point Mugu, CA: Naval Air Warfare Centre, April 1997.

[30] Agilent Technologies, "Fundamentals of RF and microwave power measurements," appl. note 64-1C.

[31] B. R. Mahafza, *Radar Systems Analysis and Design Using MATLAB*. Boca Raton, FL: Chapman & Hall, 2000.